School of Civil and Mechanical Engineering

Monitoring of Bolted Steel Plate Joints for Torque Loss and Corrosion: A Guided Wave Approach

Jay Kumar Shah

This thesis is presented for the Degree of

Doctor of Philosophy

of

Curtin University

Apr 2021

Author's Declaration

To the best of knowledge and belief this thesis contains no material previously published by any other person except where due acknowledgement has been made.

This thesis contains no material which has been accepted for the award of any other degree or diploma in any university.

Abstract

Joints are ubiquitous in the construction, manufacturing, naval, and aerospace industries. Although welded and riveted or joints had gained more popularity over the bolted joints, they are making a comeback as they offer easy dismantling, replacement, and repurposing and hence, better lifecycle management. In construction, concrete gained popularity over steel due to the perceived economy. Bolted joints are mandating a reassessment of the notion as the lifecycle assessments need to account for the ease of dismantling and repurposing of built steel facilities.

Bolted joints are susceptible to degradation. The bolts may lose tension with time, and thus, the contact pressure between the plates of the joint may be lost, leading to slippage. Moreover, corrosion of the joint may affect the performance of the joint. Therefore, it is imperative to develop a reliable technique for monitoring bolted joints. It is desirable to have a technology that can monitor automatically and preferably can move to the internet-of-things platform.

This thesis explores a guided wave technique for monitoring bolted joints. It employs systems that are conducive to automated monitoring. Two types of transduction have been attempted: embedded piezoelectric patches and a non-contact laser system. The thesis investigates the effect of torque loss, corrosion, and their combined effect. An attempt is made to correlate the non-destructive tests with parameters such as load capacity and failure modes.

The thesis has been presented in a hybrid manner as a collection of two published and five supporting chapters. It commences with a brief introduction to the motivation behind the thesis, followed by the thesis outline. A detailed literature review has been presented, highlighting the existing gaps in the literature hence identifying the key objectives of the thesis. These objectives are achieved through several experimental and numerical investigations on single-lap bolted steel plate specimens. Accelerated corrosion technique is used to simulate the joint corrosion.

The investigation initiates with an experimental study on the corroding joint using a conventional coupling transducer-based Pulser-receiver system. The findings establish a correlation between the bolt torque and the extent of corrosion. The corrosion effects on the integrity of differently tightened joints have been analyzed through destructive tension tests. While eliminating the coupling inconsistencies in the transducers, the study advances towards a baseline comparison free imaging technique using embedded piezoelectric patches. The developed images efficiently capture the quality of interfacial contact. The investigation later converges to interfacial corrosion monitoring exploiting guided wave modes existing in

different thickness regions of the joint. The experimental findings hint towards mode conversion with the advancement in corrosion. These outcomes have been cross validated with the results of a finite element based numerical model. Eventually, the patch-based investigation has been replaced by a non-contact laser system as a step to achieve automated inspection. It facilitates high energy and broadband wave excitation. The findings showed that the higher-order modes are sensitive to interfacial corrosion.

The thesis concludes with a summary of the findings while unveiling the direction for future research.

Acknowledgements

I would admit that it was the toughest section to write in this thesis. The whole journey of applying for Ph.D. applications, waiting for their outcome, and finally completing my Ph.D. work in Australia is flashing right in front of my eyes at this moment. All these experiences were only possible due to the support of all the wonderful people that I came across. I have tried my best to acknowledge everyone for their efforts.

At first, I would like to thank the Government of Australia for letting me pursue my doctoral degree in Australia. I am grateful to Curtin University to support me with the CIPR scholarship.

A big thank you to my thesis supervisor Professor Abhijit Mukherjee to give me all the freedom to test out every single childish research idea that I had during my Ph.D. I have evolved as a humble and at the same time practical researcher under your guidance. I have always enjoyed our academic and non-academic discussions. This learning has helped me to set my work standards higher.

I would also like to thank Prof. Sudeep Bhattacharjee (my master's project supervisor) and Prof. N.N. Kishore (my project investigator at NDT Lab, IIT Kanpur) for their support during my Ph.D. application. It wouldn't be possible without your recommendations to get this Ph.D.

Thanks to my family for all the unconditional love and support they have provided me. I would like to say I am no-one without your support. May God keep them safe and healthy.

Now it is the turn to acknowledge all the fossils and *relatively fresh breeds* of my Ph.D. group: Navdeep (co-supervisor cum friend), Subhra, Asha, Nimrat, Sakshi, *Sukrit,* and *Abhijit Mistri*. In the last four years, you have given me the best memories of my journey. All the road trips, picnics, delicious Indian/ Chinese meals, and logical cum time-wasting life-related discussions that you have brought into my life have made my stay in Perth memorable. It has been a wonderful experience to know you guys personally. You guys are my extended Aussie cum Indo/ Chinese/ Mexican family now. I also acknowledge all other group members (Anant, Aparna, Raja, Shivani, Hector, Hannah, and Elaheh) with whom I got little but worthy chance to personally/ professionally know.

Its turn to acknowledge all the new add-ons in my life during my time in Australia. A big thanks to my partner (now wife) Anuradha for all the undying support in the past three years. I have evolved as a responsible person by your side. I look forward to experiencing different aspects of life with you. I also thank Anu's parents to treat me like their own son and

supporting both of us during big decisions of our lives. I got wonderful friends in form of my ex-housemates: Suman and Avin. We always found a reason at laugh on our life miseries. The way you and your family members still get around together makes it feel like home. I also have many memorable dinner invitations and local trips on 'L' plates memories with Abhijit Mistri and Boral during their stay in Perth. A big cheer to Waqas for being my cricket buddy. You have always pushed me to test my limits on and off the cricket field.

When it comes to acknowledging friends form IITK, the list is huge. No words can describe the mental support that you had provided me back in my days at IITK. I acknowledge Abhijeet Shukla, Apoorva, Adarsh, Abhinav, Brijesh, Chakresh, Gaurav, Kuldeep, and Ritika for the wonderful memories we have together. From having work life balance, working with insanity towards a goal, dancing for no reason to provide undying support to your loved one you guys have taught me everything.

Finally, a big thanks to Google search, YouTube and lab Technicians at Curtin to help me sail through my research smoothly.

Dedication

This thesis is dedicated to my parents for their unconditional love. You guys are the two pillars of my life.

Table of Contents

List of Figures

List of Tables

Glossary of Terms

OECD	Organization for economic cooperation and development
SHM	Structural health monitoring
NDT	Non-destructive testing
P-wave	Pressure wave
S-wave	Shear wave
FEM	Finite element method
CAN	Contact acoustic nonlinearity
S-mode	Symmetrical mode
A-mode	Antisymmetric mode

Attributes

This thesis contains two published and one submitted for publication chapters. The co-authors of these chapters are hereby acknowledged for their contribution. The signed attribution statements have been included as follows:

Attribution Document for Chapter 3

STATEMENT OF AUTHORSHIP

Title	Ultrasonic monitoring of corroding bolted joints
Status	✓ Published Accepted by the Journal Submitted in a Journal Unsubmitted work in manuscript style
Publication details	SHAH, J.K., BRAGA, H.B.F., MUKHERJEE, A. & UY, B., *Ultrasonic monitoring of corroding bolted joints*, 2019, Engineering Failure Analysis, 102, 7-19.

Principal Author

Name (candidate)	Jay Kumar Shah
Contribution	Author has conducted the literature review and laid out the research plan based on existing gaps in literature. Author has carried out the experiments, analysis and prepared the manuscript for publication.
Certification	This paper reports on original research I conducted during the period of my HDR candidature and is not subjected to any obligations or contractual agreement with a third party that would constrain its inclusion in this thesis. I am the primary author of this paper.
Signature & date	 02 Nov 2020

Co-authorship agreement

By signing the statement of authorship agreement, each author agrees that their contribution stated by the principal author is accurate and they grant permission to the candidate to include this work in his/ her thesis.

Name of Co-Author 1	Henrique Bastos Fabrino Braga

Contribution	Author has assisted the principal author during initial stages of the experiments.
Signature & date	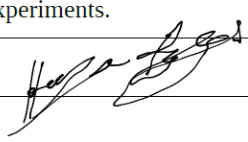 11/2/2020

Name of Co-Author 2	Abhijit Mukherjee
Contribution	Author is the supervisor of the candidate and assisted him in manuscript development, review and assessment.
Signature & date	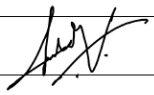 29 Nov 2020

Name of Co-Author 3	Brian Uy
Contribution	Author has assisted in development of the manuscript.
Signature & date	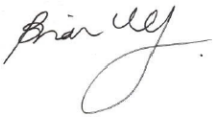 29/10/20

Attribution Statement for Chapter 4

STATEMENT OF AUTHORSHIP

Title	Monitoring and Imaging of Bolted Steel Plate Joints Using Ultrasonic Guided Waves
Status	✓ Published Accepted by the Journal Submitted in a Journal Unsubmitted work in manuscript style
Publication details	Shah, J. K., & Mukherjee, A. (2020). Monitoring and Imaging of Bolted Steel Plate Joints Using Ultrasonic Guided Waves. *Journal of Nondestructive Evaluation, Diagnostics and Prognostics of Engineering Systems*, *4*(1).

Principal Author

Name (candidate)	Jay Kumar Shah
Contribution	Author has conducted the literature review and laid out the research plan based on existing gaps in literature. Author has

	carried out the experiments, analysis and prepared the manuscript for publication.
Certification	This paper reports on original research I conducted during the period of my HDR candidature and is not subjected to any obligations or contractual agreement with a third party that would constrain its inclusion in this thesis. I am the primary author of this paper.
Signature & date	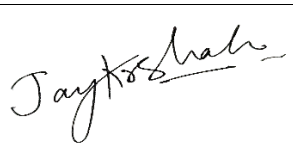 02 Nov 2020

Co-authorship agreement

By signing the statement of authorship agreement, each author agrees that their contribution stated by the principal author is accurate and they grant permission to the candidate to include this work in his/ her thesis.

Name of Co-Author 1	Abhijit Mukherjee
Contribution	Author is the supervisor of the candidate and assisted him in manuscript development, review and assessment.
Signature & date	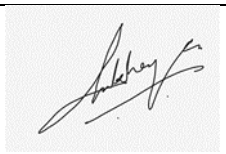 29 Nov 2020

Attribution Statement for Chapter 5

STATEMENT OF AUTHORSHIP

Title	Monitoring of Corroding Steel Bolted Joints using Embedded Piezoelectric Patches	
Status		Published
		Accepted by the Journal
	✓	Submitted in a Journal
		Unsubmitted work in manuscript style

Publication details	Shah, J. K., & Mukherjee, A. (2020). Monitoring of Corroding Steel Bolted Joints using Embedded Piezoelectric Patches

Principal Author

Name (candidate)	Jay Kumar Shah
Contribution	Author has conducted the literature review and laid out the research plan based on existing gaps in literature. Author has carried out the experiments, analysis and prepared the manuscript for publication.
Certification	This paper reports on original research I conducted during the period of my HDR candidature and is not subjected to any obligations or contractual agreement with a third party that would constrain its inclusion in this thesis. I am the primary author of this paper.
Signature & date	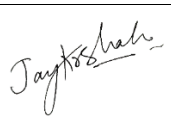 02 Nov 2020

Co-authorship agreement

By signing the statement of authorship agreement, each author agrees that their contribution stated by the principal author is accurate and they grant permission to the candidate to include this work in his/ her thesis.

Name of Co-Author 1	Abhijit Mukherjee
Contribution	Author is the supervisor of the candidate and assisted him in manuscript development, review and assessment.
Signature & date	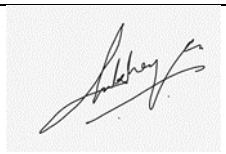 29 Nov 2020

Chapter: 1 Introduction

1.1 Motivation

Rehabilitation of existing infrastructure is a costly hurdle in achieving the goal of sustainable construction. In OECD countries, a significant share of public investment is allocated for the maintenance of in-service structures. These expenditures account for approximately 70% in European nations (OECD, 2015) whereas within Australia, an estimated budget of $30 billion has been reported (Verity et al., 2018). Such figures highlight the importance of efficient SHM techniques which can facilitate cost-efficient and timely maintenance of in-service structures. Efficient recycling of structural elements is another crucial parameter to achieve sustainable construction. Therefore, it is critical to consider the life cycle assessment of the planned construction. An ideal structure should offer labour extensive installation, easy maintenance, and effective recycling of the construction material.

Steel structures offer several advantages over concrete in terms of strength and lightweight. They can also offer easy installation and recycling provided the critical joints are bolted rather than welded or riveted (Akinade et al., 2015). To attain joint integrity, it is required to maintain adequate contact pressure between the bolted elements. Therefore, joints need to be secured with adequate torque levels during their installation. During the operational period, bolted joints are exposed to structural vibrations and harsh climatic conditions. This leads to concerns of torque loss and corrosion. These modest-looking concerns can be challenging to identify if occurred simultaneously. Insufficient torque levels result in the development of interfacial gaps which can be a favourable site for hidden rust formation.

This complex nature of the damage can go undetectable in conventional visual and audible inspections unless it reaches its advanced stage. The identification of the faulty joint gets further challenging for a multi bolt structure as the monitoring of individual bolt can become a costly and time-consuming task. Hence, considering the cost of structural rehabilitation and the limitations of traditional inspection techniques, a technology that is cost and time-efficient, comes handy, preferably non-invasive, and automated is a favourable solution to the inspection challenges of bolted joints.

There is a broad range of non-invasive techniques available, however not every technique offers a long-term solution while satisfying the above-mentioned preferences. Few examples are radiography, thermography, and electromagnetic inspections (Pickthall et al., 2011b). Radiography poses radiation hazards and requires costly equipment. It also demands a trained

operator, hence making it a specialized monitoring technique. Thermographic inspections require costly initial investments, and the outcomes are subjective to the surface temperature on the day of inspection. This may limit its use at field scale due to varying temperatures. Electromagnetic approaches such as eddy current testing are sensitive to the depth and the orientation of the damage.

Wave based inspection can offer versatile non-invasive technologies while being cost, time, and labour efficient. It is usually done in a passive and active approach. In the former method, sensors are attached to the structure to capture the audible signatures of the growing damage (Grosse et al., 2008). This method is well accepted for crack monitoring in concrete, whereas in bolted joints, torque loss and corrosion happen gradually over time and may not generate significant damage features. This approach also requires continuously active sensors around the inspection region and may face limitations in monitoring multi-bolt joints. In the latter approach, waves are induced in the structure at the time of inspection, and its interaction with the structure is interpreted to identify the damage.

Active monitoring is usually achieved by inducing standing waves (low-frequency vibrations) (Doebling et al., 1998) or high frequency travelling waves (bulk and guided waves) (Raghavan, 2007) in the structure. In the first approach, the structure is vibrated at low frequencies and the dynamic properties of the structure (resonance frequency, modal shapes etc.) are monitored. It has been argued that this approach is favoured for detecting large scale damage as local damage do not alter the global properties significantly. However, higher frequency wave interacts efficiently with the small-scale damages. Although being nondispersive in nature, bulk wave covers a localized area and may require repeated scanning at different positions for a large length of structure. Therefore, they are suited for short-distance inspections. However, guided wave covers the total thickness of the structure and travels over a longer inspection distance. Hence, a longer length can be inspected from a single point of wave excitation.

The guided ultrasonic wave-based technique (Mitra et al., 2016) has established applications in identifying a wide range of damage (micro-cracks (Y. Zhao et al., 2017)/ corrosion (Sharma et al., 2011)/ delamination (Panda et al., 2017)). It has vast applications in monitor structures made up of various types of construction materials (concrete (Pahlavan et al., 2018)/ steel (Sriramadasu et al., 2019)/ composites (Murat et al., 2016)). The core principle of this investigation lies in monitoring the wave properties (frequency (Yang et al., 2019), energy (Kaur et al., 2019), wave velocity (Chaki et al., 2007), and phase (Doyle et al., 2010)) as these are sensitive to the structural damage.

A reasonable number of guided wave-based bolted joint monitoring studies have been reported on the bolt torque loss (Nikravesh et al., 2017; Wang et al., 2013). However, no study has reported guided wave inspection on interfacial corrosion monitoring in bolted joints.

1.2 Problem Statement

Torque loss leads to poor contact between the bolted elements, hence creating interfacial gaps. These crevices serve as the ideal sites for moisture retention, later becoming a prime source of invisible interfacial corrosion. There is a possible correlation between the bolt torque and the effect of interfacial corrosion on joint integrity. The investigation of this problem is unique in nature as it covers the challenges of installation (inadequately tightened bolt) and operational (torque loss and corrosion) period of the structure. Figure 1-1 shows the schematic for the above-stated hypothesis.

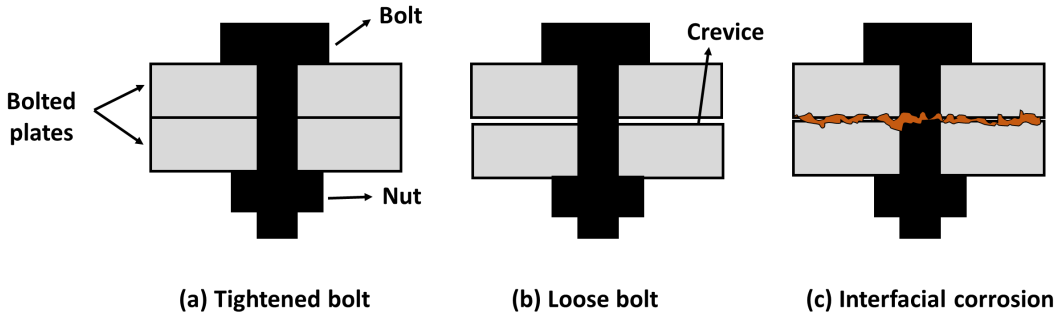

Figure 1- 1: Schematic showing interfacial condition for (a) an adequately tightened bolt; (b) loose bolt and (c) interfacial corrosion between the two plates

The key objectives of this thesis are as follows:

1) Investigation of the correlation between bolt torque and interfacial corrosion.
2) To develop a baseline free technique to estimate the quality of interfacial contact.
3) To monitor interfacial corrosion using a wide range of guided wave modes.
4) To monitor joints using potentially non-contact and automated techniques.

1.3 Thesis Outline

This thesis has been written in a hybrid manner. It consists of two published journal articles as Chapter 3 (Shah et al., 2019) and Chapter 4 (Shah et al., 2020) whereas the remaining are the supporting chapters. The thesis report original findings on joint monitoring for torque loss and corrosive conditions using guided ultrasonic wave-based technique. A brief description of the thesis outline is as follows:

Chapter 1 **Introduction** presents the motivation behind this dissertation work followed by a brief on existing gaps in the available literature. This chapter further provided the thesis statement and summarizes the layout of the investigation.

Chapter 2 **Literature Review** presents a detailed literature review tracing the progress in ultrasonic wave based investigations on bolted joints. This chapter layout the fundamental principles of guided wave monitoring followed by a discussion on existing experimental and numerical studies. It highlights the novelty and limitations of various studies. Finally, it outlines the existing gaps in the available literature and unveils a possible direction for future research.

Chapter 3 **Ultrasonic monitoring of corroding bolted joints** is a published work that investigates the correlation between the bolt torque and corrosion damage in steel plate joints. The specimens tightened at different torque values are corroded using the accelerated corrosion technique. It is followed by simultaneous ultrasonic monitoring using a conventional pulser-receiver system. The chapter reports the effect of interfacial corrosion on the signal transmission across the bolted interface. This variation in the transmitted energy successfully traced different stages of corrosion and sketched a correlation between the bolt torque and interfacial corrosion. Tension tests showed that for a similar level of corrosion, loss in strength was dependent on the initial bolt torque provided.

Chapter 4 **Monitoring and Imaging of bolted steel plate joints using embedded piezoelectric patches** is a published work that reports a potentially automated and baseline free method to trace the loss of bolt torque. A series of surface-bonded piezoceramic patches are used to record the wave interaction with the bolted interface. This interaction is interpreted for a different level of bolt tightening using a newly developed imaging technique. The scattering of a propagating wave from the bolthole is presented as contact contours at the bolted interface. This approach is further validated on a double bolted specimen. It efficiently discerned the loosened bolt from the tightened one.

Chapter 5 **Monitoring of corroding steel bolted joints with embedded piezo patches** is the extension of chapter 3 with a more sophisticated experimental investigation. This chapter investigates the properties of unique Lamb modes existing in different regions of the bolted joint as a measure to monitor interfacial corrosion. It is found that the wave modes existing in the overlapped regions are sensitive to interfacial corrosion. It has been hypothesized that the rust formation at the interface alters the contact quality between the plates. It results in Lamb

mode conversion. These findings have been cross validated with a finite element numerical model. The outcomes established the potential of ultrasonic monitoring in tracing different stages of interfacial corrosion.

Chapter 6 **Monitoring of corroding bolted interface using Laser** is the extension of Chapter 5 work. A wide range of excitation frequency signals are used to investigate the interfacial corrosion. A preliminary investigation is conducted using the patch-based experimental setup. It is found that higher-order modes attenuate rapidly with the interfacial corrosion. However, piezoceramic patches struggled to generate high energy higher-order signals. Therefore, a class IV Nd: YAG laser has been used an alternative for the actuating patch. Laser can generate high energy stress waves in the specimen along with the simultaneous generation of a wide range of excitation frequencies. This approach also alleviates the contact requirement as in the case of piezoelectric transducers and patches. The new results cross validated the preliminary results. The overall contribution of this investigation is to expand the scopes of wave-based monitoring in joint corrosion. This laser-based system has the potential to investigate large scale structures.

Chapter 7 **Conclusion** summarises the key conclusion of each investigation (Chapter 3-6) and paves the path for future research based on this thesis.

References

Akinade, O., et al. (2015). Waste minimisation through deconstruction: A BIM based Deconstructability Assessment Score (BIM-DAS). *Resources, Conservation and Recycling, 105*, 167-176.

Chaki, S., et al. (2007). Combination of longitudinal and transverse ultrasonic waves for in situ control of the tightening of bolts.

Doebling, S., et al. (1998). A summary review of vibration-based damage identification methods. *Shock and vibration digest, 30*(2), 91-105.

Doyle, D., et al. (2010). Damage detection in bolted space structures. *Journal of Intelligent Material Systems and Structures, 21*(3), 251-264.

Grosse, C., et al. (2008). *Acoustic Emission Testing: Basics for Research, Applications in Civil Engineering* (1. Aufl. ed.). Berlin, Heidelberg: Berlin, Heidelberg: Springer-Verlag.

Murat, B., et al. (2016). Scattering of guided waves at delaminations in composite plates. *The Journal of the Acoustical Society of America, 139*(6), 3044-3052.

Nikravesh, S., et al. (2017). A review paper on looseness detection methods in bolted structures. *Latin American Journal of Solids and Structures, 14*(12), 2153-2176.

OECD. (2015). *Towards a Framework for the Governance of Infrastructure*. Retrieved from https://www.oecd.org/gov/budgeting/Towards-a-Framework-for-the-Governance-of-Infrastructure.pdf

Pahlavan, L., et al. (2018). Interaction of ultrasonic waves with partially-closed cracks in concrete structures. *Construction and Building Materials, 167*, 899-906.

Kaur, N., et al. (2019). Healing and simultaneous ultrasonic monitoring of cracks in concrete. *Materials Today Communications, 18*, 87-99. doi:https://doi.org/10.1016/j.mtcomm.2018.10.022

Panda, R., et al. (2017). Characterization of delamination-type damages in composite laminates using guided wave visualization and air-coupled ultrasound. *Structural Health Monitoring, 16*(2), 142-152.

Pickthall, T., et al. (2011). *Corrosion Monitoring Equipment, A Review of Application and Techniques.* Paper presented at the CORROSION 2011.

Raghavan, A. (2007). *Guided-wave structural health monitoring.*

Shah, J., et al. (2019). Ultrasonic monitoring of corroding bolted joints. *Engineering Failure Analysis, 102*, 7-19. doi:https://doi.org/10.1016/j.engfailanal.2019.04.016

Shah, J., et al. (2020). Monitoring and Imaging of Bolted Steel Plate Joints Using Ultrasonic Guided Waves. *Journal of Nondestructive Evaluation, Diagnostics and Prognostics of Engineering Systems, 4*(1). doi:10.1115/1.4047191

Sharma, S., et al. (2011). Monitoring corrosion in oxide and chloride environments using ultrasonic guided waves. *Journal of Materials in Civil Engineering, 23*(2), 207-211.

Sriramadasu, R., et al. (2019). Detection and assessment of pitting corrosion in rebars using scattering of ultrasonic guided waves. *NDT & E International, 101*, 53-61.

Verity, S., et al. (2018). *National State of the Assets*. Retrieved from https://cdn.alga.asn.au/wp-content/uploads/2018-National-State-of-the-Assests-1.pdf

Wang, T., et al. (2013). Review of bolted connection monitoring. *International Journal of Distributed Sensor Networks, 9*(12), 871213.

Yang, Y., et al. (2019). Bolted joint integrity monitoring with second harmonic generated by guided waves. *Structural Health Monitoring, 18*(1), 193-204.

Zhao, Y., et al. (2017). Generation mechanism of nonlinear ultrasonic Lamb waves in thin plates with randomly distributed micro-cracks. *Ultrasonics, 79*, 60-67.

Chapter: 2 Literature Review

Before diving into the concepts learnt from the available literature, a brief discussion on the fundamentals of wave-based monitoring has been presented. It covers the basic aspects of wave propagation in solid media. Some results from the published chapters of this thesis are also included in this chapter to create a smooth flow in the discussion.

2.1 Fundamentals of travelling wave-based monitoring

To monitor the internal condition of the structure, the stress waves are induced in the structure at the time of inspection. This is usually achieved through piezoelectric transducers, however, in advanced setup, high power lasers can also be used. These waves propagate in the structure and interact with it internally. Any change in the medium properties alter the wave characteristics and get encoded in the wave-medium interaction. Generally, waves travel in two modes: Bulk and Guided waves.

In the former mode, waves propagate mainly as pressure (P-wave) and shear (S-wave) waves as shown in Figure 2-1a. These can be interpreted as waves that encounter no structural boundaries and assumed to be travelling in an infinite media. Bulk wave is nondispersive and preferred for localized inspections. The repeated scanning is required during the inspection of a large-dimension structure; hence it makes it a time-consuming approach. However, in guided waves, boundaries play an important role in wave propagation. These waves can be favourably seen in the plate-like structures where boundaries are in proximity causing multiple reflections resulting in wave propagation as shown in Figure 2-1b. In plates, guided waves travel as a combination of various symmetric (S_n, n = 0, 1, 2,…) and antisymmetric (A_n, n = 0, 1, 2,…) modes as shown in Figure 2-1c. The existence of these modes depends on the excitation signal frequency and plate thickness. It is to be mentioned that there are many other ways of generating guided waves in non-plate like structures. The sole purpose of this discussion is to show the difference between bulk and guided wave propagation and not to get into details of wave generation as it can be learnt from any standard textbooks on wave propagation (Rose, 2014).

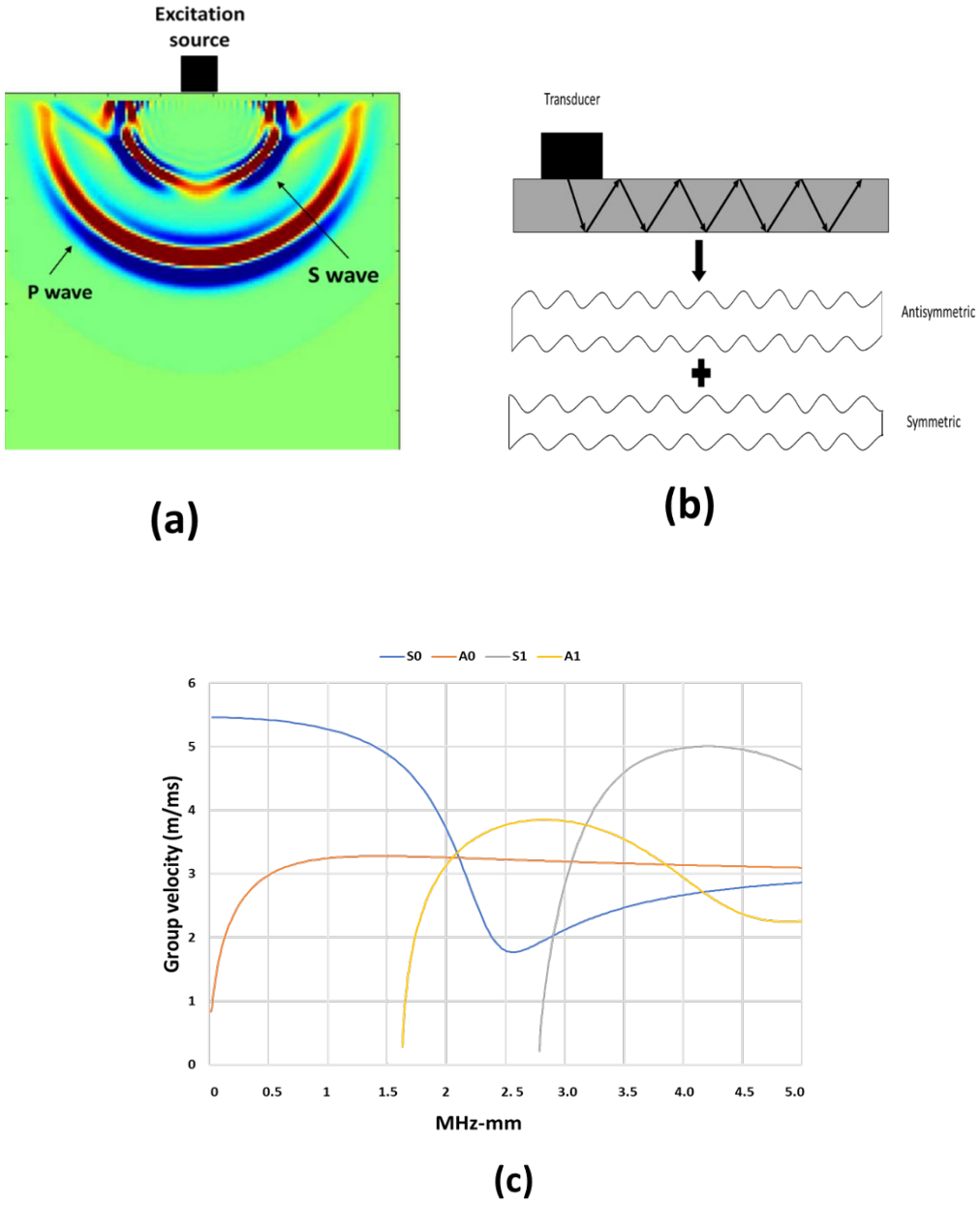

Figure 2- 1: Propagation of (b) bulk and (b) guided waves, and (c) guided wave modes existing in a steel plate

2.2 Modes of wave-based inspection

The ultrasonic inspection can be conducted only in the following two approaches:

2.2.1 Transmission

In the transmission-based investigation, separate transducers acting as an actuator and a receiver are placed on the two sides of the region of interest as shown in Figure 2-2a. The excited signal at the actuator interacts with the specimen while propagating along the specified path length. This interaction is recorded with the receiver. The change in the propagating medium's properties due to existing damage gets encoded in this interaction and can be

deciphered by monitoring the change in the wave's characteristics such as velocity, frequency, energy, phase, and time of flight.

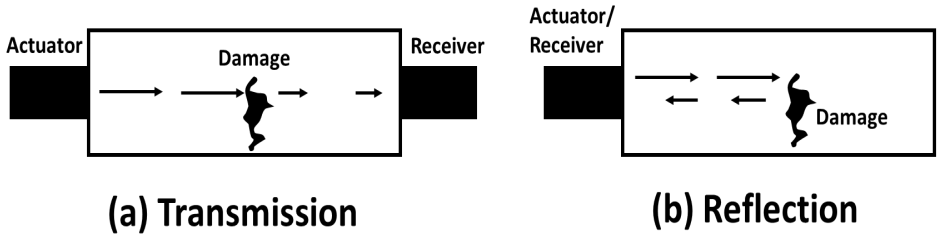

Figure 2- 2: Schematic showing configuration for inspection in (a) transmission and (b) reflection mode

2.2.2 Reflection

This mode of inspection is based on the principle that the existence of the damage in the wave propagation medium results in wave scattering due to acoustic impedance mismatch. The same transducer is used as the actuator and the receiver to record the interaction as shown in Figure 2-2b. The location of the reflection from the damage in a specimen can be traced by temporally locating the new peak in the recorded signal when compared to its healthy state counterpart. However, it requires the user to know the wave velocity in the medium for the location calculation.

2.3 Testing instruments for bolted joints

2.3.1 Types of transducers

In bolted plates, it is critical to choose the appropriate type of transducers depending on the inspection requirements. For an instant inspection, conventional transducers offer certain benefits, however, these are bulky and subjective to the quality of their contact with the specimen's surface. Therefore, for long-term and online inspections, a piezoelectric ceramic patch is a better alternative as it can be attached permanently to the specimen's surface. Being a cost-efficient option, these are one-time use and fragile if handled improperly. The laser as an actuator facilitates a significant advantage over transducers in terms of high energy output but it poses a radiation hazard to the user. Table 2-1 highlight some pros and cons of each type of transducer.

Table 2- 1: Pros and Cons of different types of transducers

Item	Pros	Cons

Piezoelectric transducer	Durable Requires minimal training	Coupling dependent Costly
Piezoelectric Ceramic patch	Low cost Can be permanently attached to the surface	Fragile One-time use Low power output
Class IV Laser	High energy output Non-contact system High precision	Radiation hazards Operator needs relevant license to operate No control over excitation frequency Costly

2.3.2 Experimental Setups

This section reviews some standard available ultrasonic testing set-ups which can be used for the inspection of bolted plates.

2.3.2.1 Pulser Receiver

It is a general-purpose ultrasonic testing setup. The pulser segment generates short bursts of electric pulses which are fed to the piezoelectric ultrasonic transducers (Taylor, 2006). Typically, conventional transducers are used which are manually coupled to the specimen with a multipurpose gel (Shah et al., 2019) whereas water (Sharma et al., 2015a) and air-coupled transducers (Grandia et al., 1995) are some other alternatives. The output from the transducer gets transmitted to the specimen in form of stress waves. This propagating wave is sensitive to change in the joint's properties e.g. changing clamping force with bolt torque loss. The reception segment of the system has the options for signal amplification and frequency filtering.

The advantage of using a Pulser-Receiver system is that different tools required for the signal processing such as amplifier and bandpass filters are inbuilt within the instrument. However, this system offers very little control over the shape of the excitation signal therefore making this system more suitable for energy attenuation (Wang et al., 2013) based measurements. For more sophisticated inspections where identification of multiple guided wave modes is required (Lowe et al., 2000a) e.g. Lamb wave modes in steel plates as shown in Figure 2-1c, it is critical to control the shape and the frequency bandwidth of the excited signal. The emphasis on

controlling the shape of the signal can be demonstrated through the following simulation results.

As per Figure 2-1c, two guided (A_0 and S_0) wave modes exist at 1.5 MHz-mm. Figure 2-3a shows that in the wave nature of recorded when a Hanning windowed shaped signal is used for the inspection. The propagating modes are easily discernible in the recorded signal whereas for a rectangular pulse as generated through a Pulser-Receiver system, these modes are non-distinctive (Figure 2-3b). This situation gets even more complicated as the number of modes coexisting at the same excitation frequency increases. Hence, it is advised to have better control over the generation of the input signal for sophisticated inspections.

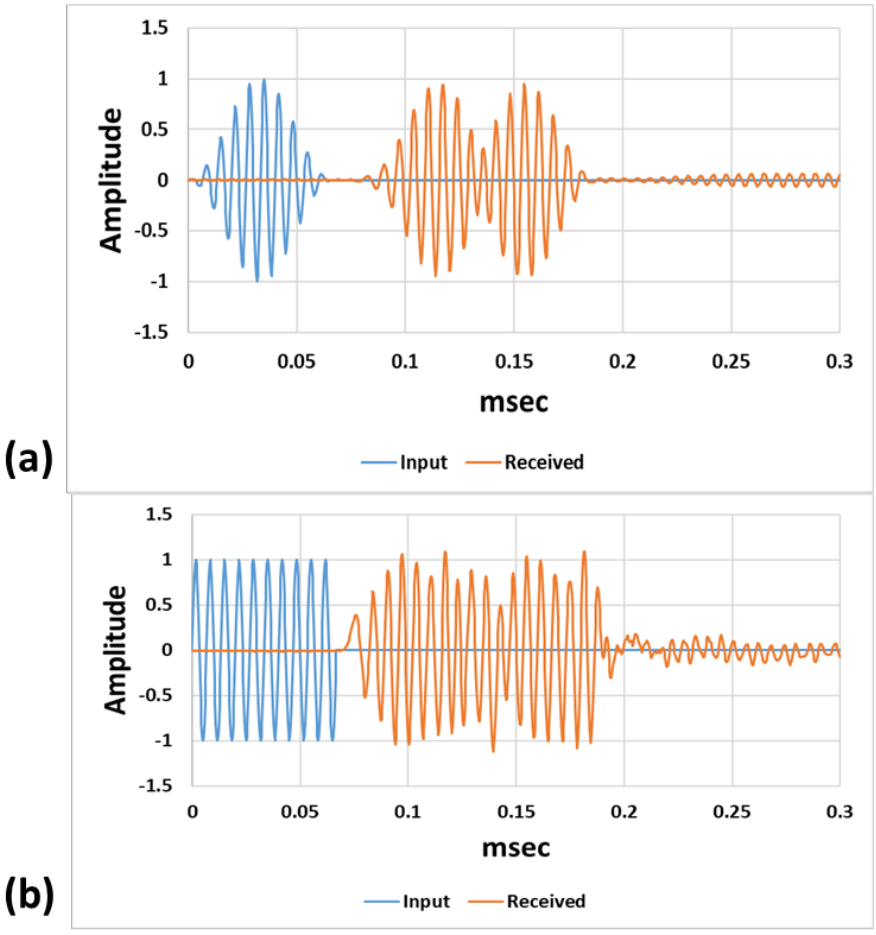

Figure 2- 3: Received signal for (a) Hanning windowed and (b) squared pulse excitation (B.P. Lowe M, 2013)

2.3.2.2 User specific setup

It is usually an assembled setup for better user control over inspection. The nature of the excited signal is controlled through an arbitrary wave function generator. The output of the

function generator is amplified using a power amplifier before being fed to the actuator. Piezoelectric patches are generally used as the actuators and receivers. This system usually does not require amplification at the receiver end. Figure 2-4 shows a typical assembly required for the inspection of bolted plates. The higher control over the input signal shape makes this setup suitable for multiple mode inspection.

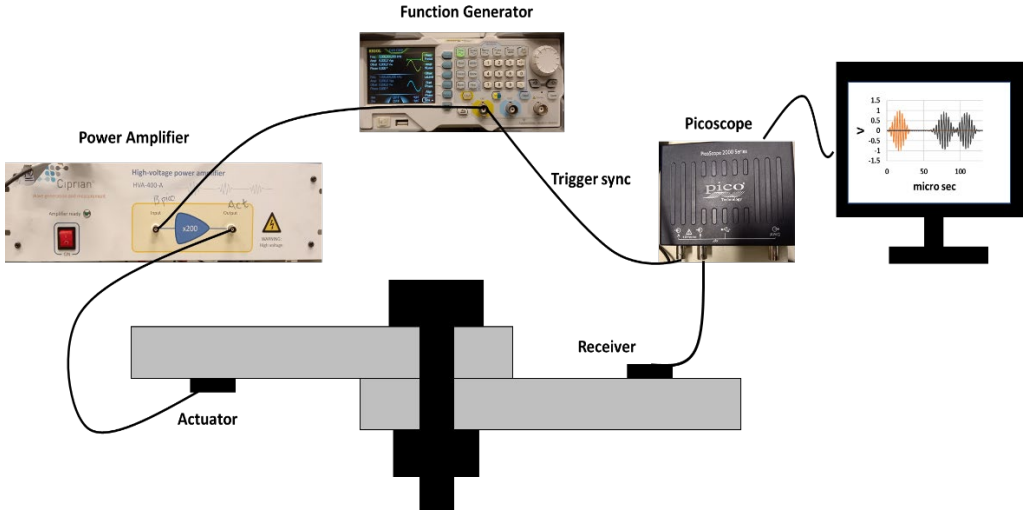

Figure 2- 4: Schematic for an assembled ultrasonic set-up

2.3.2.3 Noncontact setup

Transducer based actuation faces limitation in the inspection of large structures due to their low energy output. A class IV Laser can generate waves having up to ~1 Joule energy. These waves can travel over longer distances alleviating the signal attenuation problem even in highly dispersive media. It also eliminates the coupling requirements as in the case of conventional transducers. The principle at which laser-based excitation works is called Laser Ablation as shown in Figure 2-5.

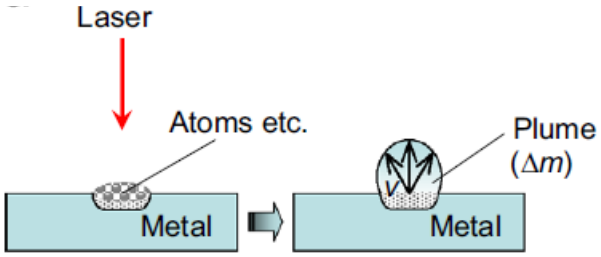

Figure 2- 5: Laser Ablation process (Huda et al., 2013)

When the laser beam hits the specimen, the local increase in the temperature at the point of excitation results in the generation of high-temperature plasma. This is followed by a large number of particles leaving the metal surface. Each particle has a certain momentum

associated to it and over a short period of time, laser-based impulse generates stress waves in the medium. This type of excitation produces a large bandwidth of frequencies and is useful for the simultaneous monitoring of a wide range of modes with changing material properties. Laser-based system can also be used as a receiver in form of laser vibrometers. Vibrometers work on the principle of beam interferometry (Staszewski et al., 2004). This instrument is capable of measuring picometers level vibrations.

2.4 Ultrasonic testing for bolt loosening

The integrity of a bolted joint depends on the contact quality between the bolted elements. However, the loss of bolt torque is inevitable due to structural vibrations and environmental factors such as corrosion. The change in torque can be correlated with the bolt load (Atta et al., 2019; Chakherlou et al., 2011) which is the controlling factor for the contact quality between the bolted plates. A travelling waves' properties are sensitive to the changes in the joint's condition. Therefore, the variation in the bolt torque can be established either by monitoring either the bolt's properties or the contact quality between the plates.

2.4.1 Monitoring through the bolt

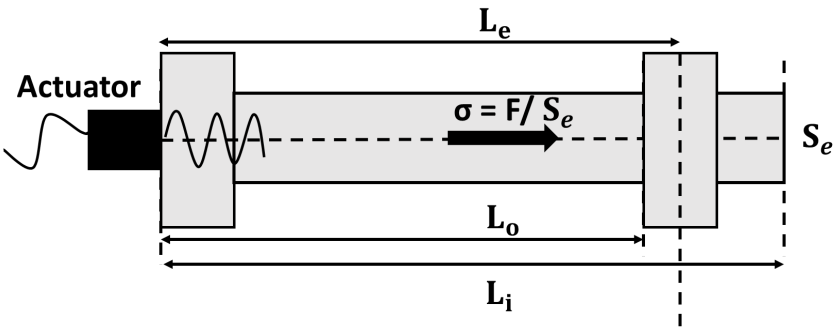

Figure 2- 6: Wave propagation in bolt

Figure 2-6 shows the effect of the bolt load (F; function of bolt torque) on the bolt's geometry. The corresponding axial stresses (σ) in the bolt results in the change in its effective length L_e. The measurement of these internal stresses is challenging without damaging the bolt like in the case of a strain gauge (Ahn et al., 2016). However, by using a propagating ultrasonic wave in the bolt, the stresses can be estimated from the wave-bolt interaction. It has been done by measuring the wave velocity (Chaki et al., 2007; Jhang et al., 2006) which is sensitive to the local stresses in the bolt. Hence, the variation in the wave velocity can give an estimate of the changing bolt torque condition. Equation 2-1 shows the relationship between the ultrasonic wave velocity and axial stress.

$$C = C_o(1 - \beta\sigma) \tag{2-1}$$

Where C and C_o are the wave velocities in bolt's stressed and unstressed condition whereas, β is the ratio of linear and nonlinear elastic constants and σ is the axial stress corresponding to the load (F). Figure 2-7 shows the result of an experimental study conducted by Jhang et al. (Jhang et al., 2006) on a high-tension bolt. They demonstrated that a linear decline in the wave velocity is observed for an increasing axial stress as expected from equation 2-1.

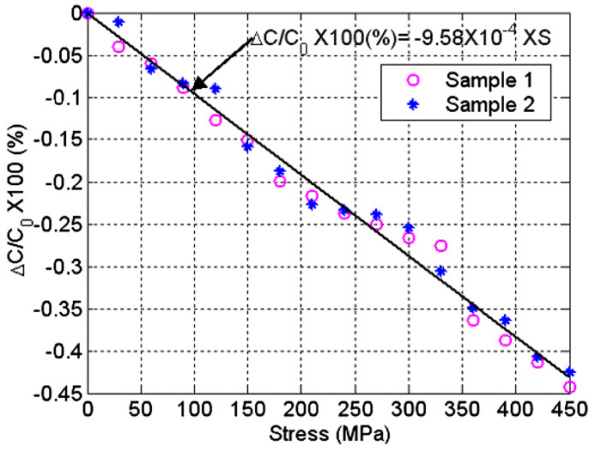

Figure 2- 7: Change of Ultrasonic velocity vs applied stress (Jhang et al., 2006)

Typically, a wave velocity-based inspection relies on the variation of the longitudinal wave velocity to estimate the bolt torque (SUDA et al., 1992; Yasui et al., 1999b). It requires calibration of the equipment for the unloaded bolt condition which makes the technique impractical to implement if the information is unavailable. This shortcoming has been improved by using the ratio of the time of flights of transverse (t_T) and longitudinal (t_L) waves in the bolt as a measure of changing bolt torque (Chaki et al., 2007). Equation 2-2 shows the correlation of this ratio and the clamping force. This method does not require any information about the unloaded bolt, hence is applicable at any instant of joint inspection.

$$\frac{T_T^\sigma}{t_L^\sigma} \cong \frac{V_L^o}{V_T^o}\left[1 - \frac{L_e}{L_i}(A_T - A_T)\frac{F}{S_e}\right] \tag{2-2}$$

Here V_L^o and V_T^o represent longitudinal and transverse wave velocities in the material and can be calculated using Lame's parameters (Chaki et al., 2007); L_e and L_i are the effective and total length of the bolt in loaded condition and As are acoustoelastic constants for the material.

It can be argued that in a real situation, change in the localized stress can be insignificant during torque loss, therefore it requires high precision in time of flight measurements to draw

any conclusion about the torque. Bolt as a waveguide may also face a unique problem in placing the actuator on a damaged bolt head surface as expected in case of bolt head corrosion (Kim et al., 2016a; Shah et al., 2019). A significant cost can also impact the inspection in the case of a multi bolt structure as monitoring individual bolt is a tedious task. These challenges limit the use of bolts as a waveguide in bolted structures.

2.4.2 Monitoring through the plate

The contact between two bolted plates deteriorates with the torque loss. Plate as a wave propagation medium supports several guided wave modes existing at different excitation frequencies (Rose, 2014). These modes have unique group velocity and attenuation properties. Hence, each mode may interact differently with the bolted interface. The monitoring through the plate also eliminates the need of inspecting individual bolts in a multi bolt structure. The following simplified contact theories can be used to demonstrate the interrelation between the bolt torque and the contact between the plates.

2.4.2.1 Contact theory

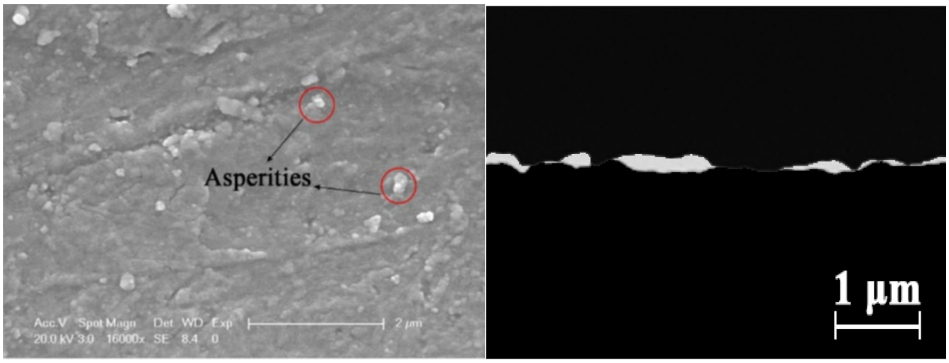

Figure 2- 8: (a) SEM image of a steel plate showing presence of asperities and (b) rough contact surface between the bolted plates (Zhang et al., 2017)

Figure 2-8a shows the scanning electron microscope images of a plate's surface and when two plates are in contact. It shows that at the microscopic level, the plate's surface is not perfectly smooth due to the presence of asperities. When put together, interfacial gaps can be seen between the plates (Figure 2-8b). It can be argued the true contact area between the two plate surfaces is always less than the nominal contact area. For plates in contact, the only contact is at the contacting tips of these asperities. When bolted together, the nominal contact area increases with the flattening of these asperities. Referring to the nature of the contact pressure provided by the bolt, the bolted interface has a variable contact profile which is highest near

the bolt while gradually fading for the regions away from the bolt. The true and the nominal contact area tend to converge only for adhesively bonded plates. The relation between the applied load and the area of contact can be explained with reference to the sinusoidal wavy surface model (Gao et al., 2006; Yang et al., 2006a) and Hertz contact theory (Johnson et al., 1987) .

2.4.2.2 Sine model

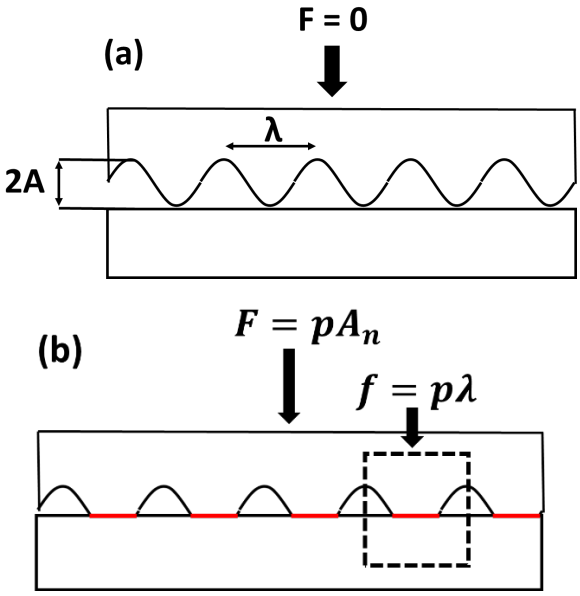

Figure 2- 9: Sinusoidal surface profile for (a) unloaded and (b) loaded condition

This model assumes the sinusoidal profile of the plate's surface as shown in Figure 2-9a. For simplification, it only considers the elastic deformation of the surface under the constraint that the amplitude (A) is smaller than the wavelength (λ). Using classical microcontact theory, plates are considered to have nil true contact area for zero mechanical load. As the load increases, the true contact area starts developing as shown in Figure 2-9b. The load experienced by an asperity (f) and the curvature (k) of the sine curve are given by the following equations (2-3 and 2-4) (Yang et al., 2006a):

$$f = p\lambda \tag{2-3}$$

$$k = \frac{4\pi^2 A}{\lambda} \tag{2-4}$$

2.4.2.3 Hertz theory

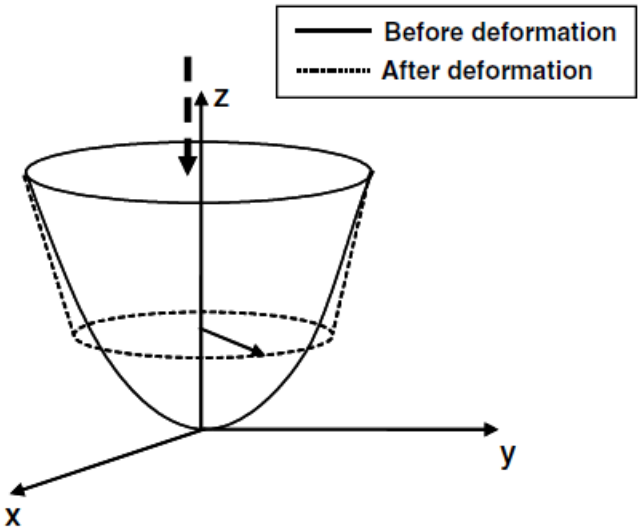

Figure 2- 10: *Undeformed and deformed geometry of a contact asperity (Yang et al., 2006a)*

This theory establishes the relation between the contact area and the applied load. Figure 2-10 shows the undeformed and deformed geometry of a circular asperity. The correlation between the geometric parameters and the contact load can be presented as equation 5 using Hertz theory:

$$f = \frac{\pi r^2 Ek}{4} \tag{2-5}$$

Here r and E denote the radius of the contact and Young's modulus of the plate material. Therefore, by using the Hertz equation for a sinusoidal surface profile, the relationship between the true contact area and the contact pressure can be summarized in the following equations 2-6 to 2-8.

$$\frac{A_t}{A_n} = 2\pi\sqrt{\frac{p}{p_o}} \tag{2-6}$$

$$\frac{A_t}{A_n} = \frac{2r}{\lambda} \tag{2-7}$$

$$p_o = \frac{\pi EA}{\lambda} \tag{2-8}$$

Here, A_t and A_n represents the true and nominal contact areas and p_o denotes the maximum Hertzian pressure. Within the limit of p_o, A_T is proportional to the square root of the pressure applied to the contact surface (Yang et al., 2006b). However, beyond this limit, the solution for the true contact diverges from the obtained solution and tend to reach the nominal contact value. This information can be exploited to determine bolt torque levels in a joint.

2.5 Different wave feature-based joint monitoring methods

The following sections reviews different methods to monitor the bolt torque using plate as a waveguide.

2.5.1 Wave attenuation

Figure 2-11a describes the effect of varying true contact on the transmission of the ultrasonic wave. At lower torque levels, the partial contact between the plates due to asperities results in poor transmission of ultrasonic waves between the two plates (Shah et al., 2019; Wang et al., 2013). However, as the true contact increases with the increase in torque as discussed in the previous, a higher fraction of the ultrasonic wave gets transmitted to the other plate. Figure 2-11b shows the experimental observation of the transmitted energy (E) between two plates obtained through equation 2-9 (Wang et al., 2013).

$$E = \frac{2\pi}{\omega_s} \sum_{t=t_s}^{t=t_f} V[t]^2, \tag{2-9}$$

Here, V is the received signal amplitude in the given time window $[t_i, t_f]$ and ω_s is the sampling frequency.

The initial increase in the energy with the applied torque can be interpreted as the development of new contacts with the flattening of asperities on the plate surface. The saturation in the energy curve at higher torque values represents the conditions when the maximum contact has been achieved by tightening the bolt manually without damaging the plates.

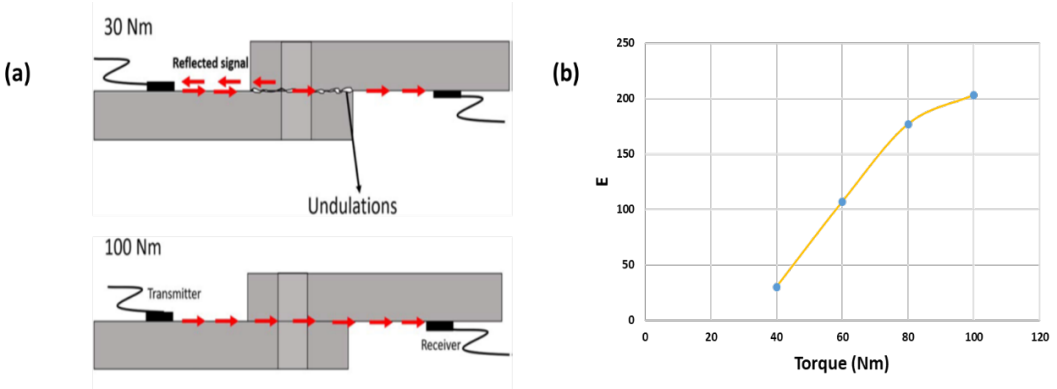

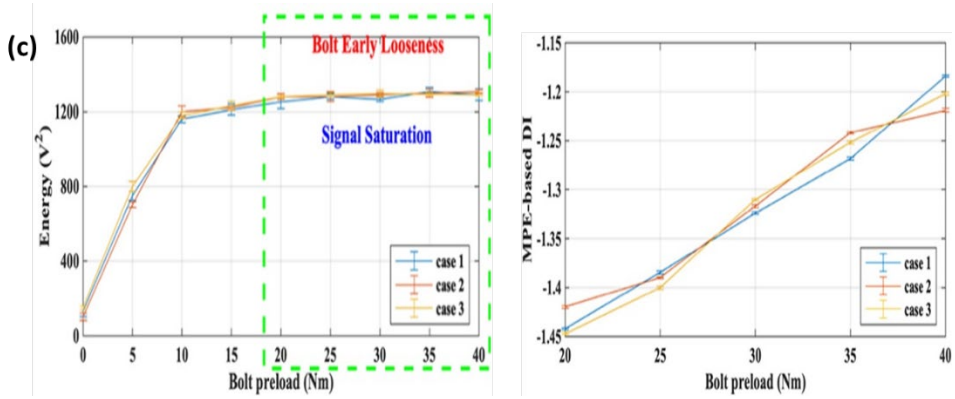

Figure 2- 11: (a) Schematic showing wave propagation in loosely tightened and fully tightened plates (b) Experimental results showing energy transmission vs bolt torque (Shah et al., 2020) and (c) variation of energy (left) and entropy based damage index (right) with bolt torque (Wang et al., 2020)

The saturation condition at higher torques makes this monitoring method suitable only for detection of higher torque loss conditions. Wang et al (Wang et al., 2020; Wang et al., 2019) reported an entropy-based damaged index to eliminate the saturation problem with energy calculation as shown in Figures 2-11c and 2-11d. This technique has the potential to track the initial stages of torque loss. However, this method needs to be explored further.

2.5.2 Frequency monitoring

The frequency of the propagating wave is another wave characteristic that is sensitive to the changing interfacial conditions. Like the variation in the transmitted energy with changing bolt torque, it is tempting to assume that the strength of the fundamental frequency goes down with the bolt loosening. However, studies have found this hypothesis true only for significant torque loss conditions. The wave interaction with the bolted interface is relatively complex for the initial stages of torque loss. It can be explained further with the analogy of the contact acoustic nonlinearity (CAN) phenomenon in the case of a microcrack (Jingpin et al., 2017; Zhao et al., 2016).

2.5.2.1 Contact Acoustic Nonlinearity

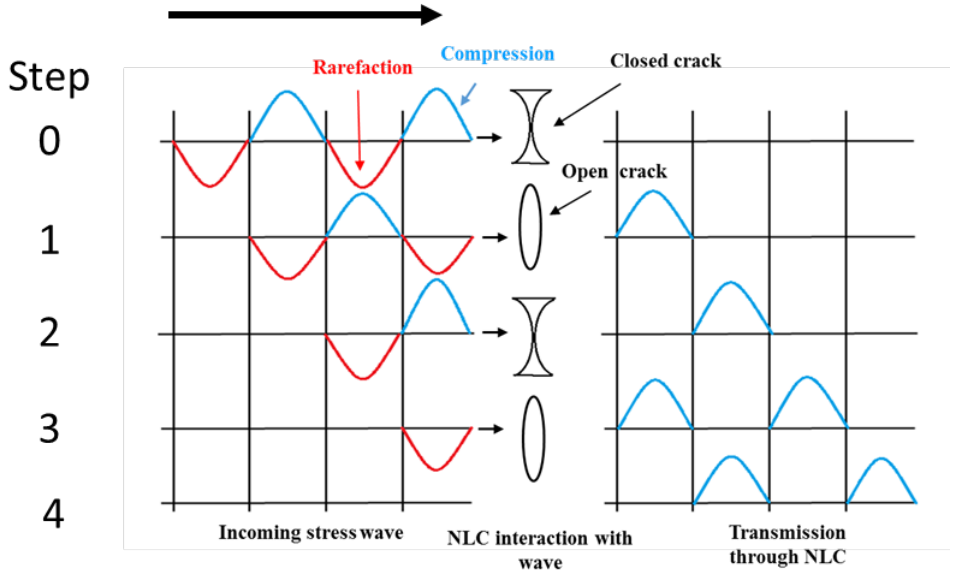

Figure 2- 12: Contact acoustic nonlinearity in a microcracks

Figure 2-12 shows the response of microcrack faces to the rarefaction and compression phase of a propagating stress wave. The crack faces come in contact during the compression phase of the stress wave whereas they separate during the rarefaction phase. This opening and the closing response of the microcrack to the propagating stress wave leads to the selective transmission of the compressive phase of the wave. This nonlinear response to the interacting wave can be illustrated using a 1D system. Assuming quadratic nonlinearity, response (R) of the system with respect to the input stress wave (S) can be written as equation 2-10:

$$R(S) = A\,S + B\,S^2 \tag{2-10}$$

Where A and B are the coefficients of the linear and the nonlinear terms. For a monochromatic stress wave, $S = a \sin(\omega t)$, R can be written as the following equations

$$R(S) = Aa \sin(\omega t) + Ba^2 \sin^2(\omega t) \tag{2-11}$$

or

$$R(S) = \frac{1}{2} Ba^2 + Aa \sin(\omega t) - \frac{1}{2} Ba^2 \cos(2\omega t) \tag{2-12}$$

Equation 2-12 has a 2ω component that is the first higher harmonic. Similarly, for an nth order nonlinearity, n-1 higher harmonics would be generated. Nonlinearity also leads to frequency modulation when an incident stress wave has a combination of two or more frequencies. For an incident wave containing two sinusoidal frequencies as $S = a \sin(\omega_1 t) + b \sin(\omega_2 t)$ on a system with quadratic nonlinearity as in equation 2-10, the response becomes:

$$R(S) = A\left(a\sin(\omega_1 t) + b\sin(\omega_2 t)\right) + \frac{1}{2}B(a^2 + b^2)\left(1 - (\cos(2\omega_1 t) + \cos(2\omega_2 t))\right) + Bab(\cos\left((\omega_1 - \omega_2)t\right) - \cos((\omega_1 + \omega_2)t) \quad (2\text{-}13)$$

The structural response of equation 2-13 contains the modulated frequency components $\omega_1 \pm \omega_2$ along with $2\omega_1$ and $2\omega_2$ components. Therefore, by spotting the side lobes around the higher frequency $\omega_1 \pm \omega_2$ the nonlinear phenomenon can be observed. However, it is important to choose a suitable ratio of the two frequencies so that the modulated and the higher frequency components distinctly manifested.

For a bolted joint, the CAN phenomenon can be expected to occur during torque loss (Amerini et al., 2011; Yang et al., 2019; Zhang et al., 2018). Due to the development of interfacial gaps, plates' surfaces interact during the compression phase of the propagating wave and separates in the rarefaction phase. This results in a clapping-like phenomenon as explained in the case of a microcrack. However, it is a non-trivial task to use the same numerical demonstration for higher-order systems. Therefore, it is critical to develop numerical models to capture torque loss related nonlinearity.

2.5.2.2 Numerical Modelling for bolted joints

To study the generation of CAN in bolted joints, it is crucial to understand the interaction of propagating waves with the changing interfacial properties which in turn are controlled by the applied torque. Hence, to achieve a realistic insight, it is mandatory to include the bolt preload and surface interaction properties in the numerical model. Finite element models (Atta et al., 2019; Shen et al., 2013; Yang et al., 2019) have been widely used to study wave interaction in bolted joints. Figure 2-13 shows a standard technique for bolt preloading where the internal surface of the bolt shank (same plane as the plate-plate interface) is prestressed with a preload (F) calculated through equation 2-14 (Atta et al., 2019).

$$F = \frac{T}{k.D} \quad (2\text{-}14)$$

Here F is the bolt preload corresponding to the applied torque (T), k is the coefficient of T and D is the nominal diameter of the bolt.

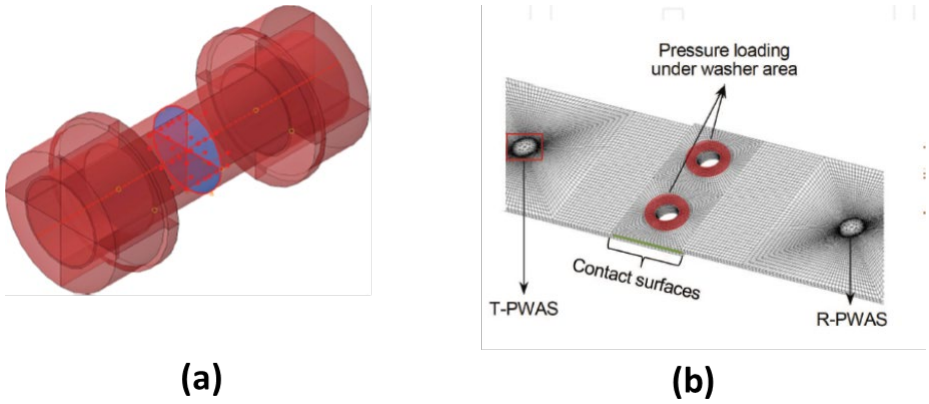

Figure 2- 13: Numerical model showing (a) bolt preloading (Krolo et al., 2016) and (b) its stress distribution around the bolt hole (Shen et al., 2013)

Once the bolt is preloaded appropriately, the next stage is to model the contact between the plates. It is challenging to exactly model the rough profile of the asperities at the plate's surface. Different techniques were adapted over the years to model the contact between bolted plates. Bao et al. (Bao et al., 2013) introduced the contact elements in their finite element model while Parvasi et al. (Parvasi et al., 2016) generated a rough surface profile by randomly adjusting the node positions. However, Clayton (Clayton et al., 2008) avoided any contact modelling to reduce the computation time. Irrespective of the complexity of the model, each technique suffers some drawbacks such as higher computational time and low convergence between experimental and numerical results. Therefore, it is crucial to use the appropriate technique depending on the user's needs.

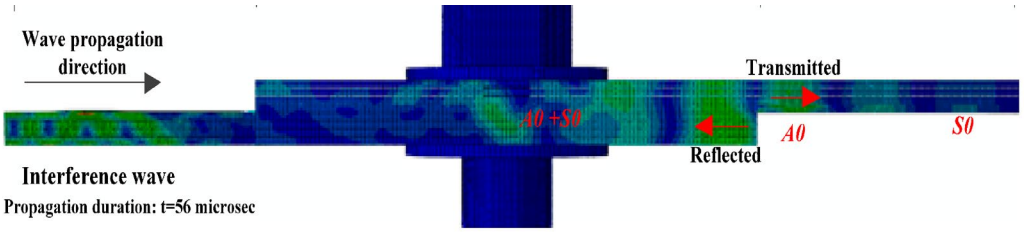

Figure 2- 14: Wave propagation in a numerical model (B. Yang et al., 2017)

The last stage is to model the wave propagation across the bolted interface as shown in Figure 2-14. Transient dynamic analysis is typically used to record the CAN-associated features in the recorded signals (Yang et al., 2017).

2.5.2.3 CAN in bolted joints

Figure 2-15 shows the experimental results obtained for a loosely tightened bolted joint. The presence of higher harmonics in the received signal indicates the CAN phenomenon occurring at the interface during wave propagation.

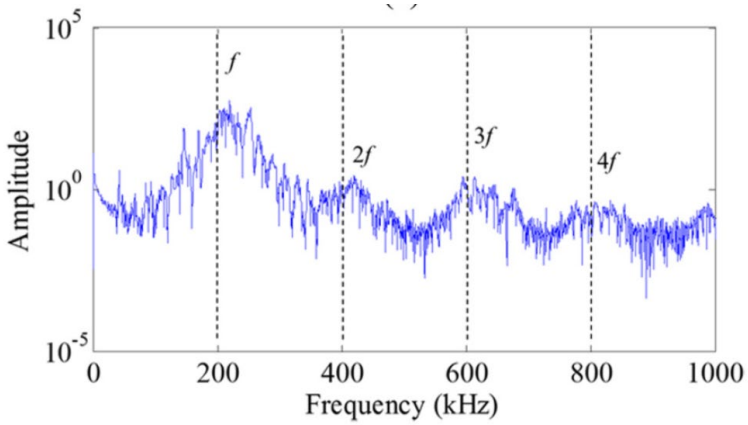

Figure 2- 15: Existence of higher harmonics in a loosened bolted joint (Yang et al., 2019)

Further estimation of the bolt torque has been carried out by adding a lower frequency excitation to the input signal. Figure 2-16a shows the anticipated response of a bolted joint for a mixed frequency excitation in its tightened and the loosened state. For poor contact between the plates, frequency modulation is expected in addition to the generation of higher harmonics as expected from equation 13. Conventionally, the natural frequency of the structure is chosen as the lower frequency. Electromechanical shaker is generally used to generate low-frequency vibrations (Zhang et al., 2017). On real structures, the use of a shaker may not be a feasible solution, therefore, a low-cost piezoelectric patch (Zhao et al., 2020b) can be an alternative for generating lower frequencies. Figure 2-16b shows the existence of modulated components near the higher frequency for loosened bolt conditions.

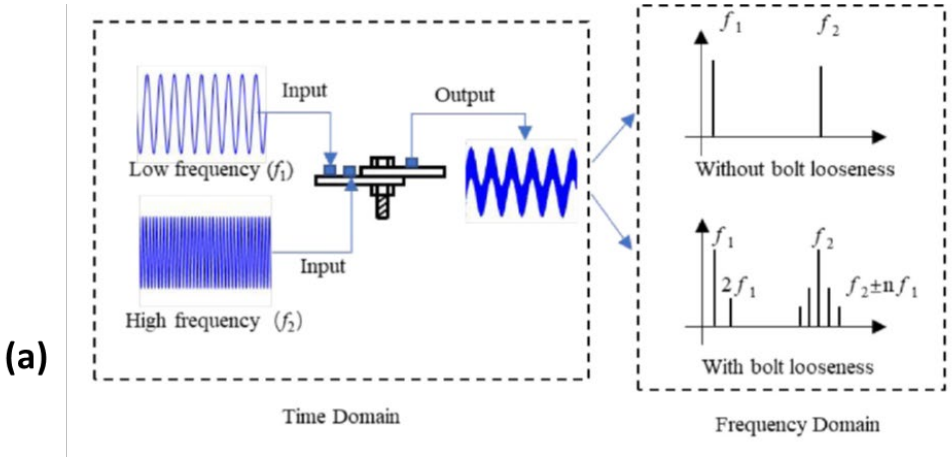

(b)

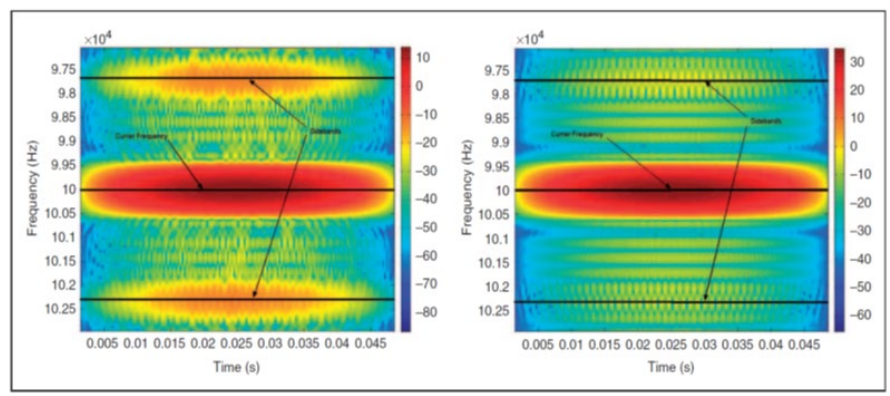

Figure 2- 16: (a) Principle of nonlinear vibroacoustic modulation (Zhao et al., 2020b) and (b) Experimental results showing the presence of modulated frequency components in a joint in its loosened and tightened bolt condition (Amerini et al., 2011)

2.5.2.4 Neglecting the aspect of instrument nonlinearity

Typically, every ultrasonic-based inspection involves the use of high power amplifiers (Shah et al., 2020; Wang et al., 2017) in the experimental setup. Amplifiers are notoriously infamous to introduce instrument related nonlinearity in the recorded signal (Anttila et al., 2013; Korpi et al., 2014). The strength of damage torque loss induced nonlinear features is relatively weaker and it can be challenging to separate them from instrumental nonlinearity. It is critical to address instrument nonlinearities to establish the outcomes of non-destructive inspection. However, limited studies have addressed the challenges of system nonlinearity (Kimoto et al., 2015).

2.6 Eliminating baseline comparison through Ultrasound imaging

In order to identify the changes in the bolt torque, all the studies mentioned above require comparison with the healthy state of the bolted joint. Hence, it may face certain limitations at the time of inspection in the absence of pristine joint data. Like ultrasound-based imaging in the medical field, imaging of joints can be proven useful to eliminate the need of baseline comparison. Imaging is based on the principle of wave reflection from the regions offering acoustic impedance mismatch. In a bolted plate, a bolt hole is a source of significant wave scattering due to different acoustic impedance of air inside it. Figure 2-17 shows the location of the bolt hole obtained from the reflected signals recorded through a series of piezoelectric patches used as actuators and receivers in pairs. Patches were used as the actuator and the receiver in pairs. The recorded signals were presented in B-scan plots which highlight the position of the bolt hole.

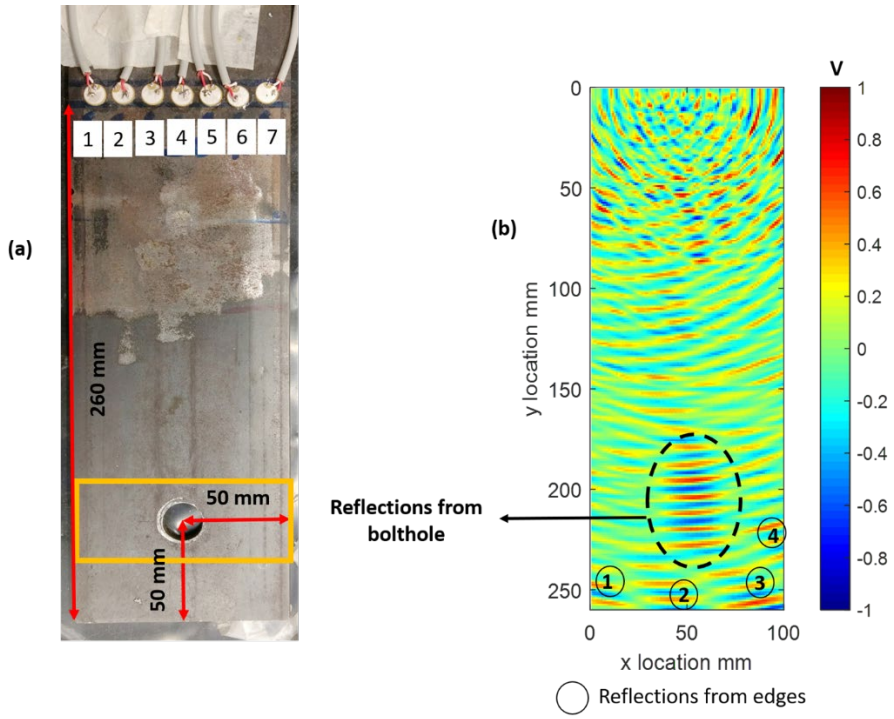

Figure 2- 17: Ultrasonic scan showing reflections from the bolt hole (Shah et al., 2020)

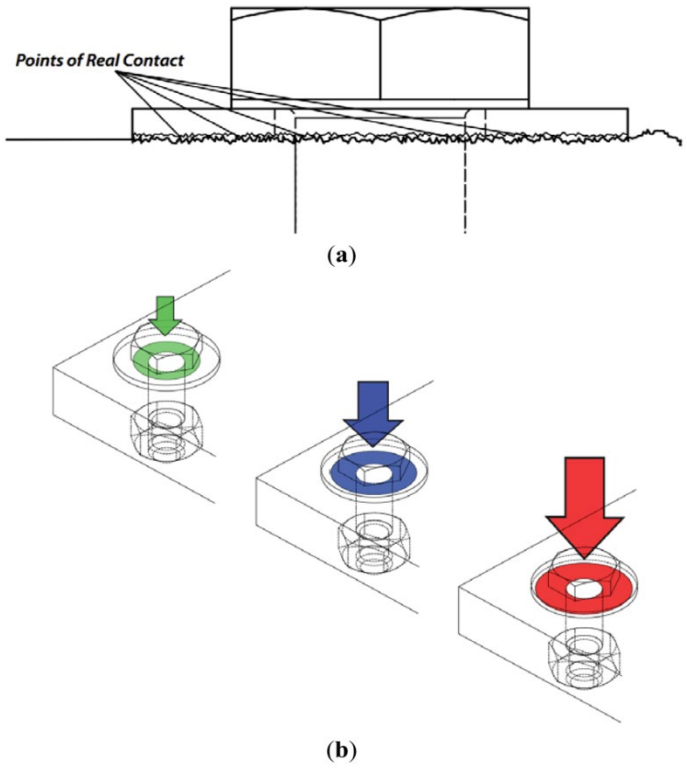

Figure 2- 18: (a) Undulation present at the washer and plate interface and (b) Growth in the contact area with the increasing bolt torque(Martinez et al., 2012)

Figure 2-18 shows a typical example of the growth of the contact region between two bolted elements (plate and a washer) at different stages of bolt tightening. For a loosened connection,

a propagating wave has a higher probability of interacting with the bolthole due to insufficient contact between the washer and the bolt. As the contact area increases at a higher torque, Martinez et al (Martinez et al., 2012) demonstrated that the reflection position will move away from the bolthole (towards the edges of the washer) denoting the growth of newer contact around the bolt hole.

Shah et al. (Shah et al., 2020) tested this hypothesis on relatively larger single bolt steel specimens and found that the contact between the washer and the plate saturates prematurely than the required bolt torque. However, they demonstrated that the contact between the plates grows gradually with the increased torque. Based on the reflected signal profile around the bolt hole, they generated contact contours using the imaging principle (Shah et al., 2020). Figure 2-19 shows that the contact was dominant near the bolt location at low torque values. However, a symmetrical lateral spread was observed around the bolt hole with the increased torque levels. This validates the generation of new contact zones away from the bolt hole. If interpreted properly, imaging techniques have the potential to determine the quality of contact between the bolted plates.

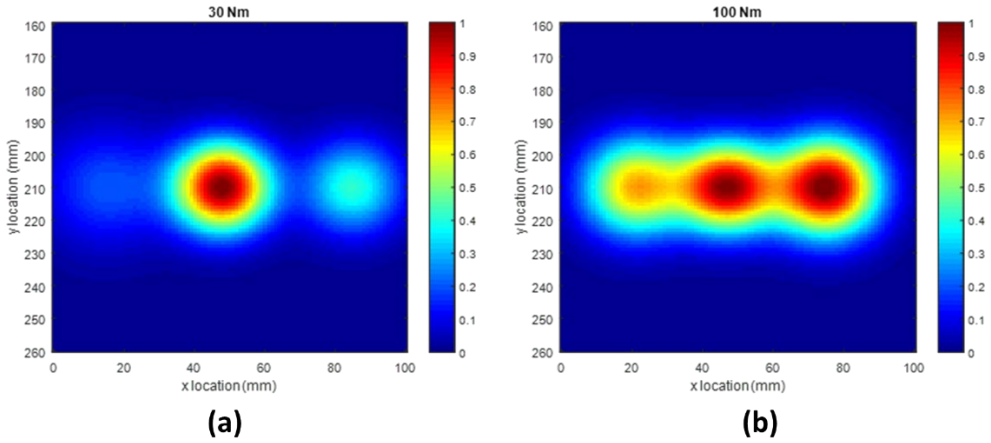

Figure 2- 19: Plots showing contact contours for a (a) loose (30 Nm) and (b) fully tightened (100 Nm) single bolt plates (Shah et al., 2020)

2.7 Challenges in monitoring multi bolt structures

A significant number of studies have been reported on single joint bolted plates. Based on the results reported, it can be stated that monitoring of wave parameters such as energy, frequency only establishes the presence of a loosened bolt in the structure. However, deciphering the location of the loosened bolt in a multi bolt structure is still an area that needs to be researched intensively through guided wave monitoring. The presence of unwanted reflections from the

boundaries and the plate interfaces further adds to the complexity of the signal interpretation. This paper reviews a few such works.

Zagarai et al. (Zagrai et al., 2010b; Zagrai et al., 2010) have exploited the phase shift to locate the faulty bolt in a satellite panel of 7 x 7 bolt matrix. The changes in local stresses during bolt loosening results in phase shift at the specific temporal location in the recorded signal. The occurrence of these shifts can be correlated with individual bolt locations if the propagation velocities of existing Lamb modes in the structure are known. Figure 2-20 shows one typical example of the phase shift obtained through the zero-crossing method.

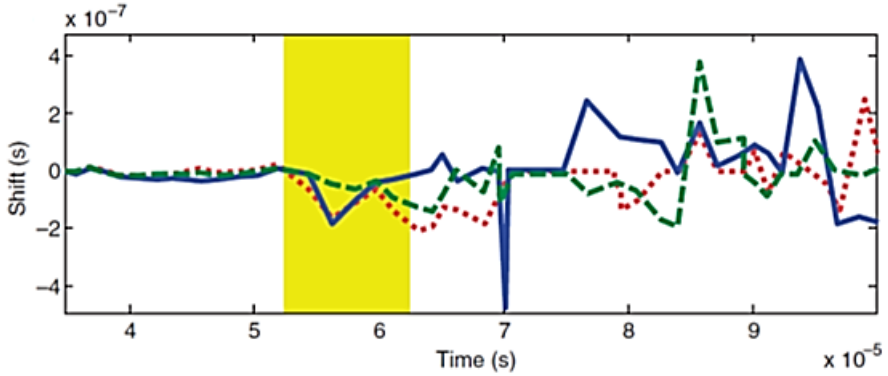

Figure 2- 20: Typical example of a phase shift due to bolt loosening (Zagrai et al., 2010b)

Fierro et al. (Fierro et al., 2017; Fierro et al., 2018) developed a damage resonance theory based on bolt-specific contact acoustic nonlinearity related frequency modulation properties. They identified frequency changes unique to individual bolt loosening in a four-bolt specimen. They have used the spectrum subtraction technique. In this process, each bolt was tightened at different levels and a mixed frequency signal was used. This subtraction technique was reported to be alleviate instrument related nonlinear features to a certain extent.

Recently, Shah et al. (Shah et al., 2020) expanded their imaging-based method to image the contact contours of a tightened (B1) and loosened bolt (B2) as shown in Figure 2-21. As discussed in section 2.6, B1 has contact contours laterally spread around the bolt hole location whereas B2 contours are localized only at the bolt location.

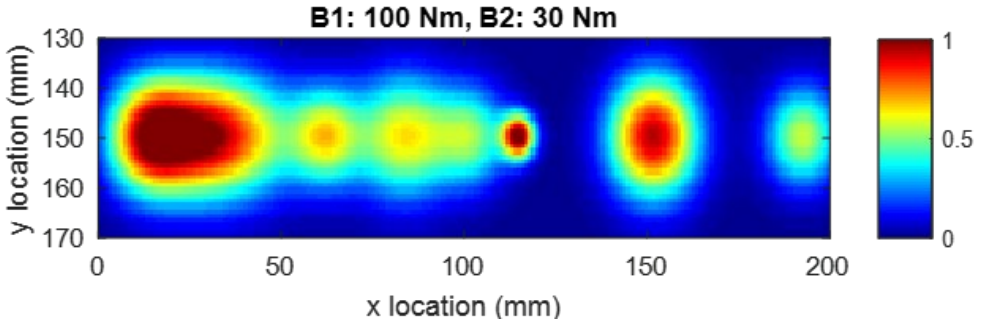

Figure 2- 21: Contact contours for a tightened (left; B1) and loose (right; B2) bolt (Shah et al., 2020)

The following section discusses the correlation between the bolt torque and interfacial corrosion damage. There is no explicit study reported which uses the guided wave technique to monitor bolt corrosion. This discussion is based on the published chapter of this thesis.

2.8 Correlation between the bolt torque and corrosion damage

Corrosion induced mass loss to the bolt and the plate leads to a reduction in the preload on the plate surface. This leads to the development of interfacial gaps between the plates. Such regions are the favourable sites for moisture retention followed by the rust formation. Since the interfacial contact is dependent on the bolt torque, a possible correlation between the torque and the nature of joint corrosion can exist. To our best knowledge, only this thesis has attempted to explore this area using ultrasonic monitoring. They inspected the bolted specimens tightened at different torque levels having different failure modes under corroding conditions achieved through accelerated corrosion (Yuan et al., 2007). The progression of corrosion at the interface was monitored through the transmission of ultrasonic wave across the interface with progressing corrosion. The authors have used a pulser receiver system for the inspection.

For a fully tightened bolt, a gradual rise in the transmitted energy was observed with initial mass loss in the bolted interface as shown in Figure 2-22a. It was hypothesized that even though the bolt was in fully tightened condition, at initial stages of mass loss calculated through Faraday's Law (Yalciner et al., 2012), rust filled the interfacial gaps making the transmission of the ultrasonic wave more effective. However, at advanced stages of mass loss, a similar decreasing trend in the transmitted energy was observed. It can be attributed to the low acoustic impedance of the rust. For loosely tightened joint, the increase in the transmitted energy was observed for a very short duration of mass loss (Figure 2-22b). It can be argued that since the interfacial gaps are relatively higher than the tightened counterpart, a certain level of mass loss was required to fill the interfacial gaps. It was found that for the same level

of mass loss, a fully tightened specimen lost ~35 % of load-bearing capacity whereas a loosely tightened specimen's load bearing capacity was unchanged (Shah et al., 2019).

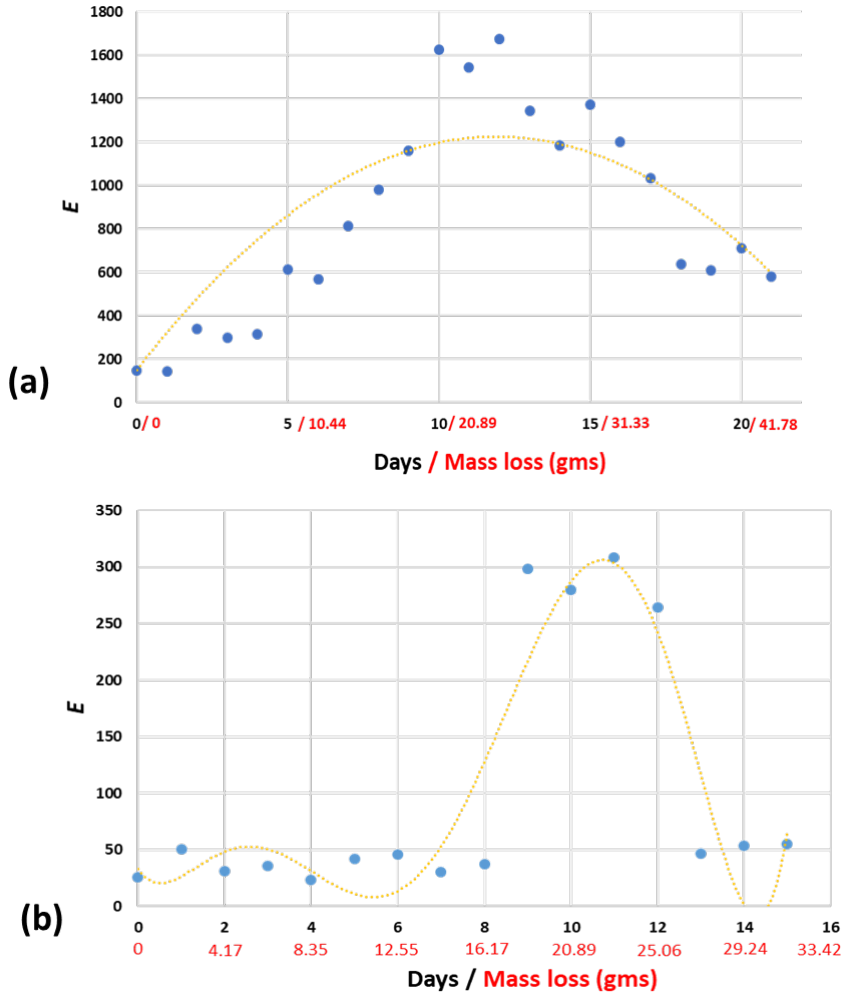

Figure 2- 22: (a): Variation in transmitted energy (E) at different stage of mass loss for (a) fully tightened and (b) loosely tightened bolted joint(Shah et al., 2019)

2.9 Signal processing

This section reviews the four most common signal processing techniques used for bolted joints.

2.9.1 Fourier Transform

The wave propagates in the plate in form of various symmetric and antisymmetric modes. With unique group velocities and attenuation properties, multiple modes can coexist at the same frequency. The identification of these modes in a recorded time signal can be a challenging task if their velocities are close to each other hence resulting in their overlapping in the recorded time signal. These modes may attenuate differently with the changing

interfacial condition of the bolted joint. Therefore, monitoring the attenuation of individual mode in the transmitted signal might not be achievable. However, in the frequency spectrum, the combined effect of attenuation in multiple modes can be monitored through the amplitude of the transmitted frequency. Hence, signal interpretation in the frequency domain can be useful. Equation 2-15 shows the relation for Discrete Fourier Transform (X_f) (Bracewell et al., 1986) of a sequence of x_n representing N successive samples x(nT) of the continuous-time signal x(T) which in this study is received signal.

$$X_f = \sum_{n=0}^{N-1} x_n W^{nf}, f = 0, 1, \ldots . N - 1 \quad (2\text{-}15)$$

where W is equal to $e^{-j2\pi/N}$

2.9.2 Short-time Fourier Transform

In Discrete Fourier transform, the temporal variation of the signal frequencies is lost. It only gives us the average of all temporally separated frequency peaks. Therefore, for a non-stationary and multi-mode signal, visualizing the recorded information on time and frequency axis plots can be useful to understand the variation of different modes over the recorded length of the signal. In short time Fourier transform (Durak et al., 2003), Fourier transform was performed over a short time window of the recorded signal. This is followed by plotting the variation of frequency components over the time length of the signal.

2.9.3 Acoustic moment

Acousto-ultrasonic parameters do not require the propagating signal to have a specific path. Common approaches such as pitch-catch and transmission methods are established to find the overt stages of bolt loosening whereas acousto-ultrasonic parameters can be used to identify initial stages of bolt loosening (Fierro et al., 2017). Acoustic moment (M) of nth order can be calculated through Energy Spectral Density (W) for each frequency (f) components in the signal as mentioned in equations 2-16 and 2-17.

$$W(f) = Y.conj(Y)/L \quad (2\text{-}16)$$

$$M_n = \int_0^{f_N} W(f) f^n df \quad (2\text{-}17)$$

Here, Y is the fast Fourier transform of the recorded signal and f_N is the Nyquist frequency. Fierro et al (Fierro et al., 2017) monitored the changes in the zeroth order acoustic moments at fundamental and higher harmonics to establish the bolt loosening in a multi bolt specimen. They calculated the acoustic moments for the individual frequency band as per the equation

$$M_f = \int_{f_l}^{f_h} W(f)df \tag{2-18}$$

where f_l and f_h are the lower and the upper bounds of the chosen frequency band.

2.9.4 Time reversal technique

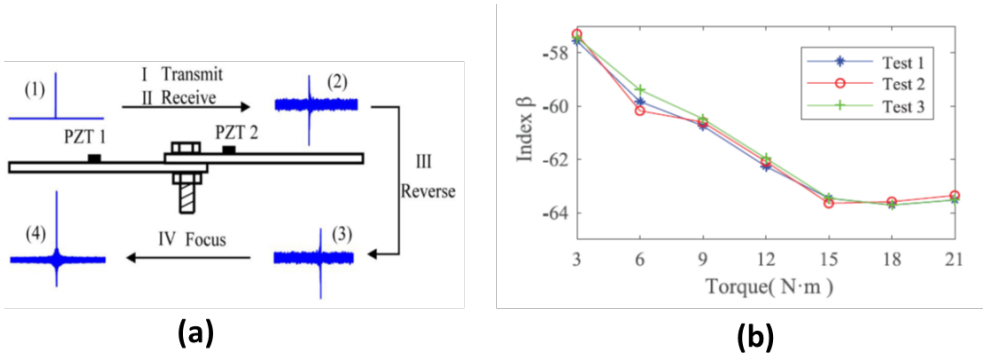

Figure 2- 23: (a) Principle of Time-reversal technique and (b) variation of damage index with bolt torque

This technique works on the principle of acoustic reciprocity i.e. the transmitted signal will maintain its characteristics if the position of the transmitter and the receiver is exchanged. Figure 2-23a shows the schematic for the ultrasonic investigation through the time reversal technique. In the first stage of inspection, PZT 1 is actuated with a pulse signal. This signal propagates across the bolted region and received on the other plate with PZT 2. The recorded signal is then reversed in the time domain. In the second stage of inspection, the role of PZT 1 and PZT 2 is reversed i.e. PZT 2 will act as an actuator and PZT 1 will serve as a receiver. The reversed signal is re-emitted into the specimen through PZT 2 and received through PZT 1. The characteristics of the received signal are used to evaluate the bolt tightness with temporal and spatial focusing techniques.

Summary and future recommendations

In the past two decades, a significant advancement in ultrasonic based monitoring of bolted joints has been made. Ultrasonic inspection has the potential to offer automated and non-invasive solutions for joint monitoring in its installation and operational period. Based on the requirement of the inspection, the health of a joint can be interpreted either by monitoring the condition of individual bolt or through the interfacial health of the bolted elements. Standard investigation includes the effect of bolt loosening on ultrasonic wave properties such as amplitude, phase and time of flight. Relatively advanced methods exploit the concept of

contact acoustic nonlinearity and have been reported to identify the initial stages of bolt loosening.

In recent years, newer studies have addressed the challenges in standard practices of joint monitoring. An entropy-based method has attempted to eliminate the energy saturation issues at high torque values. Imaging based techniques have been reported which has the potential to eliminate baseline comparison. Another study attempted to correlate the corrosion damage with bolt loosening conditions.

A major shortcoming is that most of the reported investigations are on single bolt specimens. The journey of finding an established technique applicable to monitor multi bolt structures still needs to be conquered. An ideal joint monitoring technique would be automated in nature, sensitive to minor changes in the bolt torque and can provide visual evidence of the faulty bolt in a multi bolt structure. All these factors can potentially increase the inspection frequency of the bolted structures.

References

Agarwala, V., et al. (2000). *Corrosion detection and monitoring-A review.* Paper presented at the CORROSION 2000.

Ahn, J., et al. (2016). Clamping force loss of high-strength bolts as a result of bolt head corrosion damage: Experimental research A. *Engineering Failure Analysis, 59*, 509-525.

Akinade, O., et al. (2015). Waste minimisation through deconstruction: A BIM based Deconstructability Assessment Score (BIM-DAS). *Resources, Conservation and Recycling, 105*, 167-176.

Amerini, F., et al. (2010). Detecting loosening/tightening of clamped structures using nonlinear vibration techniques. *Smart Materials and Structures, 19*(8), 085013.

Amerini, F., et al. (2011). Structural health monitoring of bolted joints using linear and nonlinear acoustic/ultrasound methods. *Structural health monitoring, 10*(6), 659-672.

Anttila, L., et al. (2013). *Cancellation of power amplifier induced nonlinear self-interference in full-duplex transceivers.* Paper presented at the 2013 Asilomar conference on signals, systems and computers.

Atta, M., et al. (2019). Prediction of failure stages for double lap joints using finite element analysis and artificial neural networks. *Engineering Failure Analysis, 97*, 242-257.

Bao, J., et al. (2013). *Linear and nonlinear finite element simulation of wave propagation through bolted lap joint*.

Beniwal, S., et al. (2015). Defect detection around rebars in concrete using focused ultrasound and reverse time migration. *Ultrasonics, 62*, 112-125.

Bickford, J. (2007). *Introduction to the Design and Behaviour of Bolted Joints*: Bpca Raton: CRC Press.

Board, N. (2008). Collapse of I-35W Highway Bridge, Minneapolis, Minnesota. Retrieved from https://www.ntsb.gov/investigations/AccidentReports/Reports/HAR0803.pdf

Bracewell, R., et al. (1986). *The Fourier transform and its applications* (Vol. 31999): McGraw-Hill New York.

Chakherlou, T., et al. (2011). An experimental investigation of the bolt clamping force and friction effect on the fatigue behavior of aluminum alloy 2024-T3 double shear lap joint. *Materials & Design, 32*(8-9), 4641-4649.

Chaki, S., et al. (2007). Combination of longitudinal and transverse ultrasonic waves for in situ control of the tightening of bolts.

Chen, X., et al. (2012). Load-differential imaging for detection and localization of fatigue cracks using Lamb waves. *NDT & E International, 51*, 142-149.

Clayton, E., et al. (2008). *Active ultrasonic joint integrity adjudication for real-time structural health monitoring.* Paper presented at the Health Monitoring of Structural and Biological Systems 2008.

Degertekin, F., et al. (1996). Single mode Lamb wave excitation in thin plates by Hertzian contacts. *Applied Physics Letters, 69*(2), 146-148. doi:10.1063/1.116902

Doebling, S., et al. (1998). A summary review of vibration-based damage identification methods. *Shock and vibration digest, 30*(2), 91-105.

Doyle, D., et al. (2009). Damage Detection in Bolted Space Structures. *Journal of Intelligent Material Systems and Structures, 21*(3), 251-264. doi:10.1177/1045389X09354785

Doyle, D., et al. (2010). Damage detection in bolted space structures. *Journal of Intelligent Material Systems and Structures, 21*(3), 251-264.

Durak, L., et al. (2003). Short-time Fourier transform: two fundamental properties and an optimal implementation. *IEEE Transactions on Signal Processing, 51*(5), 1231-1242.

Fierro, G., et al. (2017). *Identification of the Location and Level of Loosening in a Multi-bolt Structure using Nonlinear Ultrasound.* Paper presented at the 11th International Workshop on Structural Health Monitoring 2017: Real-Time Material State Awareness and Data-Driven Safety Assurance, IWSHM 2017: Real-Time Material State Awareness and Data-Driven Safety Assurance.

Fierro, G., et al. (2018). IWSHM 2017: Structural health monitoring of the loosening in a multi-bolt structure using linear and modulated nonlinear ultrasound acoustic moments approach. *Structural health monitoring, 17*(6), 1349-1364.

Gao, Y., et al. (2006). The behavior of an elastic–perfectly plastic sinusoidal surface under contact loading. *Wear, 261*(2), 145-154.

Ghosh, D., et al. (2018). Reference free imaging of subsurface cracks in concrete using R ayleigh waves. *Structural Control and Health Monitoring, 25*(10), e2246.

Grandia, W., et al. (1995). *NDE applications of air-coupled ultrasonic transducers.* Paper presented at the 1995 IEEE Ultrasonics Symposium. Proceedings. An International Symposium.

Grosse, C., et al. (2008). *Acoustic Emission Testing: Basics for Research, Applications in Civil Engineering* (1. Aufl. ed.). Berlin, Heidelberg: Berlin, Heidelberg: Springer-Verlag.

Habib, K., et al. (1997). Monitoring pitting corrosion by holographic interferometry. *Corrosion, 53*(9), 688-692.

Hay, T., et al. (2006). A comparison of embedded sensor Lamb wave ultrasonic tomography approaches for material loss detection. *Smart Materials and Structures, 15*(4), 946. Retrieved from http://stacks.iop.org/0964-1726/15/i=4/a=007

Huang, Y., et al. (2009). Real-time monitoring of clamping force of a bolted joint by use of automatic digital image correlation. *Optics & Laser Technology, 41*(4), 408-414.

Huda, F., et al. (2013). Bolt loosening analysis and diagnosis by non-contact laser excitation vibration tests. *Mechanical Systems and Signal Processing, 40*(2), 589-604.

Huo, L., et al. (2017). Impedance based bolt pre-load monitoring using piezoceramic smart washer. *Smart Materials and Structures, 26*(5), 057004.

Jhang, K., et al. (2006). Estimation of clamping force in high-tension bolts through ultrasonic velocity measurement. *Ultrasonics, 44*, e1339-e1342.

Jingpin, J., et al. (2017). Nonlinear Lamb wave-mixing technique for micro-crack detection in plates. *Ndt & E International, 85*, 63-71.

Johnson, K., et al. (1987). *Contact mechanics*: Cambridge university press.

Kim, I., et al. (2016). Tensile behaviors of friction bolt connection with bolt head corrosion damage: Experimental research B. *Engineering Failure Analysis, 59*, 526-543.

Kimoto, K., et al. (2015). A finite difference method for elastic wave scattering by a planar crack with contacting faces. *Wave Motion, 52*, 120-137.

Korpi, D., et al. (2014). Full-duplex transceiver system calculations: Analysis of ADC and linearity challenges. *IEEE Transactions on Wireless Communications, 13*(7), 3821-3836.

Kriesz, H. (1979). Radiographic ndt—a review. *NDT International, 12*(6), 270-273. doi:https://doi.org/10.1016/0308-9126(79)90086-5

Krolo, P., et al. (2016). The guidelines for modelling the preloading bolts in the structural connection using finite element methods. *Journal of Computational Engineering, 2016*.

Scalea, F., et al. (2001). Ultrasonic Guided Wave Inspection of Bonded Lap Joints: Noncontact Method and Photoelastic Visualization. *Research in Nondestructive Evaluation, 13*(3), 153-171. doi:10.1007/s00164-001-0016-8

Lim, H., et al. (2015). Noncontact fatigue crack visualization using nonlinear ultrasonic modulation. *NDT & E International, 73*, 8-14.

Lowe, M. (2013). DISPERSE.

Lowe, M. (2013). DISPERSE. *Imperial College, London*.

Lowe, M., et al. (2000). The transmission of Lamb waves across adhesively bonded lap joints. *The Journal of the Acoustical Society of America, 107*(3), 1333-1345.

Marshall, M., et al. (2006). Characterisation of contact pressure distribution in bolted joints. *Strain, 42*(1), 31-43.

Martinez, J., et al. (2012). A synthetic phased array surface acoustic wave sensor for quantifying bolt tension. *Sensors, 12*(9), 12265-12278.

Matt, H., et al. (2005). Ultrasonic guided wave monitoring of composite wing skin-to-spar bonded joints in aerospace structures. *The Journal of the Acoustical Society of America, 118*(4), 2240-2252.

Michaels, J.. (2008). Detection, localization and characterization of damage in plates with an in situ array of spatially distributed ultrasonic sensors. *Smart Materials and Structures, 17*(3), 035035.

Murat, B., et al. (2016). Scattering of guided waves at delaminations in composite plates. *The Journal of the Acoustical Society of America, 139*(6), 3044-3052.

Nagy, P., et al. (2014). Corrosion and erosion monitoring in plates and pipes using constant group velocity Lamb wave inspection. *Ultrasonics, 54*(7), 1832-1841.

Nikravesh, S., et al. (2017). A review paper on looseness detection methods in bolted structures. *Latin American Journal of Solids and Structures, 14*(12), 2153-2176.

OECD. (2015). *Towards a Framework for the Governance of Infrastructure*. Retrieved from https://www.oecd.org/gov/budgeting/Towards-a-Framework-for-the-Governance-of-Infrastructure.pdf

Pahlavan, L., et al. (2018). Interaction of ultrasonic waves with partially-closed cracks in concrete structures. *Construction and Building Materials, 167*, 899-906.

Kaur, N., et al. (2019). Healing and simultaneous ultrasonic monitoring of cracks in concrete. *Materials Today Communications, 18*, 87-99. doi:https://doi.org/10.1016/j.mtcomm.2018.10.022

Panda, R., et al. (2017). Characterization of delamination-type damages in composite laminates using guided wave visualization and air-coupled ultrasound. *Structural Health Monitoring, 16*(2), 142-152.

Paolo, Z., et al. (2017). Numerical analyses of corroded bolted connections. *Procedia Structural Integrity, 5*, 592-599.

Paolo, Z., et al. (2017). Influence of corrosion morphology on the Fatigue strength of Bolted joints. *Procedia Structural Integrity, 5*, 409-415. doi:https://doi.org/10.1016/j.prostr.2017.07.189

Parvasi, S., et al. (2016). Real time bolt preload monitoring using piezoceramic transducers and time reversal technique—A numerical study with experimental verification. *Smart Materials and Structures, 25*(8), 085015.

Peairs, D., et al. (2004). Improving accessibility of the impedance-based structural health monitoring method. *Journal of Intelligent Material Systems and Structures, 15*(2), 129-139.

Perez, I., et al. (2000). *Thermography for the characterization of corrosion damage*. Retrieved from

Pickthall, T., et al. (2011). *Corrosion Monitoring Equipment, A Review of Application and Techniques.* Paper presented at the CORROSION 2011.

Raghavan, A. (2007). *Guided-wave structural health monitoring.*

Raghavan, A., et al. (2007). Review of guided-wave structural health monitoring. *Shock and Vibration Digest, 39*(2), 91-116.

Rathod, V., et al. (2011). Ultrasonic Lamb wave based monitoring of corrosion type of damage in plate using a circular array of piezoelectric transducers. *NDT & E International, 44*(7), 628-636.

Rose, J. (2014). *Ultrasonic guided waves in solid media*: Cambridge university press.

Shah, J., et al. (2019). Ultrasonic monitoring of corroding bolted joints. *Engineering Failure Analysis, 102*, 7-19. doi:https://doi.org/10.1016/j.engfailanal.2019.04.016

Shah, J., et al. (2020). Monitoring and Imaging of Bolted Steel Plate Joints Using Ultrasonic Guided Waves. *Journal of Nondestructive Evaluation, Diagnostics and Prognostics of Engineering Systems, 4*(1).

Sharma, S., et al. (2010). Longitudinal Guided Waves for Monitoring Chloride Corrosion in Reinforcing Bars in Concrete. *Structural health monitoring, 9*(6), 555-567. doi:10.1177/1475921710365415

Sharma, S., et al. (2011). Monitoring corrosion in oxide and chloride environments using ultrasonic guided waves. *Journal of Materials in Civil Engineering, 23*(2), 207-211.

Sharma, S., et al. (2014). A Non-Contact Technique for Damage Monitoring in Submerged Plates Using Guided Waves. *Journal of Testing and Evaluation, 43*(4), 776-791.

Sharma, S., et al. (2015a). A non-contact technique for damage monitoring in submerged plates using guided waves. *Journal of Testing and Evaluation, 43*(4), 776-791.

Sharma, S., et al. (2015b). Ultrasonic guided waves for monitoring corrosion in submerged plates. *Structural Control and Health Monitoring, 22*(1), 19-35.

Shen, Y., et al. (2013). *Health monitoring of aerospace bolted lap joints using nonlinear ultrasonic spectroscopy: Theory and experiments.* Paper presented at the Proceedings of the 9th International Workshop on Structural Health Monitoring, Stanford University, CA, USA.

Silva, M., et al. (2003). Hidden corrosion detection in aircraft aluminum structures using laser ultrasonics and wavelet transform signal analysis. *Ultrasonics, 41*(4), 301-305.

Sriramadasu, R., et al. (2019). Detection and assessment of pitting corrosion in rebars using scattering of ultrasonic guided waves. *NDT & E International, 101*, 53-61.

Staszewski, W., et al. (2004). Structural health monitoring using scanning laser vibrometry: I. Lamb wave sensing. *Smart Materials and Structures, 13*(2), 251.

SUDA, M., et al. (1992). Development of ultrasonic axial bolting force inspection system for turbine bolts in thermal power plants. *JSME international journal. Ser. 1, Solid mechanics, strength of materials, 35*(2), 216-219.

Sun, Q., et al. (2019). Bolt preload measurement based on the acoustoelastic effect using smart piezoelectric bolt. *Smart Materials and Structures, 28*(5), 055005.

Tashakori, S., et al. (2018). Implementation of heterodyning effect for monitoring the health of adhesively bonded and fastened composite joints. *Applied Ocean Research, 72*, 51-59.

Taylor, S. (2006). Ultrasonic pulser-receiver. In: Google Patents.

Terrien, N., et al. (2007). Numerical predictions and experiments for optimizing hidden corrosion detection in aircraft structures using Lamb modes. *Ultrasonics, 46*(3), 251-265. doi:https://doi.org/10.1016/j.ultras.2007.02.004

Verity, S., et al. (2018). *National State of the Assets*. Retrieved from https://cdn.alga.asn.au/wp-content/uploads/2018-National-State-of-the-Assests-1.pdf

Wallace, I., et al. (2000). Direct tension indicating washers. In: Google Patents.

Wang, F., et al. (2020). Monitoring of multi-bolt connection looseness using entropy-based active sensing and genetic algorithm-based least square support vector machine. *Mechanical Systems and Signal Processing, 136*, 106507.

Wang, F., et al. (2019). Monitoring of early looseness of multi-bolt connection: a new entropy-based active sensing method without saturation. *Smart Materials and Structures, 28*(10), 10LT01.

Wang, T., et al. (2013). Review of bolted connection monitoring. *International Journal of Distributed Sensor Networks, 9*(12), 871213.

Wang, T., et al. (2013). Proof-of-concept study of monitoring bolt connection status using a piezoelectric based active sensing method. *Smart Materials and Structures, 22*(8), 087001.

Wang, Y., et al. (2017). Nonlinear Lamb waves for fatigue damage identification in FRP-reinforced steel plates. *Ultrasonics, 80*, 87-95.

Xiaoliang, Z., et al. (2007). Active health monitoring of an aircraft wing with embedded piezoelectric sensor/actuator network: I. Defect detection, localization and growth monitoring. *Smart Materials and Structures, 16*(4), 1208. Retrieved from http://stacks.iop.org/0964-1726/16/i=4/a=032

Yalciner, H., et al. (2012). An experimental study on the bond strength between reinforcement bars and concrete as a function of concrete cover, strength and corrosion level. *Cement and Concrete Research, 42*(5), 643-655.

Yang, B., et al. (2017). Lamb wave-based structural health monitoring on composite bolted joints under tensile load. *Materials, 10*(6), 652.

Yang, J., et al. (2006a). Detection of bolt loosening in C–C composite thermal protection panels: I. Diagnostic principle. *Smart Materials and Structures, 15*(2), 581.

Yang, J., et al. (2006b). Detection of bolt loosening in C–C composite thermal protection panels: II. Experimental verification. *Smart Materials and Structures, 15*(2), 591.

Yang, Y., et al. (2018). Bolted joint integrity monitoring with second harmonic generated by guided waves. *Structural Health Monitoring, 18*(1), 193-204. doi:10.1177/1475921718814399

Yang, Y., et al. (2019). Bolted joint integrity monitoring with second harmonic generated by guided waves. *Structural Health Monitoring, 18*(1), 193-204.

Yasui, H., et al. (1999). Ultrasonic measurement of axial stress in short bolts with consideration of nonlinear deformation. *JSME International Journal Series A Solid Mechanics and Material Engineering, 42*(1), 111-118.

Yu, L., et al. (2015). Crack imaging and quantification in aluminum plates with guided wave wavenumber analysis methods. *Ultrasonics, 62*, 203-212.

Yuan, Y., et al. (2007). Comparison of two accelerated corrosion techniques for concrete structures. *ACI Structural Journal, 104*(3), 344.

Zagrai, A., et al. (2010). Piezoelectric wafer active sensor structural health monitoring of space structures. *Journal of Intelligent Material Systems and Structures, 21*(9), 921-940.

Zagrai, A., et al. (2010). *Acousto-elastic measurements and baseline-free assessment of bolted joints using guided waves in space structures.* Paper presented at the Health Monitoring of Structural and Biological Systems 2010.

Zhang, M., et al. (2017). Application of subharmonic resonance for the detection of bolted joint looseness. *Nonlinear dynamics, 88*(3), 1643-1653.

Zhang, Z., et al. (2018). Contact acoustic nonlinearity (CAN)-based continuous monitoring of bolt loosening: Hybrid use of high-order harmonics and spectral sidebands. *Mechanical Systems and Signal Processing, 103*, 280-294.

Zhang, Z., et al. (2017). Vibro-acoustic modulation (VAM)-inspired structural integrity monitoring and its applications to bolted composite joints. *Composite Structures, 176*, 505-515.

Zhao, N., et al. (2019). A nonlinear ultrasonic method for real-time bolt looseness monitoring using PZT transducer–enabled vibro-acoustic modulation. *Journal of Intelligent Material Systems and Structures, 31*(3), 364-376. doi:10.1177/1045389X19891534

Zhao, N., et al. (2020). A nonlinear ultrasonic method for real-time bolt looseness monitoring using PZT transducer–enabled vibro-acoustic modulation. *Journal of Intelligent Material Systems and Structures, 31*(3), 364-376.

Zhao, Y., et al. (2017). Generation mechanism of nonlinear ultrasonic Lamb waves in thin plates with randomly distributed micro-cracks. *Ultrasonics, 79*, 60-67.

Zhao, Y., et al. (2016). *A micromechanics model for the acoustic nonlinearity parameter in solids with distributed microcracks.* Paper presented at the AIP Conference Proceedings.

Zhu, W., et al. (1998). Ultrasonic guided wave NDT for hidden corrosion detection. *Journal of Research in Nondestructive Evaluation, 10*(4), 205-225.

Chapter: 3 Ultrasonic Monitoring of Corroding Bolted Joints

Jay Kumar Shah[1], Henrique Bastos Fabrino Braga[1], Abhijit Mukherjee[1], Brian Uy[2]

[1] Department of Civil Engineering, School of Civil and Mechanical Engineering, Curtin University, Kent Street, Bentley, WA 6102

[2] Professor, School of Civil Engineering, University of Sydney, Campertown, NSW 2006

Keywords: Ultrasonics, corrosion, bolted connections, lap joints

Abstract

Ensuring adequate tightening is imperative for securing bolted connections in steel structures. Moreover, bolted joints are affected by corrosion. This paper describes a method of non-destructively assessing the condition of bolted joints. An ultrasonic pulse transmission technique for inspection of bolted joints has been described. Steel plates have been bolted by applying different levels of torque. Transmission of ultrasonic pulse through the joint with varying tightening is studied. A set of plated joints have been subjected to tensile testing to characterise the joints. The other set of joints have been subjected to accelerated corrosion and the ultrasonic measurement has been conducted regularly. After the exposure period, the joints have been subjected to tensile tests to compare with the control specimens. It is observed that the ultrasonic pulse transmission can be correlated with the initial tightening of the bolt. The effect of corrosion was also discerned through ultrasonic measurement. It is observed that the tensile behaviour of the joints due to corrosion is affected significantly by the initial tightening. The proposed method can be applied for non-invasive inspection of fresh and corroded steel structures.

3.1 Introduction

A vast number of steel structures is scrapped when they reach their end of life. Technologies that enable reuse and redeployment of these facilities can dramatically improve the sustainability of steel structures. Bolted steel joints allow easy unfastening of the parts for decommissioning and redeployment of the structures. However, it is crucial to secure the bolted joints throughout the life of the structure. In addition, for an efficient lifecycle management, it is important to monitor the joints. Corrosion is considered one of the prime reasons for deterioration and eventual collapse of steel structures. Recent collapse of Mississippi bridge (Board, 2008) has been attributed to significant corrosion of its various parts. The joints are more susceptible to corrosion than the bare plates. A technique for non-destructive evaluation of bolted steel joints is imperative for maintenance of such structures.

Techniques to monitor corrosion have been reviewed by Agarwala et al. (Agarwala et al., 2000). The most common damage inspection method is visual inspection, but it is limited to identifying surface corrosion only. Gamma and X-rays based methods (Kriesz, 1979) can penetrate the material and provide the information about thickness variations of the material. Other methods for monitoring corrosion are thermography (Perez et al., 2000) and holographic interferometry (Habib et al., 1997). However, subjective nature of inspection, low resolution results, radiation safety concerns and costly instruments restrict their application in structural monitoring. SHM through ultrasonic based monitoring techniques have been found to be time efficient, cost effective and precise. They are of generic nature as they can be used to monitor structures made up of different construction materials (Raghavan et al., 2007). The wave-structure interaction information produced by the ultrasonic waves is used to evaluate the condition of the structure by monitoring parameters like transmission amplitudes, time of flight and frequency spectrum.

Ultrasonic investigation has been successfully used for detection of hidden corrosion in aerospace structures (Silva et al., 2003; Terrien et al., 2007; Zhu et al., 1998a). Zhu et al. (Zhu et al., 1998a) used ultrasonic guided waves to examine the effects of corrosion on transmission and reflection of ultrasonic signals. Another characteristic of corrosion, mode conversion in Lamb waves upon interaction with corrosion, has been exploited to identify the corrosion pitting through finite element based simulations and experiments (Terrien et al., 2007). A non-contact laser based ultrasonic technique has been used to detect the presence of corrosion in plate like structures by monitoring the scattering of symmetrical Lamb wave modes (Silva et al., 2003). Piezoelectric wafer sensors have also been implemented to detect corrosion damage on plates by Rathod et al. (Rathod et al., 2011). Investigation by Hay et al. (Hay et al., 2006) uses computerized ultrasonic tomography algorithm to map corrosion induced mass loss in plates. Similar studies on Lamb wave based corrosion detection on plates have also been performed (Michaels, 2008; Nagy et al., 2014; Xiaoliang et al., 2007). Two studies on ultrasonic inspection of submerged plates using Lamb waves have been reported using water as a couplant (Sharma et al., 2014; Sharma et al.,2015b). These studies are on plates without joints.

Steel plated structures would always have joints and it is noticed that joints corrode early in life of the structure. In case of bolted joints, the level of bolt tightening may affect corrosion. Ultrasonic investigation has been used to monitor the leakage of ultrasonic signal from the de-bonded site in a lap joint (Scalea et al., 2001) and composite bonded joints (Matt et al., 2005). Both studies report that transmission of ultrasonic signal depends on the bonding effectiveness. Modulation in the frequency with the condition of the joint is also observed (Tashakori et al.,

2018). Wang et al. (Wang et al., 2013) detected bolt loosening by monitoring the change in contact pressure between plates with bolt tightening using piezoelectric patches. Huda et al. (Huda et al., 2013) used laser based techniques for that purpose. Signal modulation characteristics due to a fully loosened bolt has also been reported by Amerini et al. (Amerini et al., 2011).

Relatively fewer investigations have reported the effect of corrosion on bolted joints. It is observed that corrosion affects the fatigue strength of bolted joints (Paolo et al., 2017). Ahn et al. (Ahn et al., 2016) have simulated corrosion damage in the bolt head by sawing off parts of the head and experimentally investigated the loss in clamping force. An empirical relation has been reported between loss in clamping force and the volume lost in the bolt head. Numerical investigation by Paolo et al. (Paolo et al., 2017) reported the variation in the interfacial properties of the bolted plates due to bolt pretension loss as a result of corrosion damage to the bolt head.

Although there is a perception that an interrelationship exists between bolt tightening and corrosion no controlled experiments have been reported hitherto. The present paper reports a controlled experiment on bolted joints with varying levels of tightening and corrosion. Several bolted joints have been tightened by applying varying levels of torque. The joints have been subjected to controlled accelerated anodic corrosion. During the process of corrosion, the joint has been monitored non-destructively with ultrasonic pulse transmission. The specimens have been subjected to tensile force to note their residual load capacities, deformations and failure modes. Correlation between bolt torque, corrosion and mechanical performance of the joint is reported.

3.2 Experimental Program

This experimental study has four phases: 1) fabrication of the joints; 2) validation of the ultrasonic system; 3) accelerated corrosion with non-destructive testing; and 4) destructive tests.

3.2.1 Fabrication of the joints

The joints were fabricated as single bolted plate connections consisting of two mild steel plates of dimensions 400 mm x 100 mm x 5 mm and a fully threaded M16 bolt. Load bearing capacity of the specimen are calculated as per Australian standards 4100 and 1275. A bolted specimen fails at a load which is minimum among three capacities as mentioned in Table 3-1. Detailed calculations for load capacity are given in the Appendix A. These calculations do not account

for the frictional resistance due to bolt tightening. Hence, they are applicable for loose bolt condition.

Table 3- 1: Estimated capacities of the bolted joint

Capacity	Load (kN)
Bolt in Shear (f_s)	80.79
Plate in bearing (f_b)	102.50
Plate in tension (f_t)	140

$$\text{Capacity of the joint } f_j = \min(f_s, f_b, f_t) \tag{3-1}$$

3.2.1.1 Load capacity and bolt tightening

Above calculations ignore the frictional shear resistance generated by the tightening of the bolts. The force transfer in a bolted connection is shown in Figure 3-1. Due to the torque (τ) on the bolt, a normal compressive force (N) develops on the lap joint. When a tensile force is applied on the joint, a frictional resistance force (F_f) is generated. The resistance capacity of the frictional force is directly proportional to N, hence applied torque τ:

$$f_f = \mu N \tag{3-2}$$

where μ is the coefficient of static friction between the plates

Thus, the capacity of the joint is revised as:

$$f_j = \min(f_s + f_f, f_b + f_f, f_t) \tag{3-3}$$

Comparing eqns. 3-1 and 3-3 it is clear that the failure mode of the joint may switch from bolt shear to another mode if $f_s+f_f > f_b+f_f, f_t$. Thus, by controlling the bolt torque the failure mode can be switched. In the case of the present plate, an F_f exceeding 21.71 kN would cause the failure to switch from bolt shear to plate bearing.

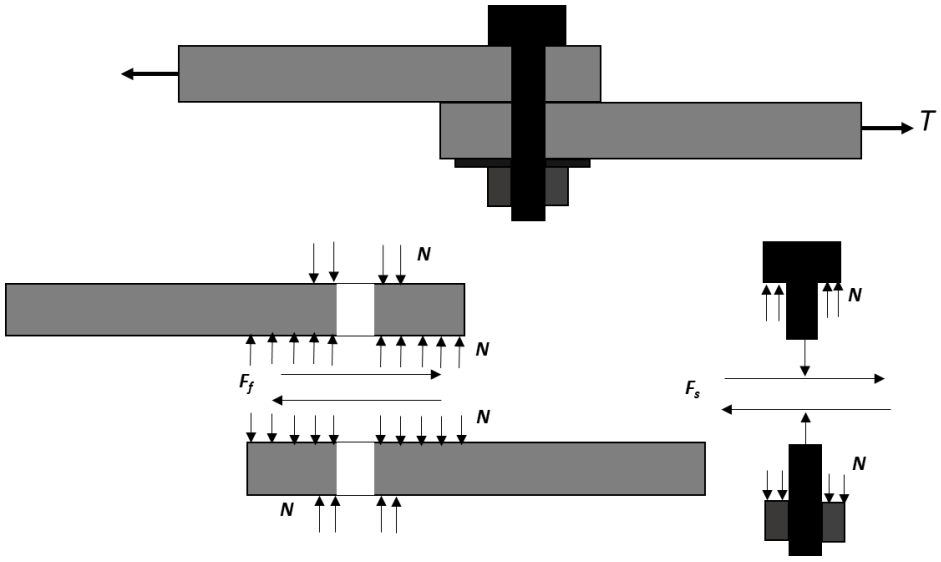

Figure 3- 1: Force distribution in a single joint bolted connection

The details of the specimens are in Table 3-2. Four bolted joints were fabricated. The first pair was tightened at 40 Nm torque and the second pair was tightened at 100 Nm torque. The specimens used have identical geometries and material properties. Both the pairs have been subjected to non-destructive testing. Two specimens (one from each pair) has been exposed to corrosion before subjecting to the tensile test and the other set was tested in tension prior to any corrosion. The failure modes of the plates have been mentioned in Table 3-2. Through destructive tests we have found that specimen S0 with a torque of 40 Nm fails in bolt shear. Specimen B0, on the other hand, fails in plate bearing. This is clearly evidenced in Figure 3-2. Thus, the failure mode did switch with the level of bolt torque. The stress-strain curve for these samples is shown in Figure 3-3. The switch in the failure mode has greatly affected the stress-strain behaviour of the joint. While the initial response of the joints was similar, their post-yield response was substantially different. S0 failed suddenly through bolt shear. B0 had a prolonged post-yield zone with around three times more ultimate strain, which serves as a good warning before the specimen failure. Later we shall report the effect of corrosion on these joints.

Table 3- 2: Details of the specimens

Torque	Corroded	Failure mode	Nomenclature
40 Nm	No	Bolt shear	S0
	Yes	To be found	SC
100 Nm	No	Plate bearing	B0
	Yes	To be found	BC

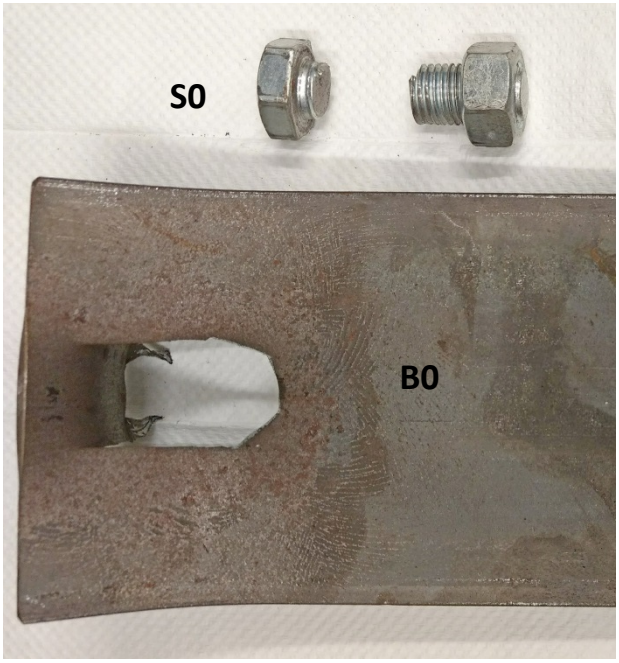

Figure 3- 2: Bolt shear and plate bearing failure in S0 and B0 specimens

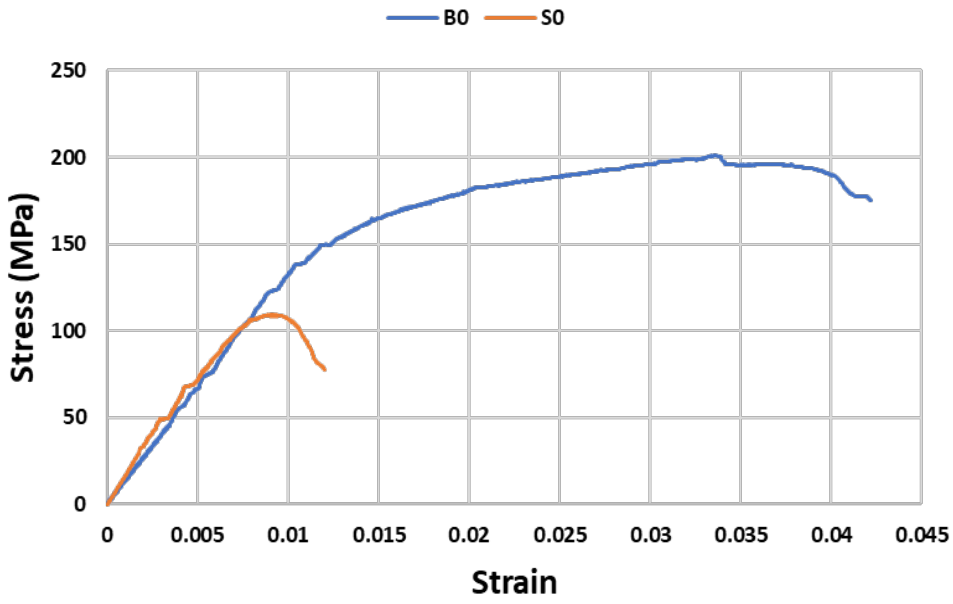

Figure 3- 3: Stress-Strain curve for B0 and S0 specimens

3.2.2 Ultrasonics investigation

The joints were subjected to guided ultrasonic pulses as shown in Fig. 3-4. The surface of the plate was polished, and a thin layer of grease was applied. A pair of 200 kHz (ULTRAN) transducers were placed securely on the greased surface. A Pulser-receiver system (JSR Ultrasonics DPR 300) was connected to the transducers to transmit an ultrasonic pulse. The pulse propagates through the interface between the plates. The propagated pulse would vary

with the condition of the interface between the plates. The interface would vary with the amount of torque applied on the bolt as well as the state of corrosion.

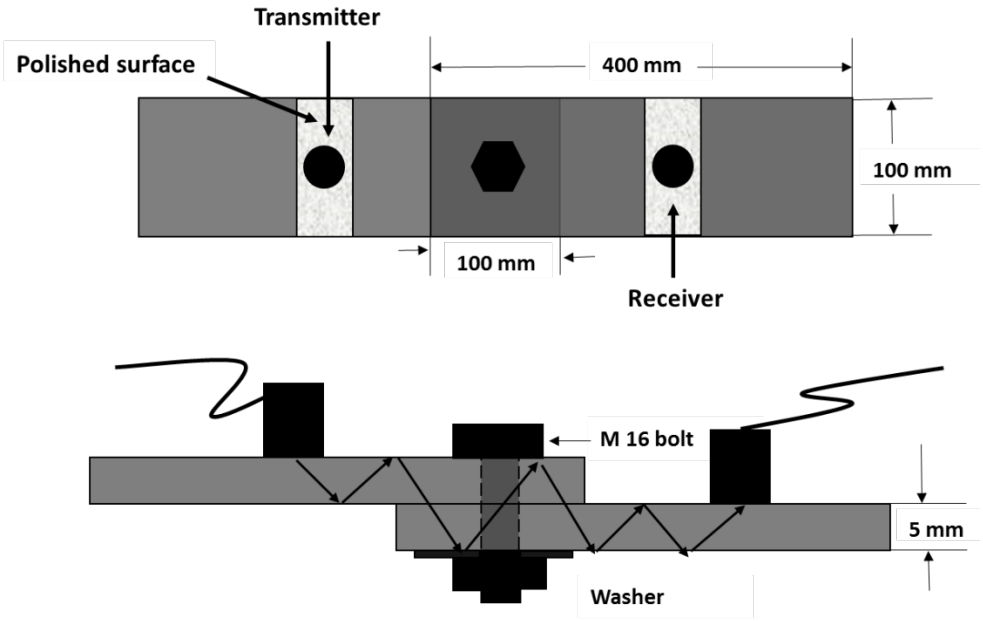

Figure 3- 4: Top and side view of experimental ultrasonic set-up

The ultrasonic signals as received from B0 and S0 specimens are shown in Figure 3-5. The overall signal amplitudes for B0 specimen are higher than that of the S0 specimen. It can be argued that the contact between plates would have undulations at microscopic scale as shown in Figure 3-6. Due to the higher torque in B0 specimen the contact force (*N*) at the interface between the plates is higher. Therefore, some undulations flatten resulting in better contact between the plates that results in higher signal transmission between the plates. Hence, the bonding effectiveness of bolted plates is dependent on the bolt tightness. Therefore, for higher torque level specimens A_T is higher.

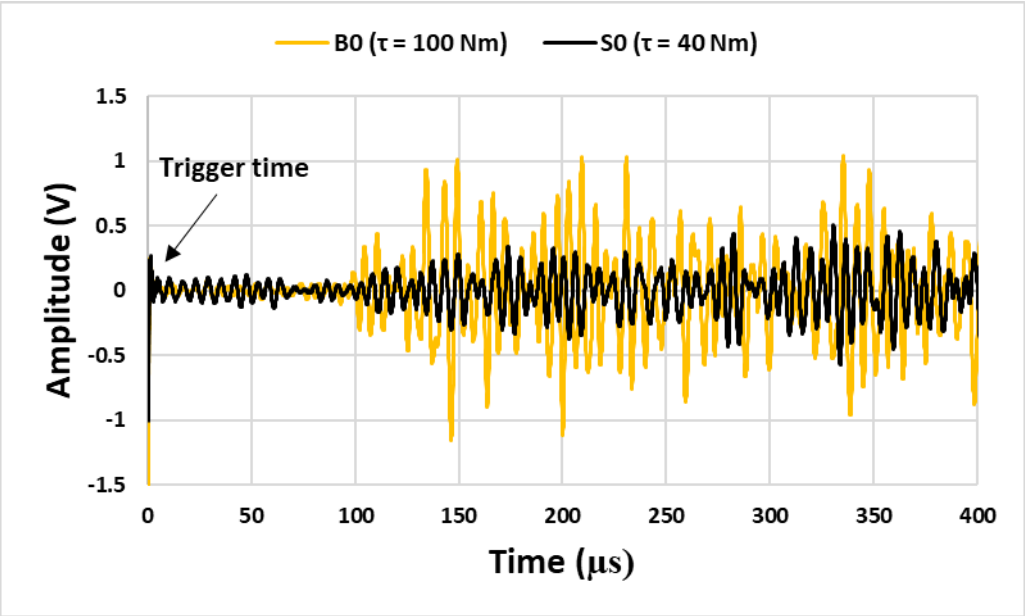

Figure 3- 5: Recorded ultrasonic signals for B0 and S0 specimens

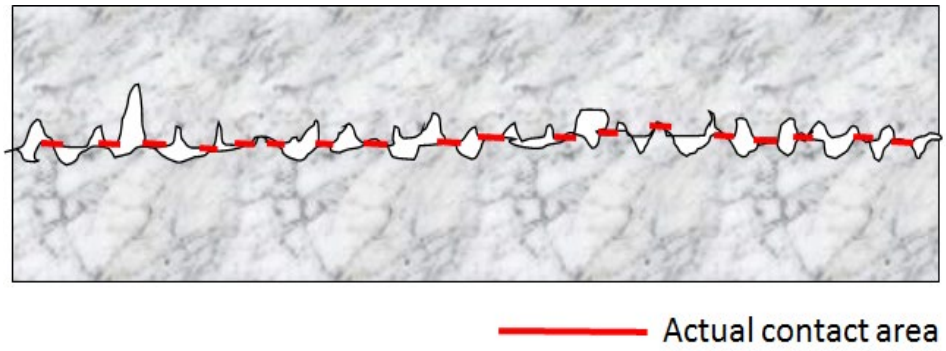

Figure 3- 6: Imperfect contact at plate's interface at microscopic scale

The transferred signal energy (E) of the received signals is calculated in discrete time domain [t_s, t_f] as per equation 3-4 (T. Wang et al., 2013).

$$E = \frac{1}{f_s} \sum_{t=t_s}^{t_f} V^2(t) \tag{3-4}$$

Here $V(t)$ is the amplitude and f_s is the sampling frequency of the discrete sensor signal.

E at different bolt torque is plotted in Figure 3-7. The relationship is linear at the start. After the torque crosses 80 Nm, there is a marked reduction in the rate of increase of *E*. Beyond this point, it was not possible to tighten the bolt any further. Similar outcome has been reported by Wang et al. (Wang et al., 2013). The initial steady increase in *E* with bolt torque signifies that the undulations at the plate interface are flattening and the effective contact area is increasing. The curve plateaus out when the undulations are too few to be flattened. Evidently, it is

possible to calibrate *E* with bolt tightening level. This investigation further explores how this relationship is affected by corrosion of the joint.

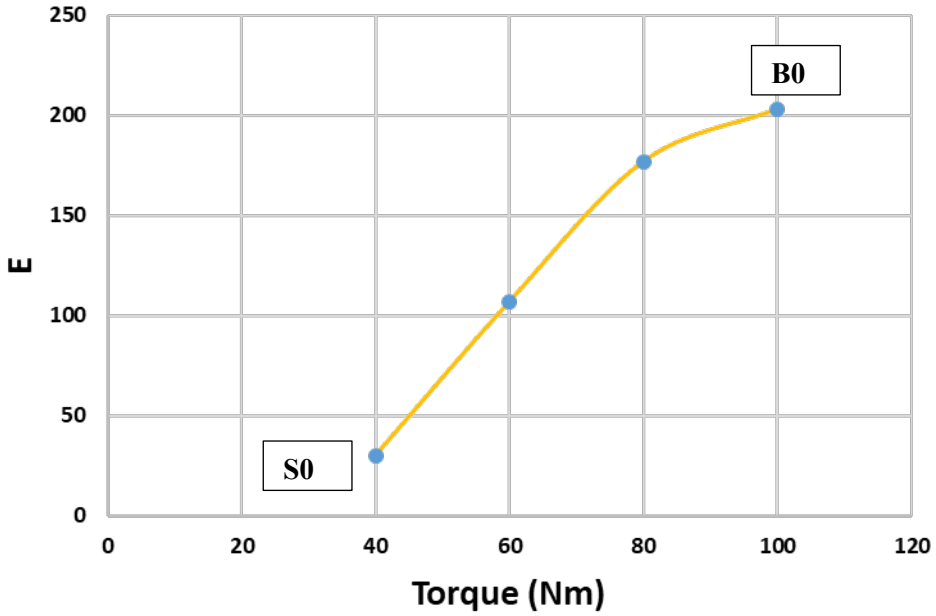

Figure 3- 7: Transferred signal energy variation in specimen at different τ levels

3.2.3 Ultrasonic monitoring during accelerated corrosion

The bolted joint was subjected to accelerated electrochemical corrosion as shown in the Figure 3-8. Two torque levels as in B0 and S0 samples, were chosen. The corroded specimens have been named as BC and SC. The galvanostatic method (Yuan et al., 2007) was chosen. A hollow cylinder was placed on the joint. The bottom of the cylinder was secured with an adhesive sealant to prevent leakage. The cylinder was filled with an electrolytic solution. For this work, we had chosen 3.5% sodium chloride in water as the electrolytic solution. The corrosion region included the bolt along with the surrounding plate region.

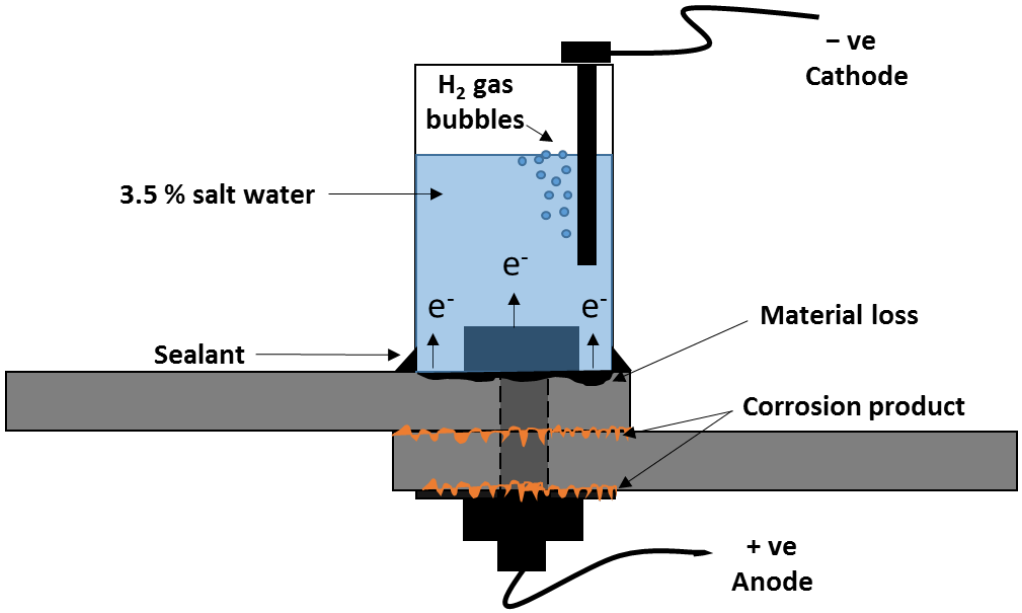

Figure 3- 8: Experimental set-up for accelerated corrosion

An electrical circuit was formed connecting the anode to the specimen and a copper rod dipped in the electrolyte as cathode to a constant mode DC power source. The anode gets oxidized and gives away the electrons under the application of an electromotive force and in the presence of chloride ions (eq. 3-5). The cathode attracts the released electrons from the anode and forms anions (hydroxyl ions) through a reduction reaction (eq. 3-6.1). The other reduction reaction at cathode (3-6.2) contributes to the liberation of hydrogen gas.

Oxidation reaction at Anode : $Fe + 2Cl^- \rightarrow Fe^{2+} + 2Cl^- + 2e^-$ (3-5)

Reduction reaction at Cathode : $O_2 + H_2O + 2\,e^- \rightarrow 2\,OH^-$ (3-6.1)

$2H^+ + 2\,e^- \rightarrow H_2$ (3-6.2)

The oxidation and reduction reactions take place simultaneously for the corrosion to occur. The hydroxyl ions combine with the ferrous ions to produce ferrous hydroxide ($Fe(OH)_2$) (eq. 3-7). Further oxidation of $Fe(OH)_2$ takes place in the presence of water and oxygen (eq. 3-8, 3-9) results in the formation of rust ($Fe_2O_3.2H_2O$) or the corrosion product.

$$Fe^{2+} + 2OH^- \rightarrow Fe(OH)_2 \quad (3\text{-}7)$$

$$4Fe(OH)_2 + O_2 + H_2O \rightarrow 4Fe(OH)_3 \quad (3\text{-}8)$$

$$Fe(OH)_3 \rightarrow Fe_2O_3.2H_2O \quad (3\text{-}9)$$

The rate of corrosion is proportional to the current flowing though the circuit. The rate of corrosion can be controlled by setting the DC power supply as a constant voltage or a constant current. In the constant voltage mode, a constant corrosion potential is maintained. In case of the constant current mode, a constant rate of corrosion is maintained. In this investigation, the specimens were subjected to a constant current setting of 0.1 Amperes for a period of 20 hours per day. The corresponding applied voltages at different times have been recorded. The mass loss due to corrosion for this condition can be calculated using Faraday's law (Yalciner et al., 2012).

$$m = \left(\frac{It}{F}\right)\left(\frac{M}{z}\right) \tag{3-10}$$

I = constant current applied for electrolysis

t = total time for which constant current is applied

F = Faraday's constant = 96500 C/mol

M = Molar mass of substance in grams per mol

z = Valency numbers of ions of the substance (electrons transferred per ion)

The estimated mass loss for this condition was approximately 2.089 grams per day. Simultaneously with accelerated corrosion, the ultrasonic pulse transmission has been measured using setup described in Section 3-2. Figure 3-9.i shows the recorded ultrasonic signals on 0^{th}, 10^{th} and 20^{th} day of corrosion experiment. It can be seen that the recorded signal's strength is highest at the 10^{th} day. We utilized the recorded data to calculate the transferred signal energy (E) across the interface at the end of each day of the experiment. Figure 3-9.ii shows the E variation for the BC specimen with time. A clear increasing trend in the E value can be seen up to day 12. After that time, a gradual decrease in E was observed.

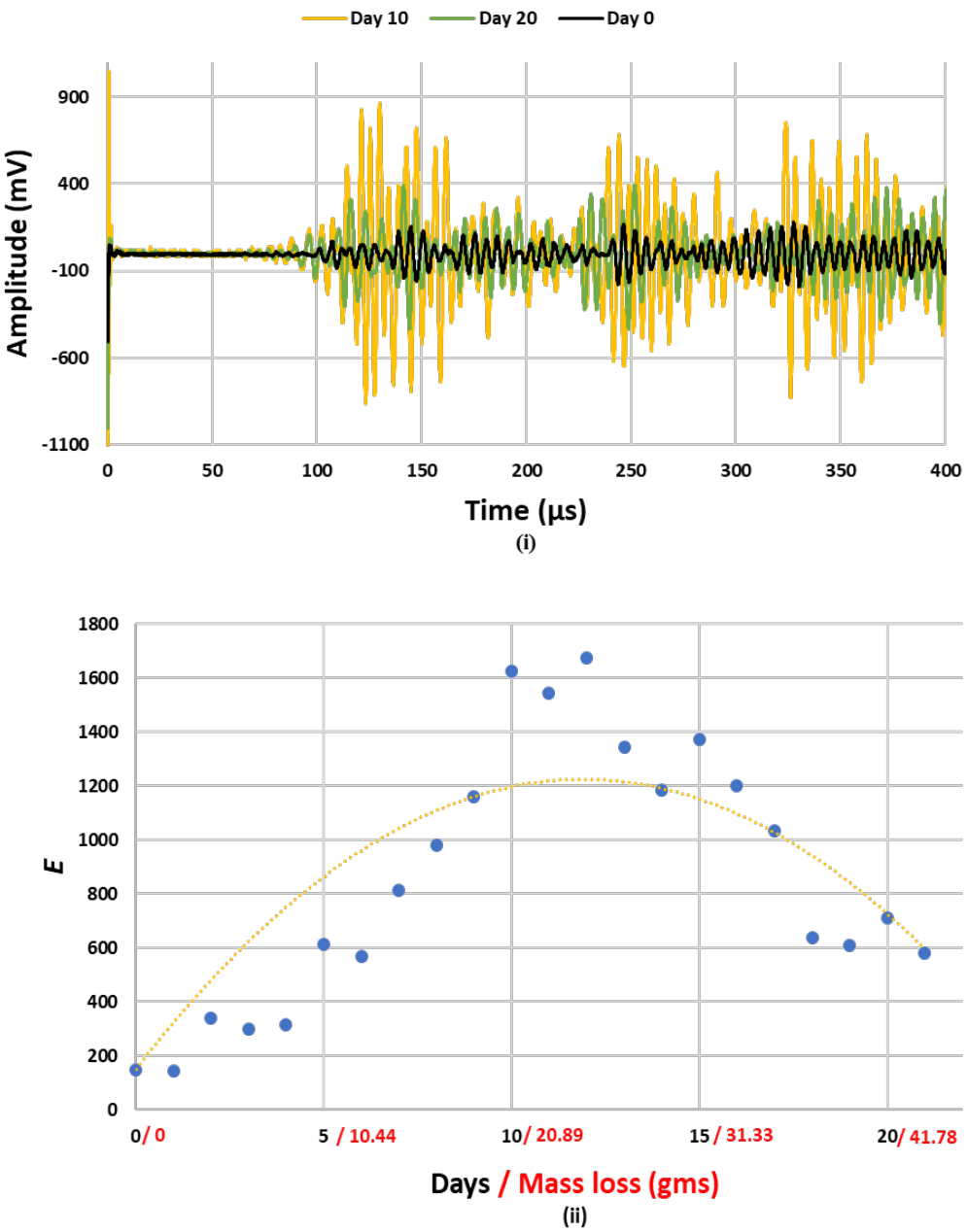

Figure 3- 9: (i) Recorded ultrasonic signal at day 0, 10 and 20 and (ii) Transferred energy (E) variation with days of corrosion/mass loss for the BC specimen

The variation in E with time is explained with the help of Figure 3-10. As explained previously, *E* increases with the increase in the interfacial contact. For a pristine specimen, even in the tightened joint, some undulations are left at the interface (pristine (Pr) stage). Hydrated ferric oxide (Fe_2O_3) formed as in equation 3-9 has a volume of about twice that of steel it replaces when fully dense. As the volume of corrosion product is more than that of the corresponding steel, it gradually fills the vacant spaces. A thin layer of corrosion product forms in the initial phase of the experiment (Initial corrosion (IC) stage). Thus, *E* increases at the initial phase of corrosion. When the corrosion product fills the entire gap, build-up of more of corrosion

product would create pressure on the corrosion product. When the pressure exceeds the endurance capacity of the corrosion product, it would crumble and the effective contact area at the interface would reduce once again (Advanced corrosion (AC) stage). Experiments were terminated when there was no significant change in the value of E with progression of corrosion.

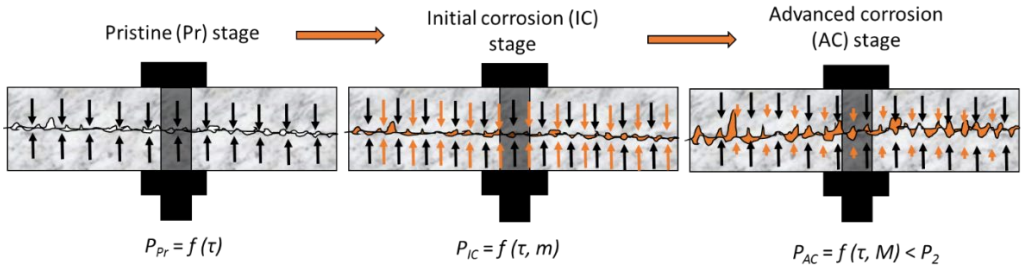

Figure 3- 10: Plate interfaces with progressive corrosion

Figure 3-10 also shows demonstrates the possible variations in the contact pressure (P) at different stages of corrosion. For a bolted specimen in its pristine (Pr) stage, contact pressure P_{Pr} at the interface is solely dependent on the bolt τ. Therefore, P_{Pr} can be described as a function of torque $f(\tau)$. For a fixed value of τ, during the initial corrosion (IC) stage, corrosion product fills the gaps at the interface generating an additional extra pressure at the interface. This additional pressure is shown in orange coloured arrows in the IC stage. At the IC stage, contact pressure P_{IC} changes with the mass (m) of steel which got converted into the rust. Therefore, P_{IC} becomes a function of m along with the τ. The additional pressure increases with the increase in volume of the rust generated at the interface. As mentioned previously, at an advanced corrosion (AC) stage this pressure exceeds the endurance capacity of the rust which results in crumbling of the rust. In this situation, additional pressure fades away with the increase in the volume of rust at the interface. This has been shown with the shortened length orange arrows in AC stage (Fig 3-10). Therefore, at this stage, P_{IC} transforms into P_{AC} which decreases as a function ($M > m$) and τ. This hypothesis is also supported by the work reported by Sharma et al. (Sharma et al., 2010), where the authors have experimentally discerned the generation of an outward pressure due to the rust formation at concrete-steel bar interface, which resulted in the cracking of the concrete.

Figure 3-11 shows the BC specimen at the end of the experiment. It can be seen that mass loss is predominantly at the bolt head and the nearby region of top plate. A thin layer of rust at the interface of the two plates was clearly visible. However, nut was relatively intact with marginal signs of corrosion. Clearly, there was minimal leakage of the electrolyte from the top to the bottom of the joint. We can conclude that the amount of corrosion is influenced by the torque applied on the bolt.

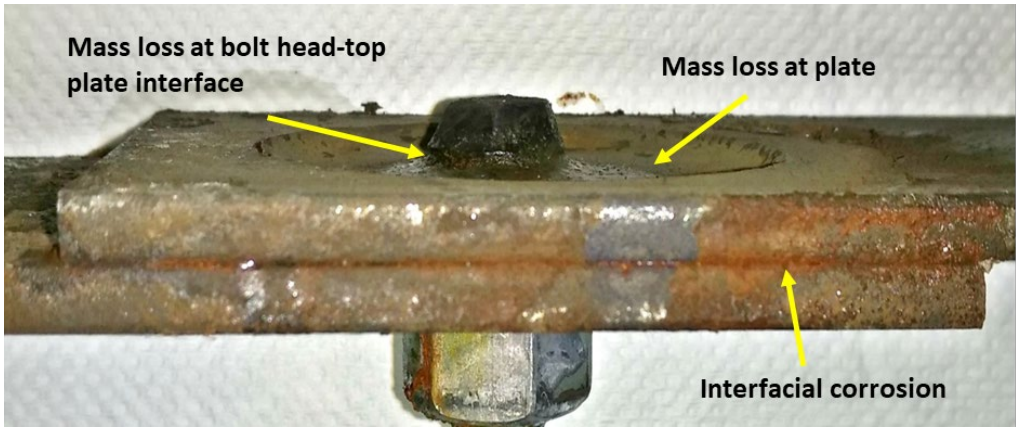

Figure 3- 11: BC specimen at the end of corrosion experiment

Figure 3-12 shows the variation in the transferred energy for the SC specimen. Unlike the increasing trend for *E* in the BC specimen, *E* remains relatively flat until the Day 9 of the experiment when there is a sudden jump in the *E* value. After reaching the peak on the Day 11, there was a similar decline pattern can be seen on the 13th day. Based on Figure 3-10, *E* declined with time. It may be noted that the bolt torque in the SC is lower. As a result, the effective area of contact is likely to be lower in this sample than in BC. Thus, it took significant volume of rust to fill up the interfacial gaps in this case resulting in a flat *E*. A more sudden jump E confirms that at that time the gaps are likely to have been filled. Beyond that time, similar to the BC specimen, as corrosion advances the rust crumbles due to additional pressure and the contact between plates becomes weaker. Therefore, *E* decreases with further corrosion.

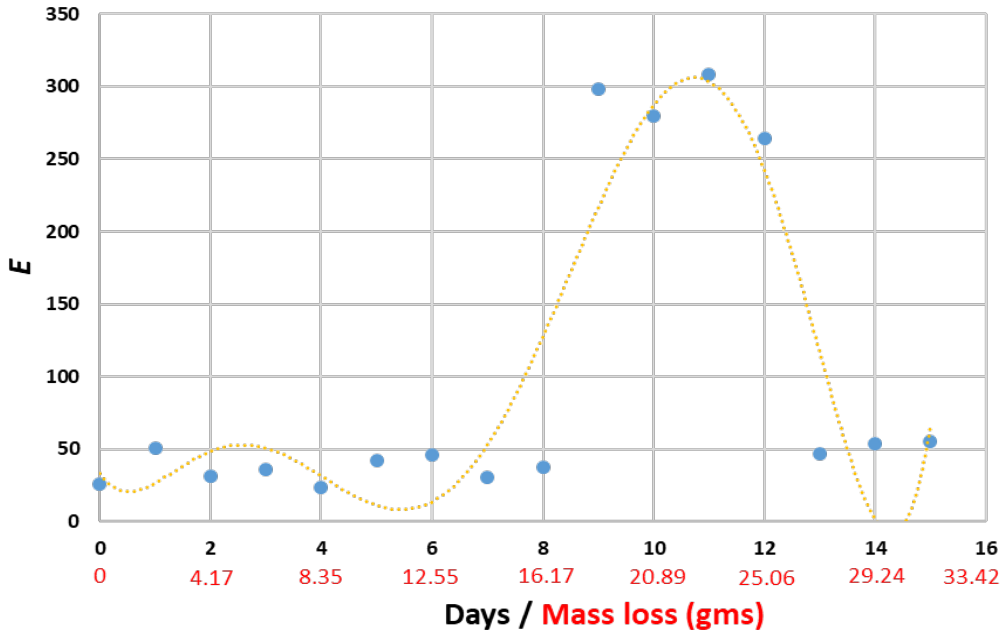

Figure 3- 12: Transferred energy (E) variation with days of corrosion/mass loss for the SC specimen

From visual inspection of the SC specimen in Figure 3-13, it can be seen that corrosion is far more widespread in this sample than in BC. Clearly, the lower bolt torque has not been able to prevent the leakage of the electrolyte. It is evident from the significant damage of the bottom nut in this case. Thus, it is reaffirmed that bolt torque does influence the corrosion of the joint.

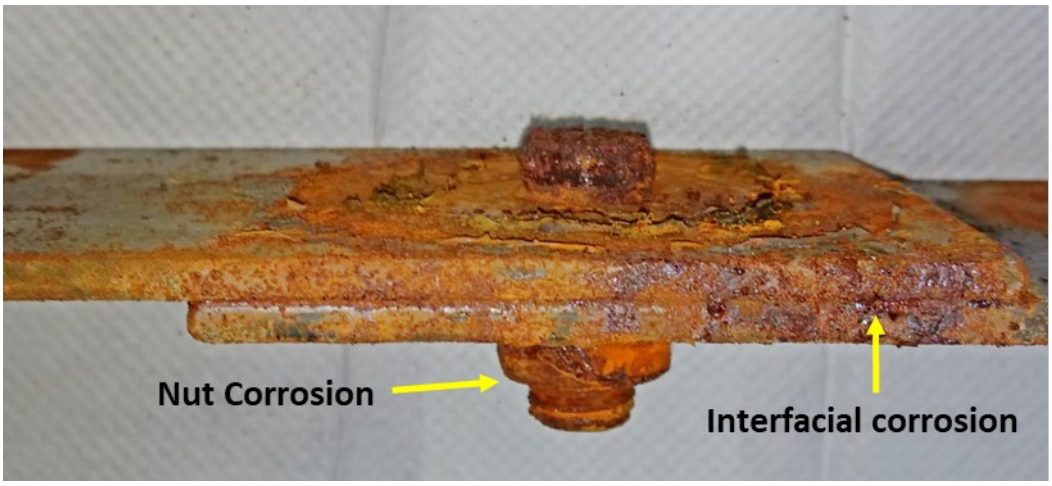

Figure 3- 13: SC specimen at the end of corrosion experiment

3.2.4 Destructive tests after corrosion

Destructive tensile tests were conducted on the specimens to investigate the effect of corrosion on load capacities. A tensile load had been applied using a servo controlled universal testing machine with a constant rate of displacement at 5 mm/min. Figure 3-14 presents the stress-strain plot of B0 and BC. At the initial phase, both specimens followed the same trend. However, at about 0.7% strain, the curves bifurcated, and BC was 40% lower than that of B0. The image of the sample after testing in Figure 3-15 shows in both samples the bolthole in the plate elongated due to bearing pressure and the bolt remained intact. The failure mode did not change after corrosion. There is a clear thinning of the top plate due to corrosion. As a result the effective area of the plate for resisting the bearing stress is reduced significantly. The strain at failure too had a significant reduction due to corrosion. Although the lost mass due to corrosion is relatively small (~3%) its effect on the reduction of plate capacity is very significant.

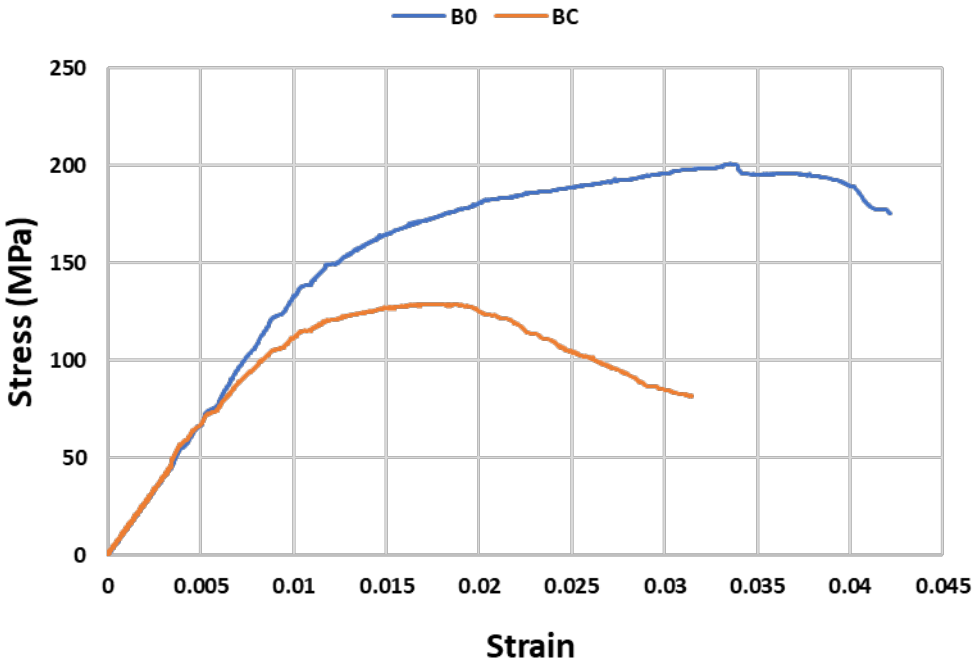

Figure 3- 14: Load-deflection plots for B0 and BC

Figure 3- 15: B0 and BC after destructive testing

Figure 3-16 shows the stress-strain plots for S0 and SC. Unlike the high torque samples, corrosion did not affect the load capacities that significantly. SC exhibited lower stiffness than S0. This is due to the loss in the diameter of the bolt that allowed higher slip between the plates. Although the strain at failure was significantly higher due to corrosion, the maximum stress on the joints was comparable. It may be noted that S0 had failed in bolt shear. SC too failed due to bolt shear. Figure 3-17 compares the bolts after failure. It can be seen that the bolt head has lost significant amount of material due to corrosion. The diameter of the bolt has reduced by less than a millimetre. Thus, the load capacity of the joint was not affected but the specimen exhibited a softer behaviour.

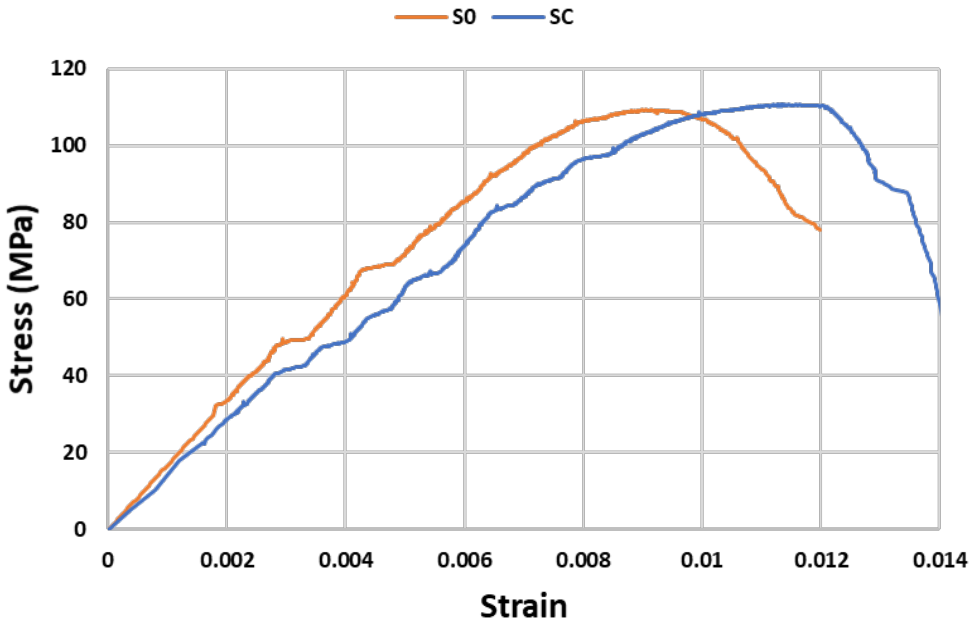

Figure 3- 16: Stress-Strain curves for S0 and SC

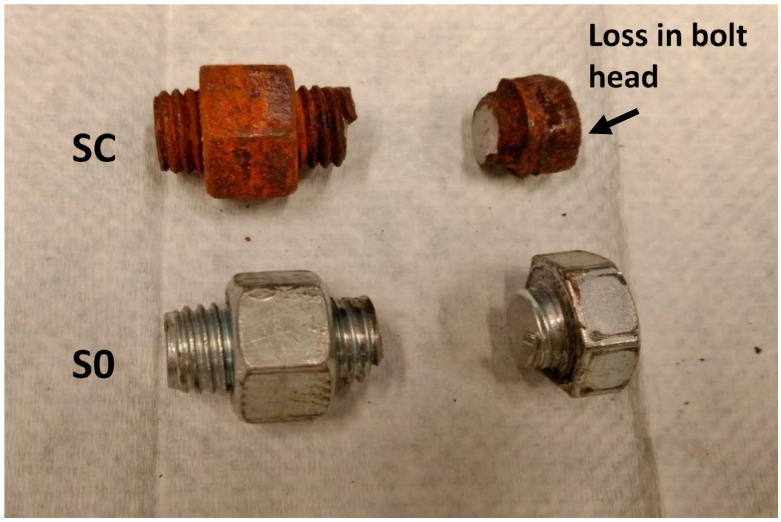

Figure 3- 17: Bolts after destructive testing of S0 and SC

It is observed, in bolted joints, the bolt torque and corrosion are interrelated. The criticality of different joint failure modes depends on bolt torque. Higher bolt torque may move the failure mode from bolt shear to plate bearing or plate tension. Corrosion affects the joints differently depending on bolt torque. It may not affect the capacity as significantly in bolt shear as in case of plate bearing or plate tension. It is possible to calibrate the state of both the joint, both in terms of bolt torque and the state of corrosion with ultrasonic pulse transmission tests.

Concluding remarks

This paper reports an experimental investigation on the interplay between the bolt torque and corrosion on the mechanical behaviour of bolted joints. A single lap joint consisting of two mild steel plates and one galvanised mild steel bolt was chosen. The joints have been monitored non-destructively simultaneously as the bolts are tightened and the specimens are corroded. Ultrasonic signal transmission signals through the joint was recorded during the entire experiment in an effort to calibrate the condition of the joint. Finally, destructive tests were conducted on the specimens to establish the relationships between the non-destructive tests and load capacities of the joints. Following major conclusions can be made from the investigation:

- The load capacity and the failure mode of a bolted joint depends on the level of bolt torque.
- The capacity goes up with tightening with diminishing returns. The failure mode of the joint can be engineered by controlling the bolt torque.
- The strength of the transmitting ultrasonic signal across the interface between the plates increases with bolt torque. Thus, the ultrasonic signal can be used for calibrating bolt torque.
- The nature and extent of corrosion in the joint depends on the bolt torque. Ultrasonic signal transmission is able to discern this difference.
- For an equivalent extent of corrosion, the load capacity of the highly tightened specimen decreases significantly due to corrosion whereas for the loosely tightened joints load capacity is not affected to that extent.

Future scopes

In present work, the scope of this investigation was limited to a single bolt. Extension of this study on more complex joints is underway and will be reported shortly. The similar investigation at different bolt tightening levels corresponding to different nature of failure modes can be investigated.

Acknowledgement

The authors gratefully acknowledge Australian Research Council for funding this investigation through grant LP150100475.

References

Agarwala, V., et al. (2000). *Corrosion detection and monitoring-A review.* Paper presented at the CORROSION 2000.

Ahn, J., et al. (2016). Clamping force loss of high-strength bolts as a result of bolt head corrosion damage: Experimental research A. *Engineering Failure Analysis, 59*, 509-525.

Amerini, F., et al. (2011). Structural health monitoring of bolted joints using linear and nonlinear acoustic/ultrasound methods. *Structural health monitoring, 10*(6), 659-672.

Board, N. (2008). Collapse of I-35W Highway Bridge, Minneapolis, Minnesota. Retrieved from https://www.ntsb.gov/investigations/AccidentReports/Reports/HAR0803.pdf

Habib, K., et al. (1997). Monitoring pitting corrosion by holographic interferometry. *Corrosion, 53*(9), 688-692.

Hay, T., et al. (2006). A comparison of embedded sensor Lamb wave ultrasonic tomography approaches for material loss detection. *Smart Materials and Structures, 15*(4), 946. Retrieved from http://stacks.iop.org/0964-1726/15/i=4/a=007

Huda, F., et al. (2013). Bolt loosening analysis and diagnosis by non-contact laser excitation vibration tests. *Mechanical systems and signal processing, 40*(2), 589-604.

Kriesz, H. (1979). Radiographic ndt—a review. *NDT International, 12*(6), 270-273. doi:https://doi.org/10.1016/0308-9126(79)90086-5

Scalea, F., et al. (2001). Ultrasonic Guided Wave Inspection of Bonded Lap Joints: Noncontact Method and Photoelastic Visualization. *Research in Nondestructive Evaluation, 13*(3), 153-171. doi:10.1007/s00164-001-0016-8

Matt, H., et al. (2005). Ultrasonic guided wave monitoring of composite wing skin-to-spar bonded joints in aerospace structures. *The Journal of the Acoustical Society of America, 118*(4), 2240-2252.

Michaels, J. (2008). Detection, localization and characterization of damage in plates with an in situ array of spatially distributed ultrasonic sensors. *Smart Materials and Structures, 17*(3), 035035.

Nagy, P., et al. (2014). Corrosion and erosion monitoring in plates and pipes using constant group velocity Lamb wave inspection. *Ultrasonics, 54*(7), 1832-1841.

Paolo, Z., et al. (2017). Numerical analyses of corroded bolted connections. *Procedia Structural Integrity, 5*, 592-599.

Paolo, Z., et al. (2017). Influence of corrosion morphology on the Fatigue strength of Bolted joints. *Procedia Structural Integrity, 5*, 409-415. doi:https://doi.org/10.1016/j.prostr.2017.07.189

Perez, I., et al. (2000). *Thermography for the characterization of corrosion damage*. Retrieved from

Raghavan, A., et al. (2007). Review of guided-wave structural health monitoring. *Shock and Vibration Digest, 39*(2), 91-116.

Rathod, V., et al. (2011). Ultrasonic Lamb wave based monitoring of corrosion type of damage in plate using a circular array of piezoelectric transducers. *NDT & E International, 44*(7), 628-636.

Sharma, S., et al. (2010). Longitudinal Guided Waves for Monitoring Chloride Corrosion in Reinforcing Bars in Concrete. *Structural health monitoring, 9*(6), 555-567. doi:10.1177/1475921710365415

Sharma, S., et al. (2014). A Non-Contact Technique for Damage Monitoring in Submerged Plates Using Guided Waves. *Journal of Testing and Evaluation, 43*(4), 776-791.

Sharma, S., et al. (2015). Ultrasonic guided waves for monitoring corrosion in submerged plates. *Structural Control and Health Monitoring, 22*(1), 19-35.

Silva, M., et al. (2003). Hidden corrosion detection in aircraft aluminum structures using laser ultrasonics and wavelet transform signal analysis. *Ultrasonics, 41*(4), 301-305.

Tashakori, S., et al. (2018). Implementation of heterodyning effect for monitoring the health of adhesively bonded and fastened composite joints. *Applied Ocean Research, 72*, 51-59.

Terrien, N., et al. (2007). Numerical predictions and experiments for optimizing hidden corrosion detection in aircraft structures using Lamb modes. *Ultrasonics, 46*(3), 251-265. doi:https://doi.org/10.1016/j.ultras.2007.02.004

Wang, T., et al. (2013). Proof-of-concept study of monitoring bolt connection status using a piezoelectric based active sensing method. *Smart Materials and Structures, 22*(8), 087001.

Xiaoliang, Z., et al. (2007). Active health monitoring of an aircraft wing with embedded piezoelectric sensor/actuator network: I. Defect detection, localization and growth monitoring. *Smart Materials and Structures, 16*(4), 1208. Retrieved from http://stacks.iop.org/0964-1726/16/i=4/a=032

Yalciner, H., et al. (2012). An experimental study on the bond strength between reinforcement bars and concrete as a function of concrete cover, strength and corrosion level. *Cement and Concrete Research, 42*(5), 643-655. doi:https://doi.org/10.1016/j.cemconres.2012.01.003

Yuan, Y., et al. (2007). Comparison of two accelerated corrosion techniques for concrete structures. *ACI Structural Journal, 104*(3), 344.

Zhu, W., et al. (1998). Ultrasonic guided wave NDT for hidden corrosion detection. *Journal of Research in Nondestructive Evaluation, 10*(4), 205-225.

Appendix A: Appendix

Notations used

Notation		Meaning
A_c	=	Minor diameter area of the bolt
A_g	=	The gross area of the cross-section
A_n	=	The net cross-sectional area, obtained by deducting from the gross area the sectional area of all penetrations and holes, including fastener holes.
A_o	=	Nominal plain shank area of the bolt
a_e	=	Minimum distance from a hole to edge of the plate
d_f	=	Diameter of the bolt
f_u	=	The tensile strength used in design
f_{uf}	=	Minimum tensile strength of the bolt
f_{up}	=	Plate ultimate stress
f_y	=	The yield stress used in design
k_r	=	Reduction factor
k_t	=	The correction factor for distribution of forces determined in accordance with Clause 7.3
N_t	=	Nominal tensile capacity
n_n	=	Number of shear planes with threads intercepting the shear plane
n_x	=	Number of shear planes without threads intercepting the shear plane
t_P	=	Plate thickness
V_b	=	Nominal plate bearing capacity
V_f	=	Nominal shear capacity of a bolt

Plate design specifications

Plate material	=	Mild steel grade 250
f_{up}	=	410 MPa (AS4100)
t_p	=	5 mm
a_e	=	50 mm
f_y	=	280 MPa
A_g	=	500 mm^2
A_n	=	492 mm^2

Plate in Tension

The nominal section capacity of a structural member in tension is the minimum of $N_t = A_g f_y =$ 140 kN and $N_t = 0.85\ k_t\ A_n f_u = 146.37$ kN

Plate in Bearing (AS4100)

$$V_b = 3.2\, d_f\, t_P\, f_{up} = 104.96 \text{ kN} \quad \textbf{(A1)}$$

For plate subjected to a component of force acting towards an edge V_b is lesser than the value in equation 1 and is given by the relation shown in equation 2.

$$V_b = a_e\, t_P\, f_{up} = 102.5 \text{ kN} \quad \textbf{(A2)}$$

Bolt design Specifications

Bolt grade	=	8.8
Bolt diameter	=	16 mm
Thread type	=	Fully threaded
f_{uf}	=	830 MPa (AS4100)
k_r	=	1.0 (AS4100)
n_n	=	1
n_x	=	0
A_c	=	157 mm^2 (AS1275)

Bolt in shear capacity (AS4100)

$$V_f = 0.62\, f_{uf}\, k_r\, (n_n\, A_c + n_x A_o) = 80.79 \text{ kN}$$

Chapter: 4 Monitoring and Imaging of Bolted Steel Plate Joints using Ultrasonic Guided Waves

Jay Kumar Shah and Abhijit Mukherjee
School of Civil Engineering and Mechanical Engineering, Curtin University, Kent Street, Perth, WA, 6102, Australia

Abstract

Steel structures with bolted joints are easily dismantled and repurposed. However, maintaining joint integrity is a challenge. This paper reports a non-destructive methodology to monitor steel bolted joints. Piezo electric ceramic patches have been surface bonded in the joint for transmission and reception of guided ultrasonic waves. Both single and multiple bolted joints have been investigated. It has been demonstrated that the variation in acoustic impedance due at the bolt interface can be discerned and calibrated with bolt torque level. The recorded reflections from interfaces are used as inputs for a newly developed imaging algorithm. The proposed method has the potential to be a reference free and fully automated method.

Keywords: Bolt loosening; bolted joints; ultrasonics; imaging; torque; pre-tension loss

4.1 Introduction

Developing sustainable construction technologies is a formidable challenge in Civil Engineering. Repurposing and upcycling of structural components is a great strategy for improving sustainability of constructed facilities. Steel structures have an edge over concrete in recycling provided the joints can be easily dismantled. This requirement mandates that the key joints must be bolted instead of welding or riveting (Akinade et al., 2015). Bolted joints must be secured with adequate bolt tension that in turn provides joint integrity by maintaining contact pressure between the plates in the joint. Therefore, during installation, a bolted joint is secured by providing an appropriate level of bolt torque. During their service period, bolted joints are prone to damages such as creep, corrosion and fatigue cracking. A typical bolted joint consists of a large number of bolts and manual inspection and retightening of bolts is infeasible. Hence, technologies to enable quick, easy and preferably automated maintenance of bolted joints are seminal towards the goal of achieving sustainability of steel structures.

Standard methods to monitor bolt installations include bolt tension indicators (Wallace et al., 2000) and bolt torque control (Bickford, 2007). An example of tension indicator is usage of special washers with protruding features. Flattening of these protrusions at a predetermined

compression gives a visual proof of adequate bolt tightening. However, the process is not reversible; thus, it is unable to indicate subsequent bolt loosening. Bolt torque measurement systems too are unable to indicate loosening. Impact hammer tests are conducted to identify bolt loosening where an inspector analyses the vibrational response of the bolt (Nikravesh et al., 2017). Such practices are time consuming, expensive and dependent on the expertise of inspectors. An automated inspection technique with permanently attached sensors can alleviate these challenges.

Other well-known techniques to monitor bolt condition during service life include strain measurements, electrical impedance measurements and digital image correlation. Strain gauges fitted in bolts have been reported to determine bolt elongation during tightening (T. Wang et al., 2013) and change in pretension in the bolt during service life (Ahn et al., 2016). However, it is not feasible to install strain gauges on all bolts. Thus, representative bolts/washers can be instrumented (Sun et al., 2019; Yang et al., 2006b) and an estimate on overall condition of the joint is made based on the this information. Further, strain gauges are known to have a drift and they are notoriously fragile. An overall check on a bolted joint can be made through the impedance technique or through digital image correlation. In Impedance based methods, electrical or electromechanical response of a joint is recorded and compared with a baseline measurement (Huo et al., 2017; Peairs et al., 2004). In digital image correlation technique, the zone of interest is photographed periodically and the images are correlated to discern its health (Huang et al., 2009). Both these techniques need a baseline information of the initial condition of the joint.

Guided ultrasonic wave (GUW) based techniques offer a variety of inspection methods using a relatively simple setup with transducers connected to signal generators and recorders. GUW based joint inspections can adopt both linear and nonlinear approaches. Linear acoustic properties such as velocity of the guided wave, time of flight and phase depend on the axial force in the bolt. In a straight forward approach, bolt tightness can be assessed monitoring GUW through the bolt (Chaki et al., 2007; Jhang et al., 2006; Yasui et al., 1999b). However, inspection of each bolt in a joint can be tedious. Since the loss of bolt torque reduces the plate contact pressure, a superior monitoring technique can be developed using the plates as a waveguide. In this method, the transducers are placed on the plates instead of the bolts. Parameters such as transmitted wave energy (Shah et al., 2019; Wang et al., 2013) and phase shift (Doyle et al., 2009; Zagrai et al., 2010b) through the plates have been measured.

Due to loss of bolt tension, wave propagation can lead to interfacial vibrations causing clapping between the bolted plates generating contact nonlinearity. This nonlinear

phenomenon is known to generate higher harmonics of the excitation frequency (Amerini et al., 2010b; Y. Yang et al., 2018; Zhang et al., 2017). In the presence of more than one excitation frequency, frequency modulation can be observed (Zhang et al., 2017; Zhao et al., 2019). However, in addition to the contact, there are other sources of nonlinearity. The nonlinearity in the incident wave can be amplified by the use of power amplifiers, which has sometimes been ignored (Amerini et al., 2011; Yang et al., 2018). Power amplifiers have been found to be a source of significant instrument induced nonlinearity (Anttila et al., 2013; Korpi et al., 2014). Therefore, discerning bolt induced nonlinearity from instrument nonlinearity can be a challenging task in a multi bolt joint. Limited attempts have been made in this regard by using baseline subtraction (Kimoto et al., 2015).

Majority of GUW based joint monitoring have employed wave transmission mode. Although an overall condition of the joint can be obtained using the transmission mode, it does not pinpoint the loose bolt in a multi bolt structure. More recently, efficacy of wave reflection in pinpointing defects have been highlighted (Fierro et al., 2018; Zagrai et al., 2010b). However, these studies used a baseline signature for comparison. In this study, we report a reflection based baseline free method to determine the bolt condition. Reflection mode inspection combined with an imaging technique can offer damage detection along with its localization (Beniwal et al., 2015; Ghosh et al., 2018). This method has been resorted to for imaging of cracks in plate structures (Chen et al., 2012; Lim et al., 2015; Yu et al., 2015). However, only attempts of imaging bolted joints are reported [(Martinez et al., 2012), (Marshall et al., 2006)]. Martinez et al. (Martinez et al., 2012) used a transducers-wedge arrangement to generate surface acoustic waves on the washer-plate interface of a single bolt joint. They generated B-scans of the reflected ultrasonic signals from the interface captured in a synthetic array. They demonstrated that the shift in the location of first reflection from the interface can be used to monitor the changing torque. Marshall et al. (Marshall et al., 2006) produced contact pressure maps to draw a similar conclusion. No application on multi-bolt joints have been reported in these works. This article has attempted to extend the application of the proposed method on the double bolted joint.

It is important to choose appropriate type of transducers for a long-term automated monitoring of joints. Commonly used piezoelectric transducers require coupling gel and an appropriate pressure to hold on to the waveguide surface. Therefore, the efficacy of such inspection is subjective to the quality of contact and the inspector's skills. On contrary, piezoelectric patches are can be permanently attached on the surface and relatively cost efficient. Therefore, patch is a potential candidate for automated monitoring of joints. Other than choosing an appropriate sensor, it is crucial to select an optimum excitation frequency for the inspection. A travelling

wave guided by the boundaries of the plate propagates as Lamb waves which is combination of several symmetric (S_n, n = 0, 1, 2,..) and antisymmetric (A_n, n = 0, 1, 2,..) modes as shown in Figure 4-1. The existence of these modes and their group velocities depend on the excitation frequency and the thickness of the plate. For our study, a frequency which can generate distinct and less attenuative modes (usually lower order modes) can be considered optimum. Such frequency can be determined through analytical solutions cross validated with the experimental results.

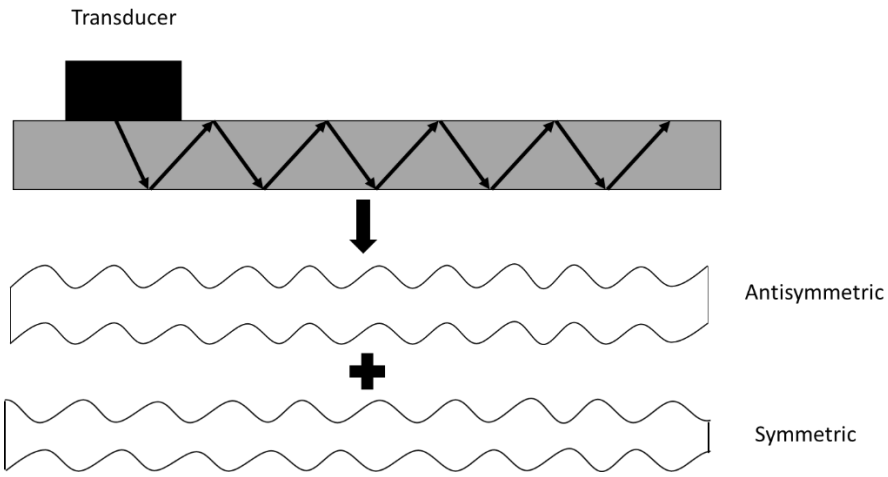

Figure 4- 1: Wave propagation in plates

In this work, we present a non-invasive and a potential baseline free imaging approach for monitoring torque levels in bolted joints. Single and multi-bolt steel joints tightened at varying torques were monitored through surface bonded piezoelectric patches. The recorded bolt-wave interaction was fed into the imaging algorithm. A post processing was done in order to identify torque levels.

4.2 Specimen preparation

Bolted joints, as shown in Figure 4-2, have been fabricated. The single joint consisted of two identical mild steel plates of dimension 400 mm x 100 mm x 5 mm joined together with a M16 fully threaded bolt. The double joint had two 400 mm x 200 mm x 5 mm plates joined together using two M16 bolts. The plates were assembled by placing the bolts in the hole of diameter 18 mm. The bolts were tightened by applying a specific torque on them with a torque wrench.

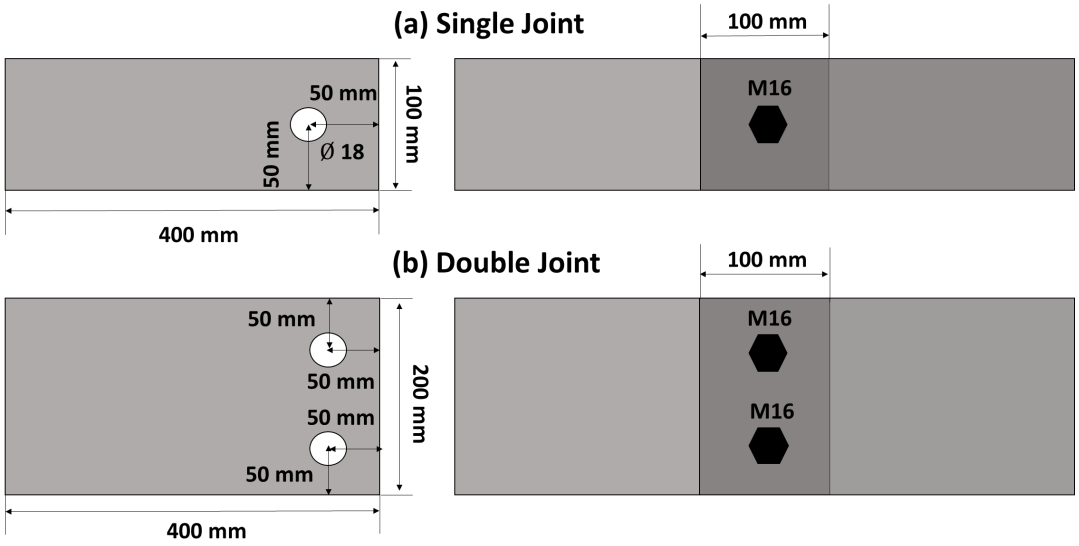

Figure 4- 2: Schematic diagram for a (a) Single and (b) Double joint

4.3 Experimental program

4.3.1 Selection of wave mode and excitation frequency

The coexistence of several Lamb wave modes in a plate make GUW based inspection difficult to interpret. Therefore, it is critical to identify an optimum excitation frequency. Figure 4-3 shows the dispersion curves for different Lamb wave modes travelling in a 5 mm thick plate. These curves have been obtained using a commercial software called DISPERSE (Lowe et al., 2013). For frequencies lower than 300 KHz, only two fundamental modes S_0 and A_0 exist in the plate, whereas higher order modes get generated above 300 kHz. To avoid overlapping of different modes in the signal, we have chosen a frequency well below 300 kHz. Another advantage is that the S_0 and A_0 modes travel at significantly different velocities, hence these can be identified at distinct arrival times in the recorded signals.

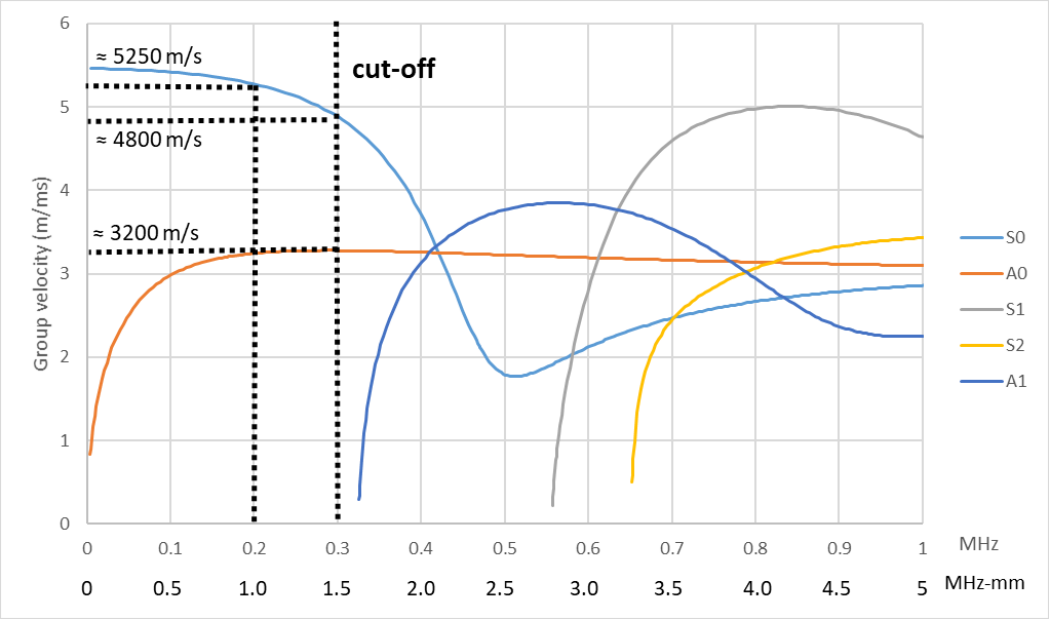

Figure 4- 3: Group velocity of a 5 mm thick steel plate using DISPERSE

The transducers are attached on the surface of the plate. This particular sensor placement and the excitation frequency favours generation of relatively strong antisymmetric modes as discussed by Degerketin et al. (Degertekin et al., 1996). In the range of 200 kHz-300 kHz, it can be noticed that the group velocity of the S_0 mode changes continuously in between 5200 m/s to 4800 m/s whereas the group velocity of the A_0 mode remains constant at approximately 3200 m/s. It makes A_0 a more convenient mode for inspection. For the experimental validation, we attached two piezoceramic patches (10 mm dia; 0.5 mm thick; Warsash Scientific Pty Ltd.) at 300 mm distance on the plate. A 200 kHz 5.5 cycle Hanning window tone burst signal was excited into the plate. The signal was generated using a function generator (RIGOL DG1035) and amplified with a power amplifier (Ciprian HVA 400 A). No amplification at the receiving end was used. Figure 4-4 shows a typical signal where the arrival of two fundamental modes can be distinctly identified. The signal was recorded for a time period of 400 µs. It can be seen that the A_0 mode has significantly higher energy content than the S_0 signal. This process was repeated for four different frequencies 175 kHz, 200 kHz, 225 kHz and 250 kHz. We chose to use 200 kHz frequency as the inspection frequency as it had the highest A_0/S_0 energy ratio and it also generates non-overlapping modes. The energy content in each of the mode is calculated using equation 4-1 (Yang et al., 2006a), where f_s is the sampling frequency of the signal (6.25 MHz in this study), V is the amplitude at discrete time 't' and t_s and t_f represent the starting and finishing time limits of the mode interval as marked in Figure 4-4. These values are approximately 53 µs and 76 µs for the S_0 mode and 80 µs and 103 µs for the A_0 mode.

$$E = \frac{1}{f_s}\sum_{t=t_i}^{t_f} V^2(t) \qquad (4\text{-}1)$$

The group velocity of each mode was calculated from distance-time-velocity relation. The arrival time of the highest peak in each mode (≈ 60.4 µs for S_0 mode and ≈ 92 µs for A_0 mode) was used for the velocity calculations. This corresponds to respective group velocities of approximately 4950 m/s and 3200 m/s for S_0 and A_0 mode which lie in the velocity range observed in Figure 4-3.

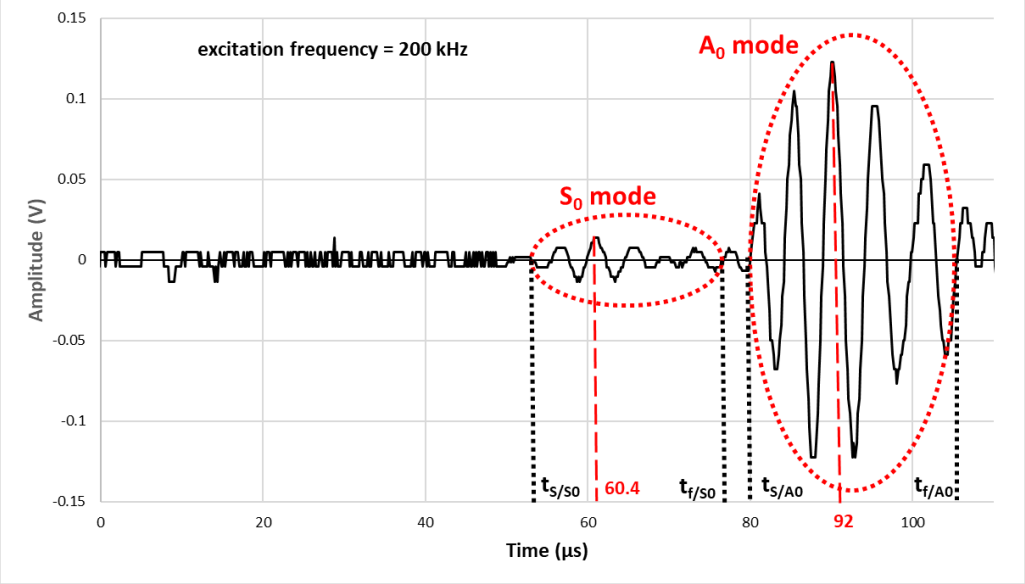

Figure 4- 4: Recorded signal for a 200 kHz signal

4.3.2 Preliminary ultrasonic investigation (Transmission mode)

In order to validate the effectiveness of A_0 mode for the inspection of bolted joints, a single joint was subjected to ultrasonic wave in transmission mode as shown in Figure 4-5. An amplified 200 kHz and 1.5 V_{P-P} 5.5 cycle tone burst signal was transmitted across the joints as shown in Figure 4-5a. The transmitted signal was recorded for different bolt torque values and the variation in the energy (E) of A_0 mode was calculated as per the equation 4-1. Figure 4-5b shows the variation of E at different bolt torques. It can be seen that with linear increase for initial tightening, E tends to saturate at higher torque values signifying the maximum possible tightening. Similar outcomes have been reported in (Shah et al., 2019; Wang et al., 2013; Yang et al., 2006a)

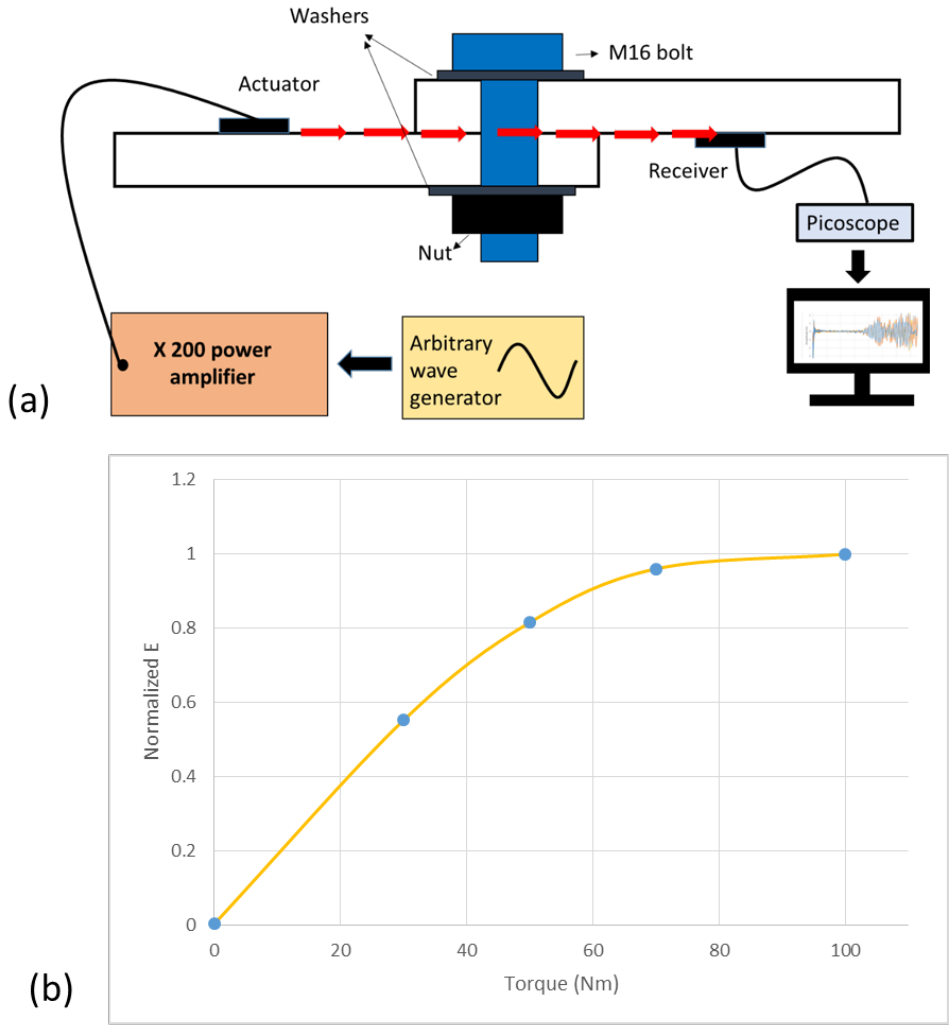

Figure 4- 5: (a) Schematic for transmission mode experimental setup (b) Variation in E with the bolt torque values

It is noted that initially E increases linearly with torque. At around 30 Nm torque, the rate of increase in E starts to slow down and it hits a plateau at around 80 Nm. Figure 4-6 shows a possible wave propagation scenario for 100 Nm and 30 Nm bolt torque. The plates have undulations at microscopic levels, and they are not in complete contact. At a lower torque (<30 Nm), a considerable fraction of the energy is reflected at the uneven contact area and from the bolthole. As the contact pressure increases, the undulations tend to flatten resulting in increase in contact area between the plates, therefore a higher fraction of the energy is transmitted across the joint. At 100 Nm, the contact pressure is significant to flatten all undulations and there is no further increase in the transmitted energy. In other words, the fraction of energy left in the transmitting plate can be used as an indicator of the contact pressure and hence, bolt torque.

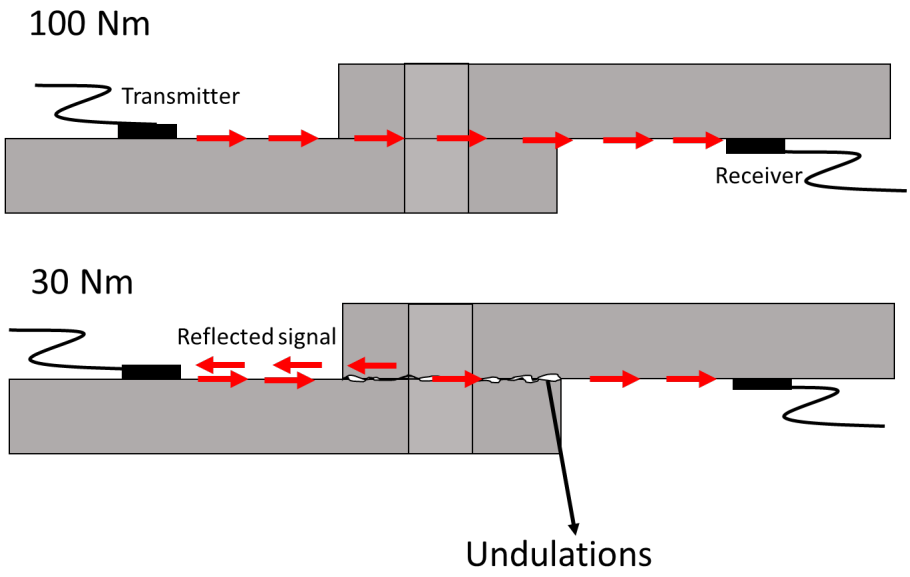

Figure 4- 6: Wave propagation across a bolted joint with bolt torque 100 Nm (top) and 30 Nm (bottom)

4.3.3 Reflection mode inspection

4.3.3.1 Ultrasonic imaging

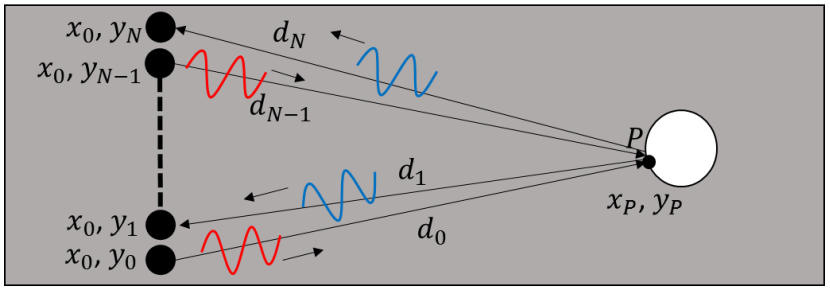

Figure 4- 7: Schematic representation of the imaging principle

Figure 4-7 shows schematic for the imaging principle used in this study. Successively positioned patches at locations (x_0, y_{i-1}) and (x_0, y_i) where, i = 0 to N act as actuator and receiver. The excited ultrasonic signal travels and interacts with point P located at (x_P, y_P) and travels back to the receiver covering a total distance of d_{i-1}+ d_i. Since the pixels located at the bolthole offer significant acoustic impedance mismatch, the intensity of reflected signals from such a location is prominent. The time of flight T corresponding to reflections from P can be calculated as follows

$$T = \frac{(d_{i-1}+d_i)}{c};\ (i=1, N) \qquad (4\text{-}2)$$

Here, c is the approximate velocity of A_0 mode in the plate. For each receiver location, reflected signal R scattered from P is extracted from the recorded time signals at each corresponding Ts, hence,

$$R(T) = \sum_{i=1}^{N}(P(x_0, y_i, T)) \quad (4\text{-}3)$$

represents the information about the P properties. Similarly, reflections for all pixels in the chosen domain were recorded to create an image of the specimen. For the bolted joint as shown previously in Figure 4-5a, undulations are present at both the washer-plate interface and at the plate interface as shown in Figure 4-8. Therefore, sensors array can be placed along any of the two interfaces as it is crucial to minimize the number of interfaces which may cause unwanted reflections of the signal. Now onward, investigations with sensors at former and latter interface type will be referred as configuration A and B as shown in Figure 4-9.

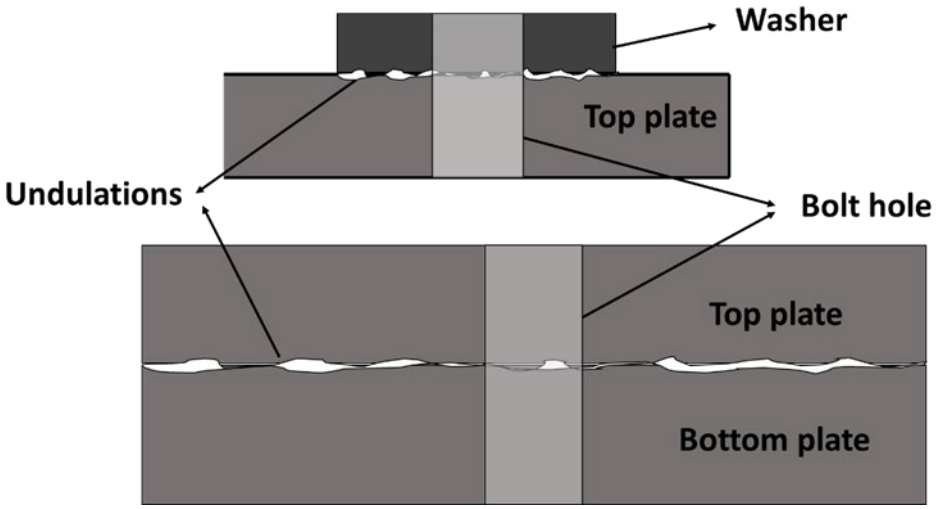

Figure 4- 8: Undulations at washer-plate interface (top) and plate-plate interface (bottom)

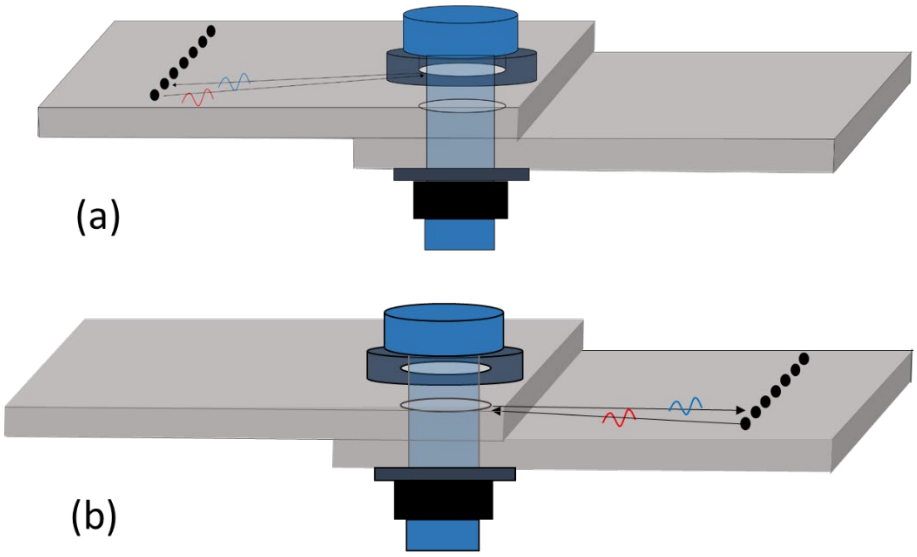

Figure 4- 9: Schematic for configuration (a) A and (b) B

4.3.3.2 Single plate

To validate the imaging algorithm, we first image a single plate with a bolthole which is a much simpler case than a bolted joint as it has many interfaces to offer. Seven patches with a centre-to-centre distance of 13.5 mm were surface bonded at a distance of 260 mm from the edge of the plate as shown in Figure 10a. Five amplified cycles of 200 kHz and 1.5 V_{P-P} sinusoidal wave was used as an input for the patch. The ultrasonic scan, as shown in Figure 10b was created as described in the section above. The near field effect is visible up to a distance of 50 mm from the patches. The reflection from the bolthole can be clearly spotted at the bolthole location. Some reflections from the edges are also observed. However, the bolthole can be identified from the image. As the input had five cycles of sine wave, five compression and rarefaction bands have formed. In this image, the location of the hole is clearly identified.

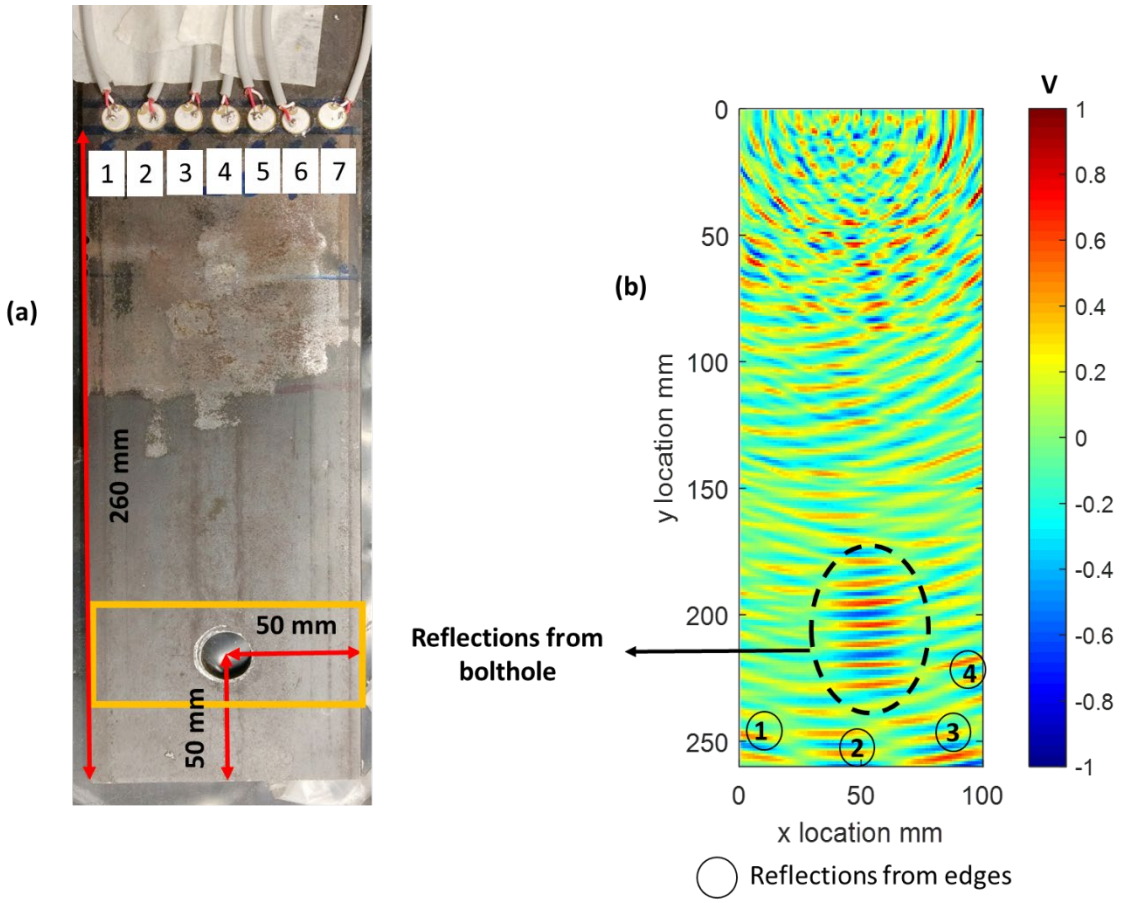

Figure 4- 10: (a) The specimen and (b) its ultrasonic scan

The next step is to obtain a realistic image of the hole. For this purpose, an intensity (I) variation analysis was done in a specific window (yellow window in Figure 4-10a) around the detected pressure wave. This windowing technique was chosen to reduce the interference of undesired reflection from the plate boundaries. In our case it was critical to cover the bolthole in the window, also without losing the information of pressure band. This was implemented by setting a limit (190 to 230) on the 'y' in equation 4. The intensity at each pixel can be rewritten as

$$I\,(T) == \sum_{x=0}^{100}\left(\sum_{y=190}^{230}(R(T))^2\right); \qquad (4-4)$$

Figure 11a shows the intensity (I) variation in the chosen window. It is observed that the I peak at the bolthole location. As equation 4-4 shows that the variation of I is obtained through the summation of independent pixel intensities acquired through experiments. As the pixel intensities are affected by several factors, they need smoothing to discern the contact pressure. It can be noticed that the variation of intensity in the chosen window resembles closely to a

Gaussian distribution. Therefore, a Gaussian fit was used to smoothen the reflected intensity. The resulting curve is plotted as coloured contour in Figure 4-11b. This may be interpreted as the likelihood diagram for the location of the bolt, maximum (red) at the centre and gradually going down towards the edge. The result is a realistic representation of the bolthole. However, there is small peak at the right end of the Figure. This may be interpreted as another contact point developing as a result of small undulations on the plate surfaces.

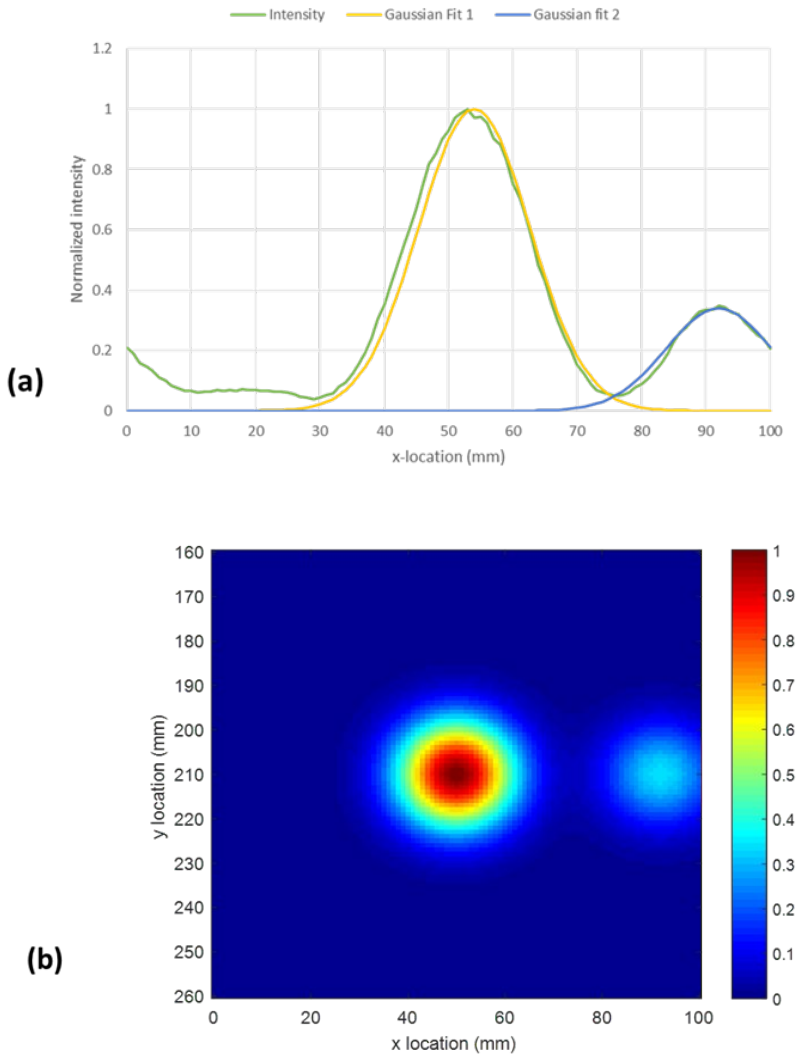

Figure 4- 11: (a) Intensity variation of the received signal (b) contact contour highlighting the bolthole location

4.3.4 Configuration A

This section describes the results for Configuration A. The initial torque was minimal with hand tightening of the bolt, followed by tightening with a torque wrench. It is to be noted that it was not possible to identify the torque value for hand tightened case. The hand tightened case just represents the severe case of bolt loosening throughout this paper. Figure 4-12a-c

show the ultrasonic scans at different torques. The pressure bands from the bolthole disappear with slight rise in torque. With increasing torque, the contact pressure between the plate and the washer increases as do the pressure between the plates. As a result, more and more energy leaks into the second plate and the reflected signal is attenuated.

The intensities across the plate at different torques have been plotted in Figure 4-12d. A clear peak at the bolthole location is visible for the hand tightened case. At this stage, the interfacial gaps allow the propagating waves to interact with the bolt hole. As the torque increases the intensity drops rapidly. This is due to two possible factors 1) more energy leaks through the joint into the second plate; 2) the reflections are spread over a larger area due to higher contact pressure. It is also observed that the peaks occur well beyond the diameter of the washer, which indicates that the reflections from the interface between the two plates are also received in this configuration.

It can be observed that for 30 Nm and 100 Nm torques, no pressure band was observed around the bolthole even when there was significant difference in the corresponding transmitted energy as observed in Figure 4-5b. Thus, it can be stated that the effect of increasing torque on undulations at washer-top plate interface tends to saturate prematurely. It is due to the smaller contact area between washer and the top plate. Instead, it can be argued that the larger overlapped area between the plates can offer gradual change in the contact with the increasing torque. Thus, it is expected that a clearer picture of the condition of the joint will emerge in Configuration B.

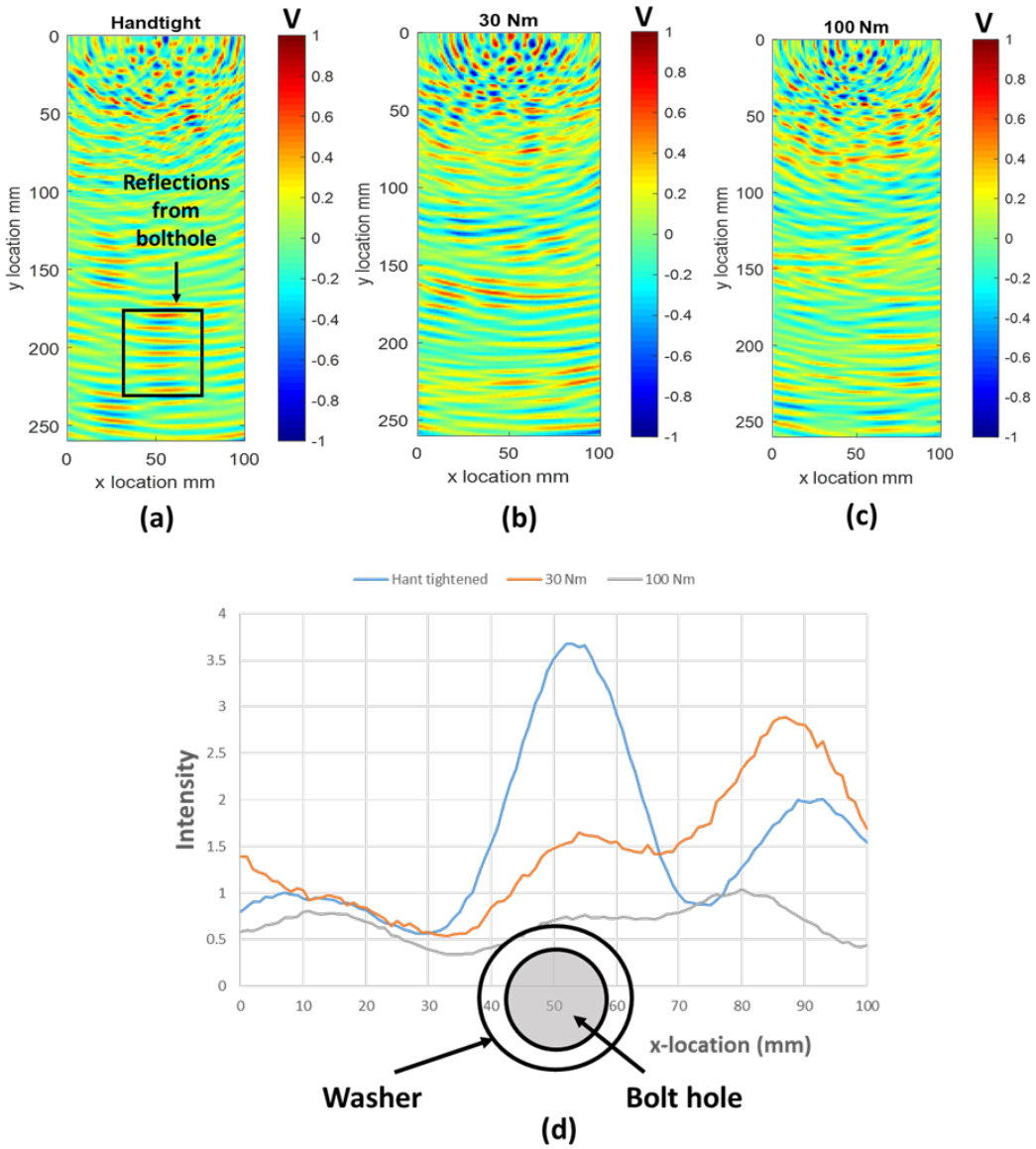

Figure 4- 12: (a) Configuration A based ultrasonic scans for (a) hand tightened, (b) 30 Nm and (c) 100 Nm bolt torque single joint, (d) intensity variation

4.3.5 Configuration B

Figure 4-13 shows the results for Configuration B at different bolt torques. Compared to Configuration A, a much clearer pressure band is observed at different torque levels. In case of hand tight and a torque of 30 Nm, the dominant reflections are from the bolthole. At a torque of 50 Nm, the reflection from the hole is relatively faint with a sign of lateral spreading. This indicates the spreading of the contact area between the plates with increasing torque. The signal further spreads laterally with torques of 70 Nm and 100 Nm with the bolthole scarcely identifiable. At this stage, significant areas of the joint are in contact beyond the hole. The new plate-to-plate interfaces reflect most of the energy with little contribution from the bolthole.

Clearly, Configuration B is better than Configuration A for monitoring bolt torque. The next step is to attempt to map the contact areas at different torques through the intensity plots.

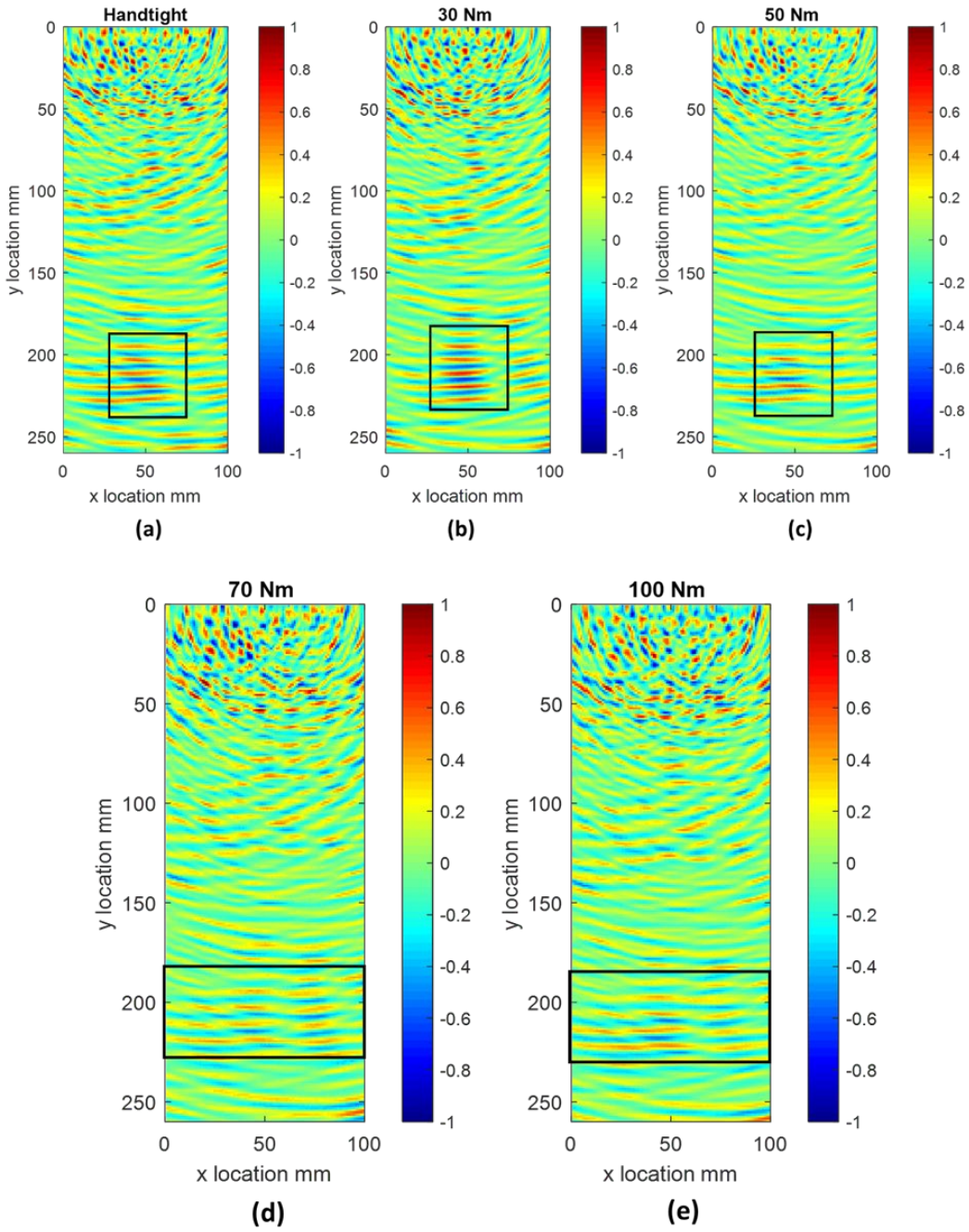

Figure 4- 13: Configuration B ultrasonic scans for (a) hand tightened (b) 30 Nm (c) 50 Nm (d) 70 Nm and (e) 100 Nm bolt torque

Figure 4-14 shows intensity variations obtained at different bolt torques. Figure 4-14a shows that at low torques there is a strong peak from the bolthole. With increasing torque, the reflected energy spreads resulting in gradual reduction in the amplitude of the peak corresponding to the bolthole and development of reflection away from the hole. Figure 4-14b presents the normalized representation of intensities. The initial peak corresponds to the centre

of the hole. As the torque increased, a strong alternate developed to the right of the hole at 80 mm. A weaker peak developed to the left of the hole at 20mm. They should correspond to the new contacts that have developed with increasing bolt torque. It can be seen that the contact areas are not symmetrical. It is expected as the plate undulations can be random, so does the contact area. This intensity normalization eliminates the requirement of baseline comparison to estimate the bolt preload. The reported conclusions are generic and can be applied to any number of joints.

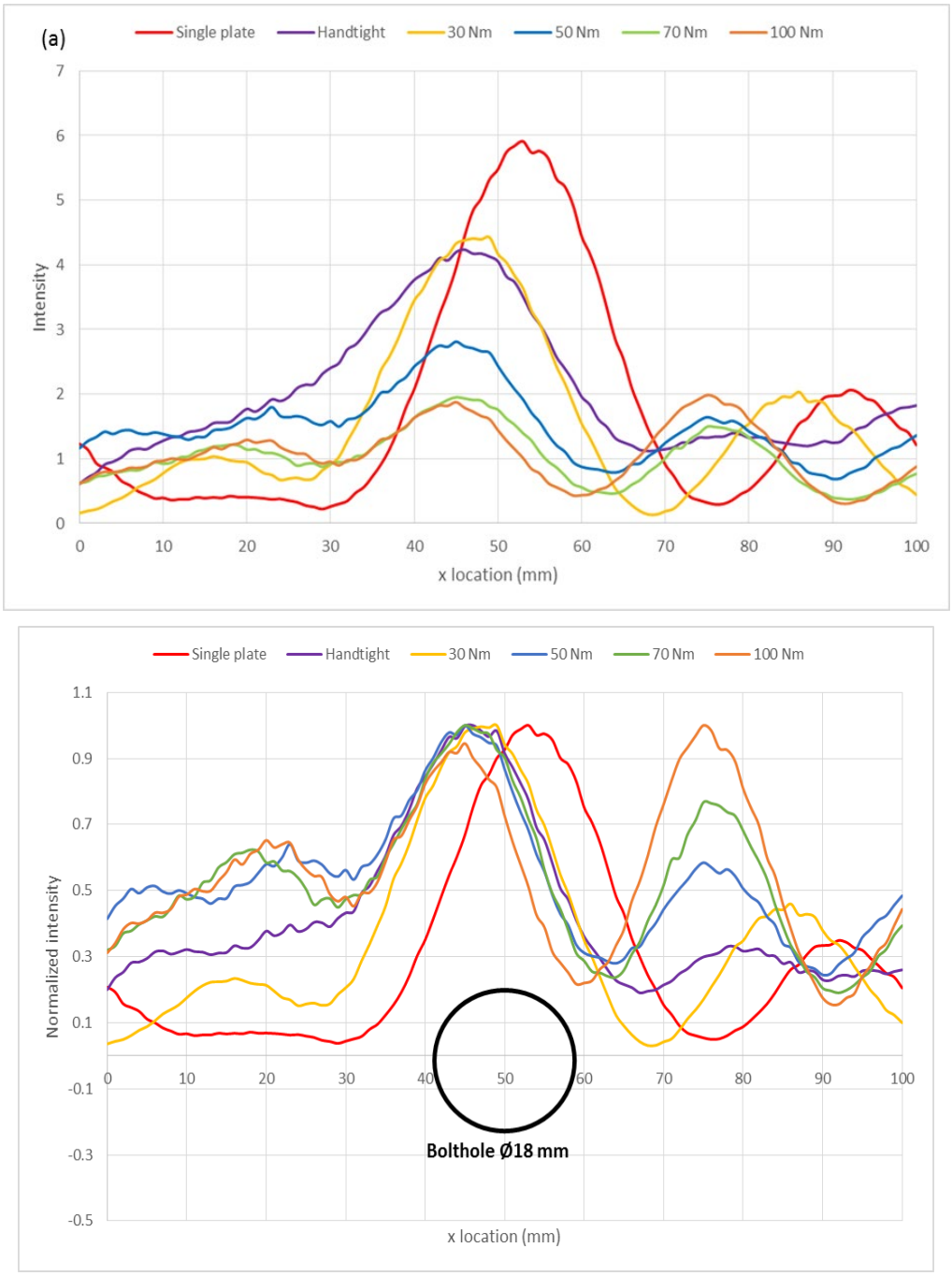

Figure 4- 14: (a) Raw intensity and (b) normalized intensity variation at different torque levels

Figure 4-15 shows the contours of the estimated contact pressure. Until the torque of 30 Nm, the contact is mainly around the bolthole. Above that torque, the contours spread on both sides of the hole. The new contact areas grow with the increasing torque. At 100 Nm torque, the side pressures exceed that of the pressure at the centre. This torque also corresponds to the maximum possible tightening that could be achieved manually without damaging the specimen.

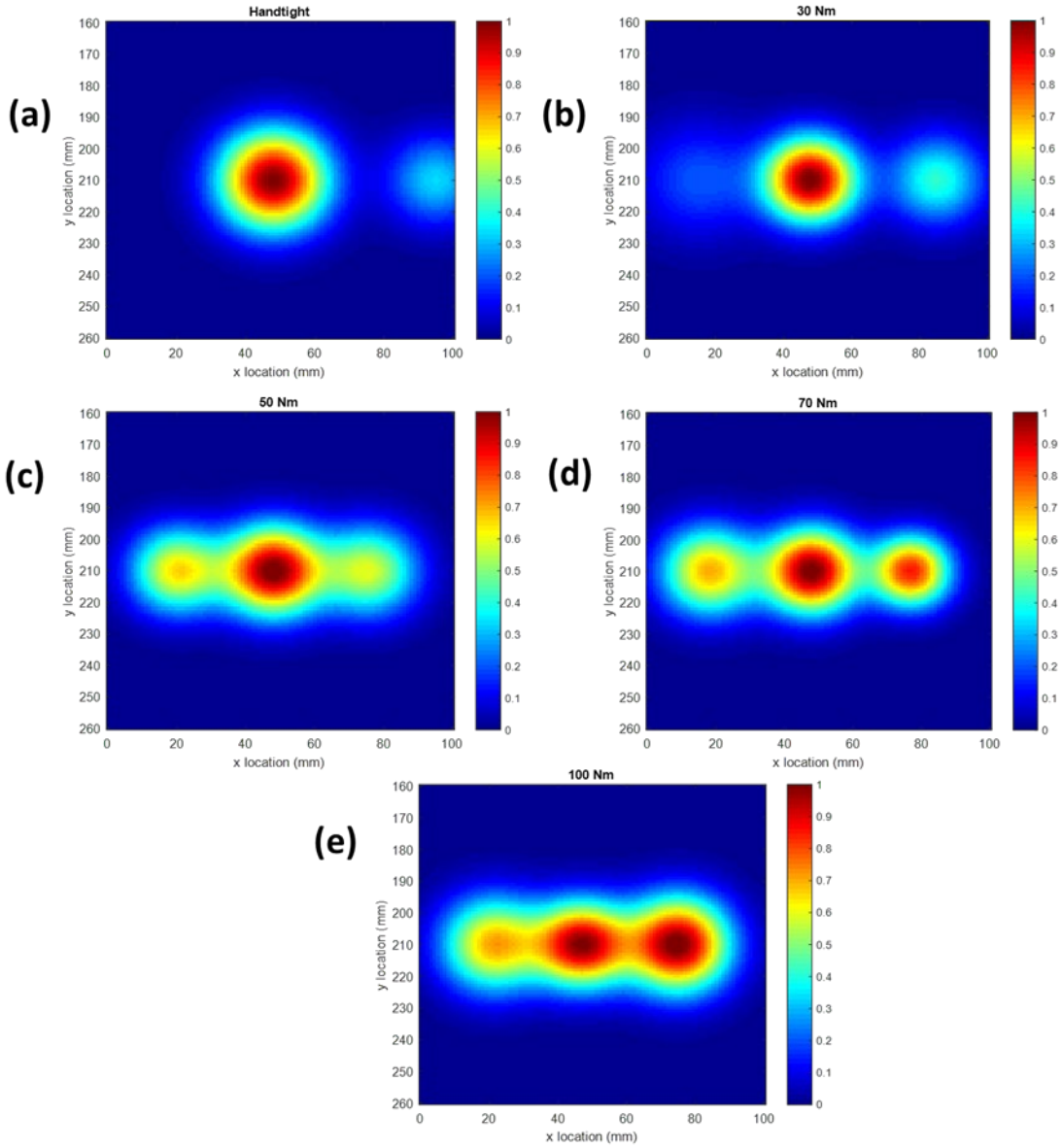

Figure 4- 15: Contact contours for Configuration-B scans of single bolt joint at (a) hand tightened (b) 30 Nm (c) 50 Nm (d) 70 Nm and (e) 100 Nm torque

Based on this experiment, it is concluded that Configuration B is more suitable for the scanning of bolt torque. As the bolt torque increases the contact area spreads on both sides of the hole.

However, they may not be symmetric depending on the undulations in the plates. The next section presents the scans for a double bolted joint.

4.3.6 Double joints

Figure 4-2b showed the joint under inspection. A set of thirteen equidistant patches was used for the scanning. Two bolts are referred as B1 and B2. Figure 4-16 shows pressure band at bolthole locations for a single plate with two boltholes. Similar to single plate results, intensity variation in the chosen window of interest (x: 0-200 mm; y: 135-165 mm) is represented in the form of contact contours. Two bolthole locations can be clearly discerned in the Figure. Based on single joint analysis, the whole idea is to achieve adequate bolt torque when we observe relatively less reflection from bolthole or laterally distributed contact contours.

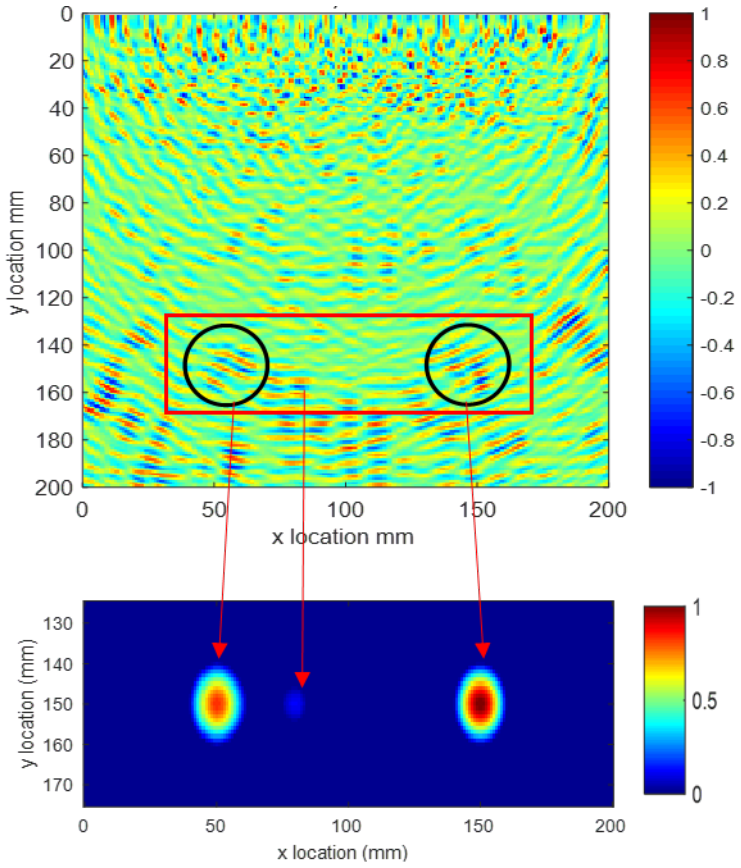

Figure 4- 16: Ultrasonic scan and its corresponding contact contour of a single plate with two boltholes

Figure 4-17 shows ultrasonic scans of the double bolt joint specimen at different torque levels. Figure 4-17a shows that similar to the single joint case, reflections from boltholes are prominent when 30 Nm torque has been applied to both B1 and B2. Significant patches of reflections from the back and side walls are also visible. In Figure 4-17b, the applied a torque at B1 is 100 Nm while B2 has 30 Nm. It can be seen that reflection from B1 is significantly smeared whereas B2 still shows significant reflection from bolt hole. When both the bolts have

a torque of 100 Nm (Figure 4-17c), the reflections from the bole hole has almost disappeared and a more distributed patch of lower pressure amplitude is obtained. The reflections from the back wall are also less prominent indicating that wider contact area between the plates have allowed less wave energy to reach the back wall.

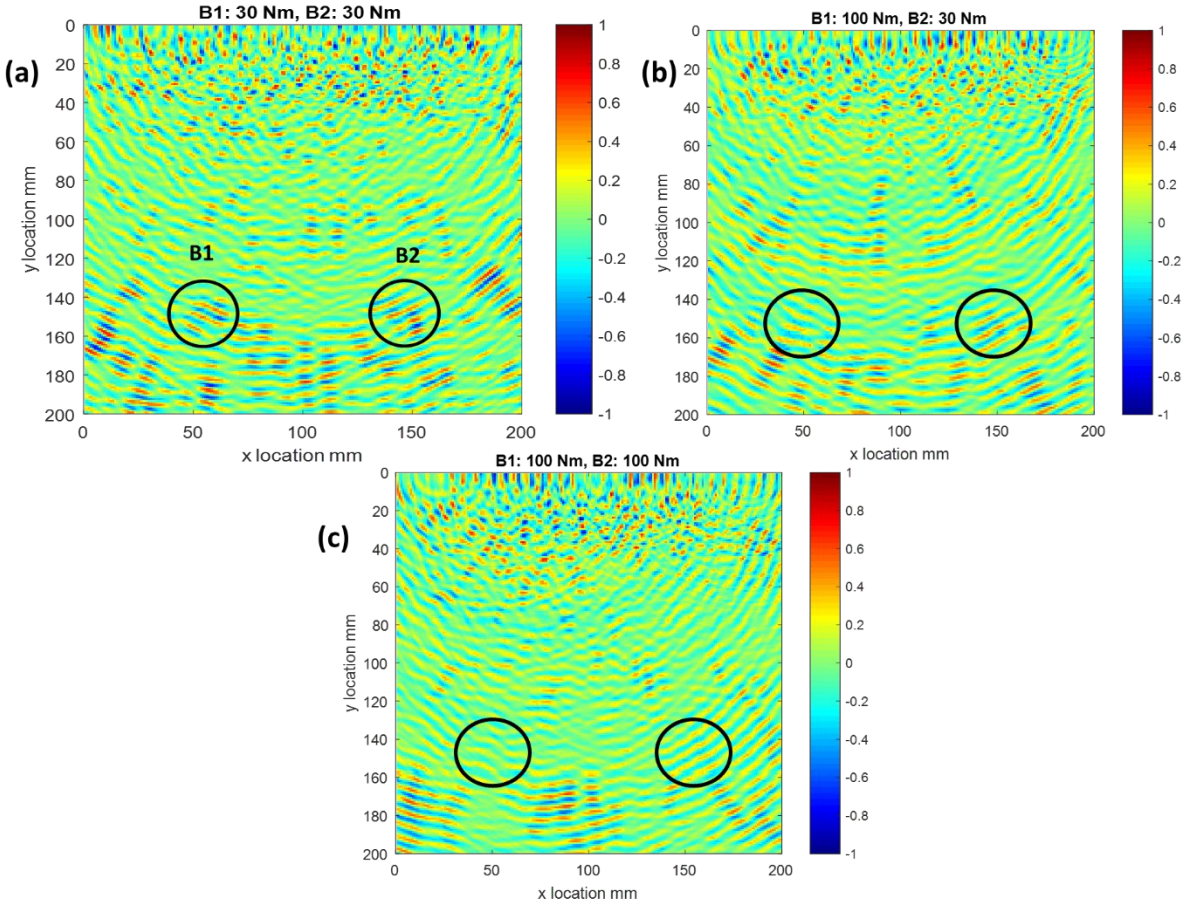

Figure 4- 17: Configuration B ultrasonic scans for double joints tightened at (a) 30 Nm each, (b) 100 Nm and 30 Nm (c) 100 Nm torques each

Figure 4-18 shows the normalized intensities in the imaging domain for different torques. It can be observed that at 30 Nm a clear peak at the bolt location is obtained. When B1 had a torque of 100 Nm, the peak corresponding to B1 diminished and a number of other peaks appeared around that location. The new peaks can be attributed to the new contacts developed between the plates. B2 at 30 Nm still retained the original peak at the location of the bolt. For 100 Nm torque on each bolt, the peak at B2 diminished and smaller peaks developed as in case of B1 when it was applied with 100 Nm torque.

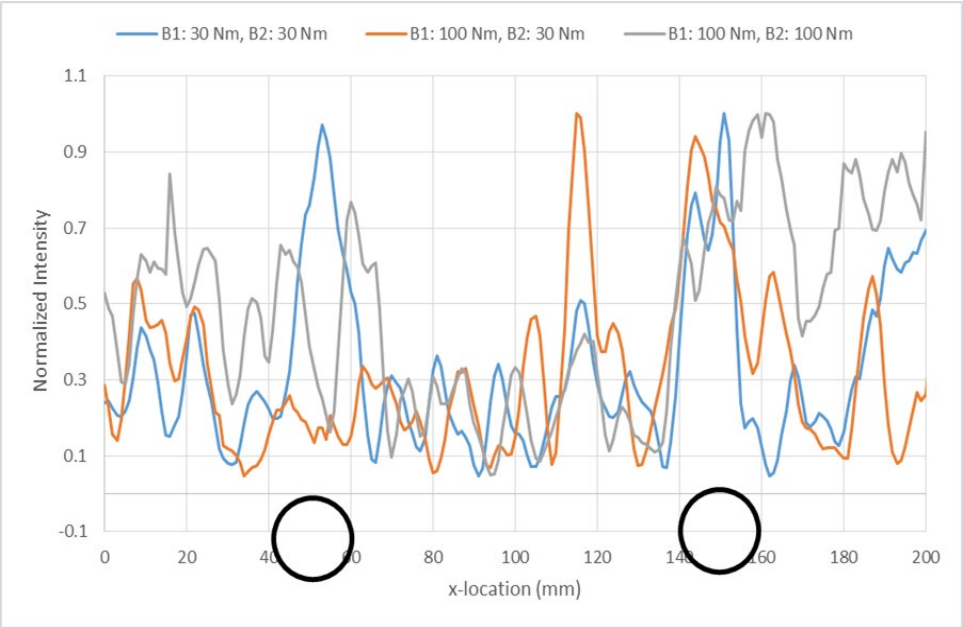

Figure 4- 18: Normalized intensity variation throughout the imaging domain

The smoothening of these curves using a Gaussian fit was done for the development of contact contours. Figure 4-19 shows the contact contours for various torques at B1 and B2. For 30 Nm bolt torque at both B1 and B2 (Figure 4-19a), understandably, the contours are concentrated around the bolt holes with some smaller contact areas. In Figure 4-19 b, B1 is at 100 Nm while B2 is at 30 Nm torque. In B1 the contact area has spread while that at B2 has remained close to Figure 4-19a. The contours are well spread out along the bolt line in Figure 4-19c as the torque reaches 100 Nm at both B1 and B2. Thus, the present scanning methodology has been able to realistically map the contact pressures with varying bolt torques.

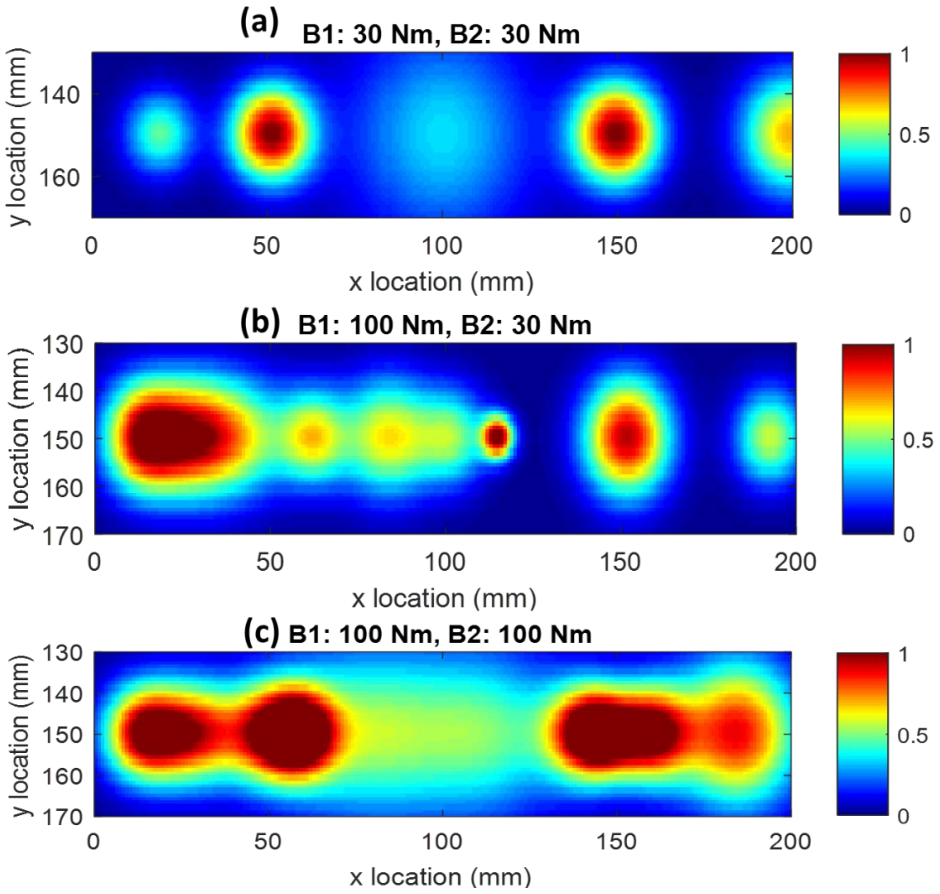

Figure 4- 19: Contact contours for (a) both bolts at 30 Nm torque; (b) 100 Nm and 30 Nm and (c) both at 100 Nm

Concluding remarks

This paper presents a non-destructive experimental study to monitor torque in steel plate joints with single and multiple bolts. Ultrasonic signals generated through surface bonded piezoelectric patches have been used to monitor the bolt torque level. The joint has been studied in reflection mode. An imaging technique has been developed to provide a visual representation of contact pressures developed due to bolt torque. Following are the major conclusions from the investigation:

- Ultrasonic wave transmission across the bolted interface increases with the increase in torque. This information can be used for determining the quality of contact between the bolted plates.
- The scanning of plate interface provides efficient bolt torque monitoring over a wide range of torque values than the washer-plate interface scanning.
- Reflection of ultrasonic signal from interfacial gaps can be utilized to calibrate the torque levels of joints.
- Reflection from a bolt hole is prominent at low torque values whereas laterally spread reflections around bolt hole represent joints with higher torque. This information is generic and does not require any baseline comparison.

This investigation demonstrates the success of the present baseline free imaging technique for relatively simple geometries. It needs to be further investigated for more complex geometries where multiple reflections from the bolts may overlap. In such a case, it may be imperative to use the baseline signature of the joint to improve the efficacy of the method. Performance of the present technique for complex joints is being investigated and will be reported in future.

Acknowledgement

This research has received financial support from Australian Research Council Linkage Project grant LP150100475. We would also like to thank our colleague Subhra Majhi for his initial help with the imaging methodology.

References

Ahn, J., et al. (2016). Clamping force loss of high-strength bolts as a result of bolt head corrosion damage: Experimental research A. *Engineering Failure Analysis, 59*, 509-525.

Akinade, O., et al. (2015). Waste minimisation through deconstruction: A BIM based Deconstructability Assessment Score (BIM-DAS). *Resources, Conservation and Recycling, 105*, 167-176.

Amerini, F., et al. (2010). Detecting loosening/tightening of clamped structures using nonlinear vibration techniques. *Smart Materials and Structures, 19*(8), 085013.

Amerini, F., et al. (2011). Structural health monitoring of bolted joints using linear and nonlinear acoustic/ultrasound methods. *Structural Health Monitoring, 10*(6), 659-672. doi:10.1177/1475921710395810

Anttila, L., et al. (2013). *Cancellation of power amplifier induced nonlinear self-interference in full-duplex transceivers.* Paper presented at the 2013 Asilomar conference on signals, systems and computers.

Beniwal, S., et al. (2015). Defect detection around rebars in concrete using focused ultrasound and reverse time migration. *Ultrasonics, 62*, 112-125.

Bickford, J. (2007). *Introduction to the Design and Behaviour of Bolted Joints*: Bpca Raton: CRC Press.

Chaki, S., et al. (2007). Combination of longitudinal and transverse ultrasonic waves for in situ control of the tightening of bolts.

Chen, X., et al. (2012). Load-differential imaging for detection and localization of fatigue cracks using Lamb waves. *NDT & E International, 51*, 142-149.

Degertekin, F., et al. (1996). Single mode Lamb wave excitation in thin plates by Hertzian contacts. *Applied Physics Letters, 69*(2), 146-148. doi:10.1063/1.116902

Doyle, D., et al. (2009). Damage Detection in Bolted Space Structures. *Journal of Intelligent Material Systems and Structures, 21*(3), 251-264. doi:10.1177/1045389X09354785

Fierro, G., et al. (2018). IWSHM 2017: Structural health monitoring of the loosening in a multi-bolt structure using linear and modulated nonlinear ultrasound acoustic moments approach. *Structural Health Monitoring, 17*(6), 1349-1364. doi:10.1177/1475921718806141

Ghosh, D., et al. (2018). Reference free imaging of subsurface cracks in concrete using R ayleigh waves. *Structural Control and Health Monitoring, 25*(10), e2246.

Huang, Y., et al. (2009). Real-time monitoring of clamping force of a bolted joint by use of automatic digital image correlation. *Optics & Laser Technology, 41*(4), 408-414.

Huo, L., et al. (2017). Impedance based bolt pre-load monitoring using piezoceramic smart washer. *Smart Materials and Structures, 26*(5), 057004.

Jhang, K., et al. (2006). Estimation of clamping force in high-tension bolts through ultrasonic velocity measurement. *Ultrasonics, 44*, e1339-e1342.

Kimoto, K., et al. (2015). A finite difference method for elastic wave scattering by a planar crack with contacting faces. *Wave Motion, 52*, 120-137. doi:https://doi.org/10.1016/j.wavemoti.2014.09.007

Korpi, D., et al. (2014). Full-duplex transceiver system calculations: Analysis of ADC and linearity challenges. *IEEE Transactions on Wireless Communications, 13*(7), 3821-3836.

Lim, J., et al. (2015). Noncontact fatigue crack visualization using nonlinear ultrasonic modulation. *NDT & E International, 73*, 8-14.

Lowe M, B. (2013). DISPERSE. *Imperial College, London*.

Marshall, M., et al. (2006). Characterisation of contact pressure distribution in bolted joints. *Strain, 42*(1), 31-43.

Martinez, J., et al. (2012). A synthetic phased array surface acoustic wave sensor for quantifying bolt tension. *Sensors, 12*(9), 12265-12278.

Nikravesh, S., et al. (2017). A review paper on looseness detection methods in bolted structures. *Latin American Journal of Solids and Structures, 14*(12), 2153-2176.

Peairs, D., et al. (2004). Improving accessibility of the impedance-based structural health monitoring method. *Journal of Intelligent Material Systems and Structures, 15*(2), 129-139.

Shah, J., et al. (2019). Ultrasonic monitoring of corroding bolted joints. *Engineering Failure Analysis, 102*, 7-19.

Sun, Q., et al. (2019). Bolt preload measurement based on the acoustoelastic effect using smart piezoelectric bolt. *Smart Materials and Structures, 28*(5), 055005.

Wallace, I., et al. (2000). Direct tension indicating washers. In: Google Patents.

Wang, T., et al. (2013). Review of bolted connection monitoring. *International Journal of Distributed Sensor Networks, 9*(12), 871213.

Wang, T., et al. (2013). Proof-of-concept study of monitoring bolt connection status using a piezoelectric based active sensing method. *Smart Materials and Structures, 22*(8), 087001.

Yang, J., et al. (2006a). Detection of bolt loosening in C–C composite thermal protection panels: I. Diagnostic principle. *Smart Materials and Structures, 15*(2), 581.

Yang, J., et al. (2006b). Detection of bolt loosening in C–C composite thermal protection panels: II. Experimental verification. *Smart Materials and Structures, 15*(2), 591.

Yang, Y., et al. (2018). Bolted joint integrity monitoring with second harmonic generated by guided waves. *Structural Health Monitoring, 18*(1), 193-204. doi:10.1177/1475921718814399

Yasui, H., et al. (1999). Ultrasonic measurement of axial stress in short bolts with consideration of nonlinear deformation. *JSME International Journal Series A Solid Mechanics and Material Engineering, 42*(1), 111-118.

Yu, L., et al. (2015). Crack imaging and quantification in aluminum plates with guided wave wavenumber analysis methods. *Ultrasonics, 62*, 203-212.

Zagrai, A., et al. (2010). Piezoelectric wafer active sensor structural health monitoring of space structures. *Journal of Intelligent Material Systems and Structures, 21*(9), 921-940.

Zhang, M., et al. (2017). Application of subharmonic resonance for the detection of bolted joint looseness. *Nonlinear dynamics, 88*(3), 1643-1653.

Zhang, Z., et al. (2017). Vibro-acoustic modulation (VAM)-inspired structural integrity monitoring and its applications to bolted composite joints. *Composite Structures, 176*, 505-515.

Zhao, N., et al. (2019). A nonlinear ultrasonic method for real-time bolt looseness monitoring using PZT transducer–enabled vibro-acoustic modulation. *Journal of Intelligent Material Systems and Structures, 31*(3), 364-376. doi:10.1177/1045389X19891534

Chapter: 5 Monitoring of Corroding Steel Bolted Joints with Embedded Piezo Patches

Jay Kumar Shah[1] and Abhijit Mukherjee[2,*]

[1] PhD Candidate, Department of Civil Engineering, School of Civil and Mechanical Engineering, Curtin University, WA 6102

[2] Professor, Department of Civil Engineering, School of Civil and Mechanical Engineering, Curtin University, WA 6102

Abstract

Steel structures with bolted joints facilitate easy installation, dismantling and repurposing. However, these joints must be monitored over their service lives against degradation due to bolt loosening as well as corrosion. This study reports an experimental online monitoring technique using embedded piezo patches. Steel bolted joint with specific bolt torque has been fabricated and subjected to accelerated corrosion. Simultaneously, the joint was monitored using the ultrasonic guided waves produced by the embedded piezo-ceramic patches. The patch was excited by an input wave. The wave characteristics were determined by using a simplified model of the joint. From the experimental results, a hypothesis for the corrosion behaviour of bolted joints has been developed and validated using a detailed finite element model. The techniques have been used together to identify the most effective way for monitoring corrosion. It has been found that the transition of Lamb wave modes from individual plate to the overlapped region can be utilized to establish onset of interfacial corrosion. A correlation between these modes and the state of corrosion is established.

Keywords: Bolted steel joints; accelerated corrosion; ultrasonic monitoring; Lamb wave modes; numerical models

5.1 Introduction

Reusing and repurposing of built facilities is essential for sustainable construction. Bolted steel structures are ubiquitous as they can be easily built, dismantled and repurposed (Akinade et al., 2015). To ensure structural safety of the bolted joint, adequate contact pressure between the plates must be maintained throughout their service lives. However, bolts may become loose due to a variety of reasons and corrosion is one of the prime causes. Steel in the joint region is more susceptible to corrosion than in other areas as the complex geometry of the joint can create pockets for corrosion. Moreover, joints are more difficult to access and monitor. Corrosion induced material loss at bolt head results in loss of torque. The loss results in the

development of interfacial gaps between plates, which creates a passage for corrosive agents, which accelerates the degradation of the joint (Bayliss, 2004). However, early detection and intervention can avoid further rapid deterioration. Therefore, it is crucial to develop an efficient non-destructive technique for monitoring corrosion of bolted joints.

A review on various corrosion monitoring techniques is available in Agarwala et al. (Agarwala et al., 2000) and Pickthall et al. (Pickthall et al., 2011a). Visual inspection is a widely accepted inspection method, but it is limited to identifying rusts only when they are visible. Moreover, it is manual, hazardous, expertise dependent and expensive. Radiography techniques (Kriesz, 1979) can be used to identify corrosion induced thickness loss; however, it too is manual, requires expensive equipment and also poses radiation hazard to the user. Techniques like magnetic flux leakage and eddy current testing are sensitive to surface temperature and depth at which the damage is present (Pickthall et al., 2011a). However, they are difficult to automate. Technologies that monitor the joint by using mechanical waves can be automated for remote monitoring. These techniques record minute oscillations in the joint to determine its state. A class of these techniques detect the acoustic emissions at the time of corrosion. In this case, the sensors must operate all the time to capture the acoustic events. The induced wave techniques, on the other hand, can be operated at the will of the operator as they use a transmitter-receiver pair to monitor the joint. These techniques have the potential to offer a versatile, automated and fast inspection with cost efficient equipment (Raghavan, 2007). However, waves can disperse and attenuate rapidly making it difficult to scan a large structure.

Waves guided by the boundaries of structural elements can travel longer distances compared to bulk waves. Guided waves in plates propagate as a combination of Lamb modes (Rose, 2014). These modes have unique velocities and attenuation properties. Thus, it is possible to customize the inspection by proper selection of the modes. Some applications of Lamb modes for detection of hidden corrosion in aerospace structures have been reported (Silva et al., 2003; Terrien et al., 2007; Zhu et al., 1998b). Hidden corrosion has been observed through transmission and reflection of Lamb waves both experimentally (Zhu et al., 1998b) and numerically (Terrien et al., 2007). Scattering of symmetric Lamb modes was used as an indicator for corrosion in plate like structures using a non-contact laser system (Silva et al., 2003). Rathod et al. (Rathod et al., 2011) monitored corrosion using a circular array piezoelectric transducers and localize the corrosion pits. A computerized ultrasonic tomography was conducted to localize corrosion induced mass loss in aircraft parts (Hay et al., 2006). Mukherjee et al. (Sharma et al., 2015a; Sharma et al., 2015c) conducted ultrasonic scanning of corroding steel plates in submerged condition using the water as a couplant. They

were able to create an image of the corroded areas. All these studies are done only on relatively simple plate geometries without any joint.

Joints are observed to suffer higher corrosion than members due to their complex geometries that can create pockets for accumulation of moisture and corrosive chemicals. In case of bolted joints, the geometry is further complicated by the presence of multiple bolts that may have uneven torque levels. Ultrasonics can be used in monitoring bolt torques. Conventionally, bolt torques have been monitored by wave propagation through bolt itself (Chaki et al., 2006; Yasui et al., 1999a). However, this can generate information for only the bolt under inspection and monitoring a joint with many bolts can be tedious. Corrosion in the bolt head imposes another challenge for securing the transducers there. The entire joint can be monitored by using the plates instead of the bolt as waveguides (Shah et al.). Parameters such as wave energy (Shah et al., 2019; Wang et al., 2013) and phase shift (Doyle et al., 2010; Zagrai et al., 2010a) have been explored. Another approach is to extract the nonlinear features such as higher harmonics (Amerini et al., 2010a; Yang et al., 2019), sub harmonics (Zhang et al., 2017) and frequency modulations (Zhang et al., 2017; Zhao et al., 2020a) of wave-interface interaction to identify the onset of bolt loosening. These methods have been applied on fresh bolted joints and the authors are unaware of any prior report of investigation of corroding joints with these techniques.

Relatively fewer investigations are available on corroding bolted joints and most of them are through destructive tests. One of the challenges is to induce controlled corrosion in bolted joints. Anodic current technique has been applied for inducing accelerated corrosion and observe its effect on fatigue (Zampieri et al., 2017) and tensile strength (Wang et al., 2020) of bolted joints. Ahn et al. (Ahn et al., 2016) experimentally investigated the loss of clamping force due to artificially induced corrosion damage to the bolt head. They further monitored its effect on tensile load bearing capacity of the joint (Kim et al., 2016b). Paolo et al.(Zampieri et al.,2017) numerically investigated the change in interfacial properties due to corrosion damage to the bolt head. The studies revealed severe reduction in the capacity of bolted joints due to corrosion. Thus, a non-destructive technique for monitoring corroding bolted joint is essential.

The authors, for the first time, have used ultrasonic guided waves to create images of the plate contact areas in bolted joints (Shah et al. 2020). They also reported ultrasonic wave based inspection of corroding bolted joints initially tightened at different torque levels (Shah et al., 2019). It was observed that corrosion damage depends on the level of bolt tightening achieved. The study highlighted that it is essential to detect corrosion at its onset to ensure the safety of the joint. Previous research has used the attenuation of wave amplitude when it passes through

the joint as a measure of corrosion. However, wave amplitudes may alter due to a variety of reasons. Some research on adhesively bonded joints have reported variations in Lamb wave modes when they pass through the joint (Lowe et al., 2000b; Puthillath et al., 2013). This technique is not dependent on wave attenuation; however, it is not directly applicable for bolted steel joints because in adhesive joints, the bond is achieved through adhesion while in case of bolted joints it is achieved through the contact pressure generated by means of bolt torque. Thus, bolted joints have a variable contact pressure, which gradually diminishes away from bolt. Formation of rust at the plate interface progressively alters the contact pressure. Varying contact between plates is likely to alter the Lamb modes, thus give a clue to the onset of corrosion.

5.2 Research framework

This study reports an online ultrasonic investigation of bolted joints subjected to a controlled corrosion. The parameters for ultrasonic investigation were selected based on the Lamb modes of the waveguide. The joint was regularly monitored throughout the process of corrosion using an embedded ultrasonic setup. Figure 5-1 shows the outline of the present investigation. It has three major components: 1) simplified simulation to identify the modal characteristics; 2) experimental observations and 3) numerical validation. A simplified simulation of the guided wave passing through the joint is performed to determine the suitable input for the experimental work. The joint has been subjected to the guided wave while a controlled accelerated corrosion experiment has been performed. The experimental results have been analysed and validated with a detailed numerical model.

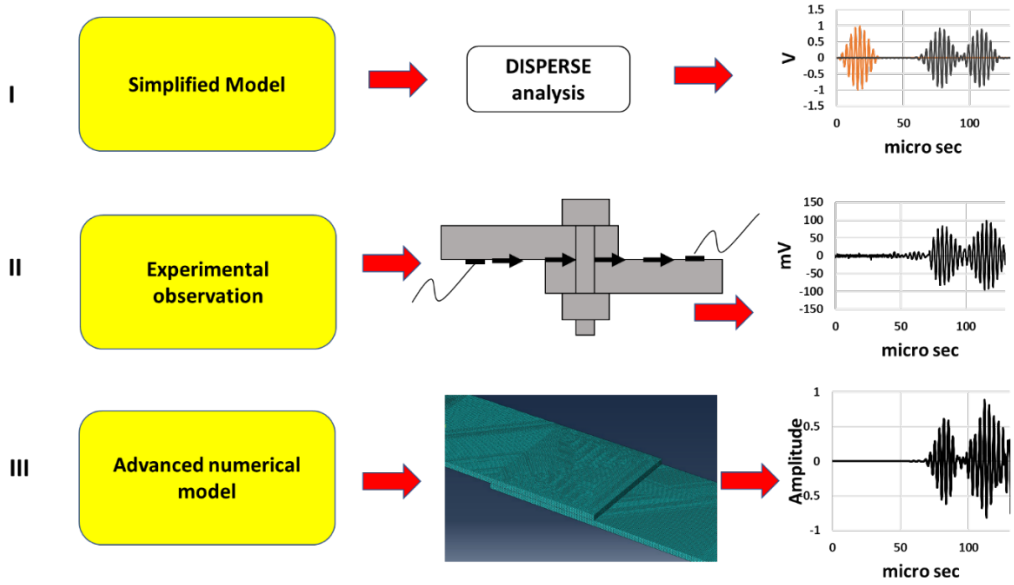

Figure 5- 1: Outline of the present investigation

5.3 Selection of input

In the joint, two plates overlap resulting in a sudden change in thickness of the plate. When the guided wave propagates through the joint, various symmetric and antisymmetric modes are generated. The existence of these modes and their corresponding group velocities depend on the excitation frequency and the thickness of the plate. When the thickness changes at the joint, the modes alter, and they can be vital in assessing the condition of the joint. However, to decipher individual modes from the received signal is challenging. Study of Lamb modes in two simple models, one consisting of just the plate and the other the overlap region, can be a vital tool. We have used DISPERSE (Lowe M, 2013) software for tracing the wave modes in the joint. The plate thickness is 5 mm and at the overlap it is 10 mm.

Figure 5-2 shows the variation of group velocities in steel with frequency-thickness product. We select a window from 1.5 to 3 MHz-mm. At the left end, only S0 and A0 modes exist while at the right end S0, A0, S1 and A1 modes are present. For the 5 mm thick plate, if we select a frequency of 300 kHz, the frequency-thickness product is 1.5 MHz-mm in the plate, but it is 3 MHz-mm at the overlap. Thus, when the wave passes through the plate only S0 and A0 modes would propagate while at the overlap additional modes are expected. The additional modes attenuate as the wave leaves the lap and renters the 5 mm thick region. However, these conversions would depend on plate undulations (Wang et al., 2013; Shah et al., 2019), contact pressure and bolt torque. When the bolt torque is minimal, the plates behave individually of 5 mm thickness. As the bolts are tightened, the effective thickness gradually rises to a maximum of 10 mm. Thus, the frequency band shaded in Figure 5-2 can offer a clue to bolt tightening. The velocity of the A0 mode is relatively steady through the band. Thus, we should expect a steady time of flight for this mode that can serve as a reference for determination of the movement of other modes. The velocity of the other modes varies significantly within the zone. Variations in their arrival times should reveal the condition of the joint.

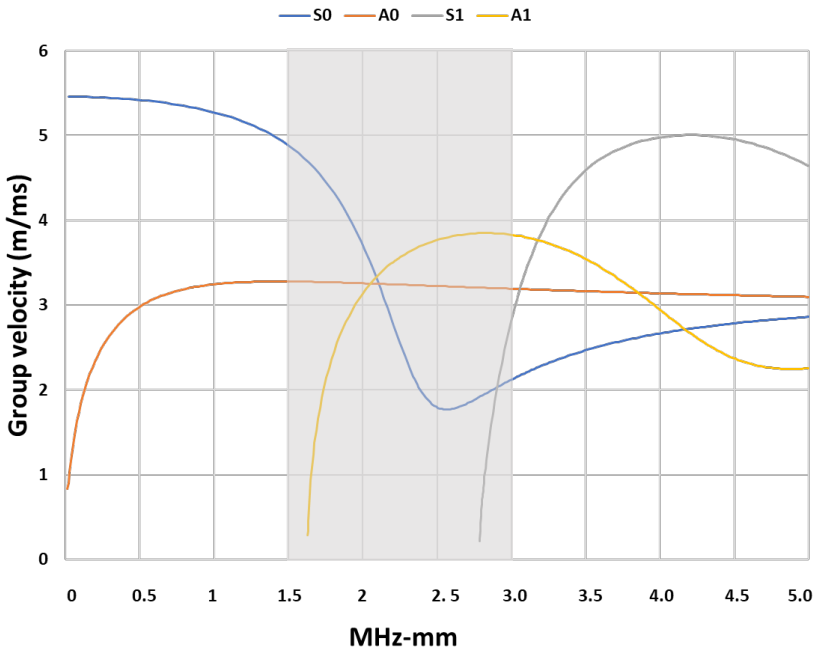

Figure 5- 2: Dispersion curves for the steel plate

Two plates of length 300 mm each and of thickness 5 and 10 mm were modelled using DISPERSE. They were subjected to a 10 cycle Hanning windowed sine input signal at 300 kHz frequency. Figure 5-3a presents the input and received signals for the 5 mm thick plate. Two distinct peaks are obtained. Figure 5-3b shows the modal contributions separately. It is confirmed that S0 arrives first at around 80 μs followed by A0 at 110 μs. In case of the 10 mm thick plate (Figure 5-3c) the distinct peaks are lost and a major peak at around 100 μs is discernible. Separation of the modal contributions (Figure 5-3d) reveals that four modes are present in this signal. It is also established that for 300 mm propagation distance, even the higher order modes such as S1 mode in 10 mm region contributes significantly to the total signal. Thus, with the chosen transducer location and signal, a significant change in the modal contribution is envisaged when the wave passes through the joint. It must be kept in mind that two plates of different thicknesses have been modelled in DISPERSE and the jump in thickness at the lap is ignored. However, this analysis lets us make a judicious selection of input wave parameters for the experimental investigation.

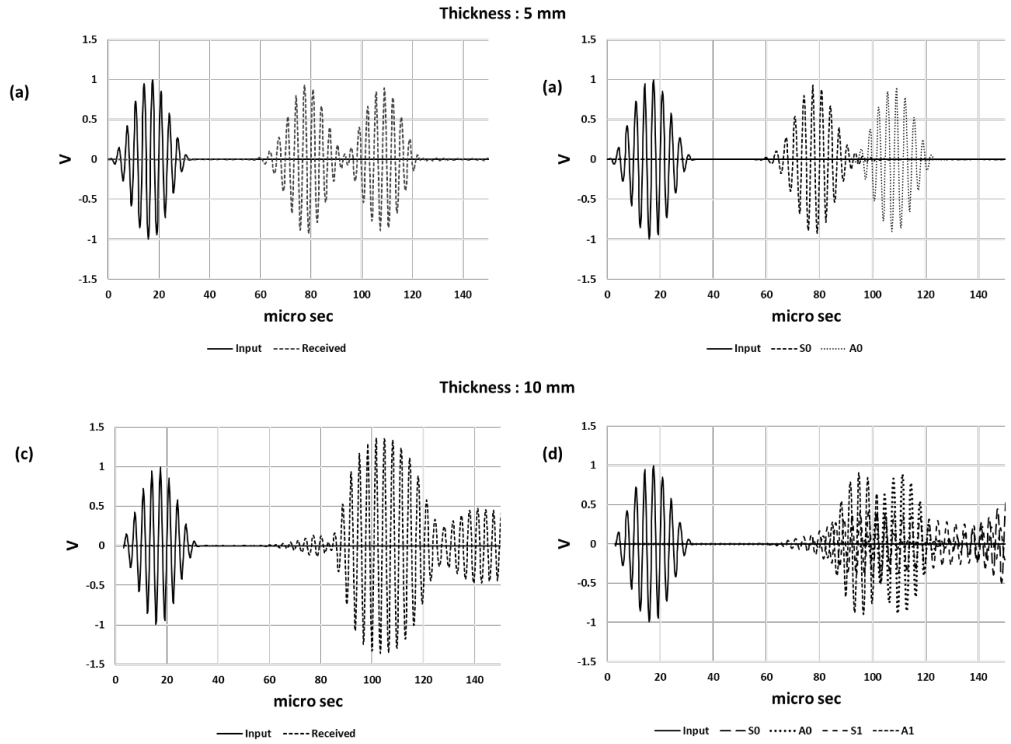

Figure 5- 3: Received signal (a & c) and the mode contributions (b & d) in a 5 mm and 10 mm thick steel plate.

5.4 Experimental work

The experiment was conducted on mild steel bolted joint specimens. Piezoceramic patches were surface bonded on the plates as ultrasonic transducers. The joints were subjected to accelerated anodic corrosion. Simultaneously, transmission of ultrasonic waves was studied.

Figure 5-4 presents the single bolted steel joint investigated in this study. It consisted of two 400 mm x 100 mm x 5 mm mild steel plates. The plates were lapped by 100 mm and bolted through a hole with an M16 fully threaded bolt. The bolt was given a torque of 100 Nm. This is the fully tightened condition.

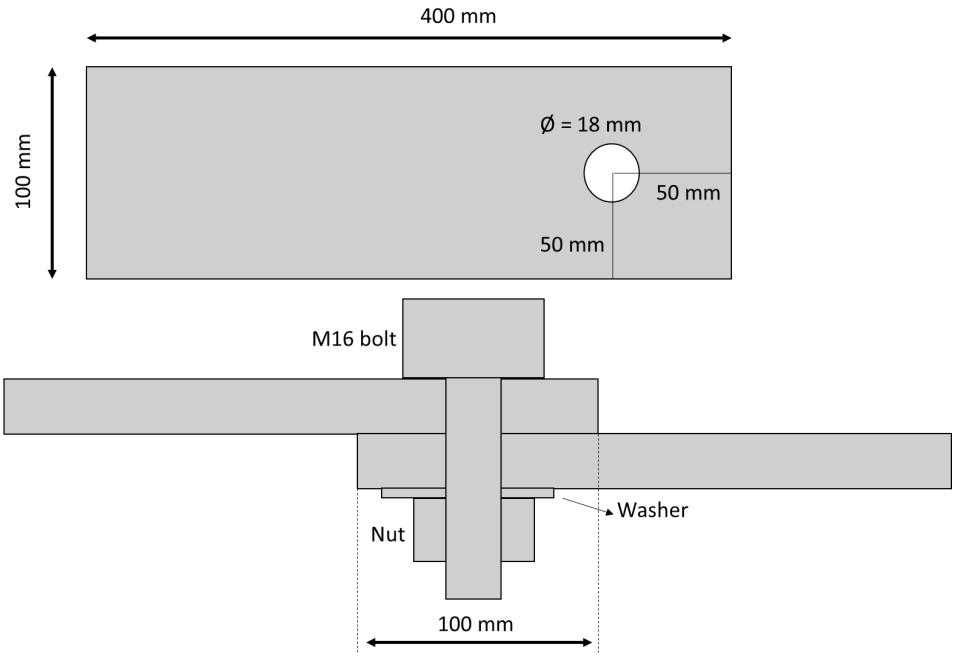

Figure 5- 4: Schematic of fabricated specimen

5.4.1 Accelerated corrosion

The specimen was subjected to electrochemical corrosion where the bolt head and the overlapped region of top plate are exposed to corrosive conditions. An electrolytic bath having 3.5% saltwater solution was secured on top plate with silicone gel, as shown in Figure 5-5. To accelerate the corrosion process, an electric circuit was formed with the bolt as anode and a metal rod dipped in the electrolytic solution as cathode of a DC power source. A constant current of 0.1 A was maintained in the circuit. The mass loss (m) in the specimen is governed by Faraday's law,

$$m = \left(\frac{It}{F}\right)\left(\frac{M}{z}\right) \tag{5-1}$$

where;

I = constant current applied for electrolytes

t = total time for which constant current is applied

M = molar mass of the corroding material in gram per mole

F = Faraday's constant (96500 C/mol)

z = valency number of ions of the corroding material

The details of corrosion mechanism can be found in our previous study (Shah et al., 2019).

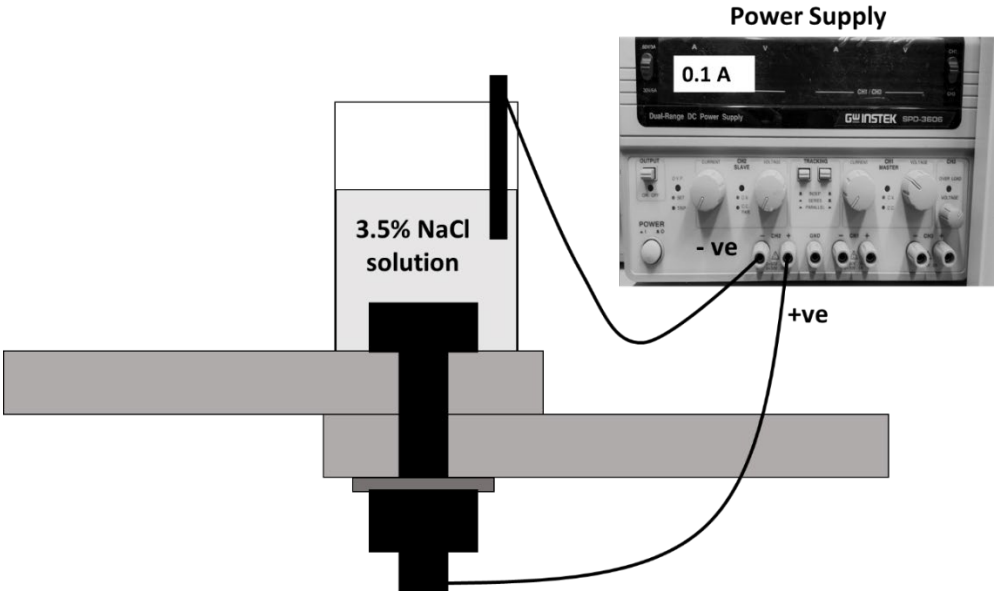

Figure 5- 5: Corrosion set up

5.4.2 Ultrasonic setup

The ultrasonic waves were generated by means of piezoceramic patches (10 mm dia, 0.5 mm thickness; Warsash Scientific) surface bonded on the plates. The patches were placed at the opposite sides of the joint as shown in Figure 5-6. One of them acts as transmitter and the other as receiver. A function generator (RIGOL DG1035) was used to generate ultrasonic signal. The signal was amplified with a power amplifier (Ciprian HVA 400 A) before being fed to the transmitting patch. The wave passes through the joint and is received by the patch placed on the opposite side. The received signal is digitized and recorded using a Picoscope and a computer. No amplification was used at the receiving end.

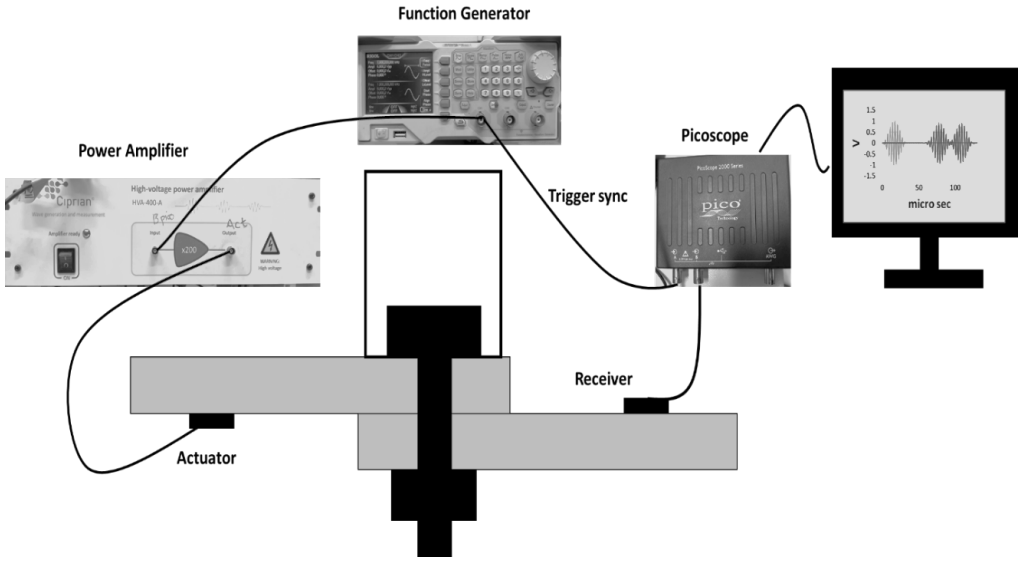

Figure 5- 6: Experimental setup for ultrasonic testing

5.4.3 Simultaneous corrosion and ultrasonic measurements

Each epoch of the experiment consisted of a phase of accelerated corrosion followed by ultrasonic monitoring. The total mass of the fresh specimen was 4018 grams. The joint was corroded to obtain an approximate mass loss of 2 grams as calculated from equation 1 (~20 hours/ epoch). Then the bath was emptied and left for air drying for 4 hours. It was followed by the ultrasonic measurements. The bath was filled with fresh saltwater for the next epoch. This cycle was continued until an estimated mass loss of 1% was achieved.

5.5 Experimental results

Figure 5-7a shows the signal recorded from the pristine joint. It is of interest to compare this signal with those generated through DISPERSE. In the single plate region of the joint, it is expected to observe modes corresponding to the 5 mm plate, while in the lapped region, additional modes as observed in the 10 mm plate (Figure 5-3c) can be expected. The experimental signal closely matches that of the 5 mm plate. The arrival time of the first two modes closely matches with that of S0 and A0 mode as found by DISPERSE for 5 mm plate (Figure 5-3b). Therefore, it can be stated that in the pristine plate, only the modes corresponding to the thickness of individual plates propagate. This result shows that although additional modes might have been generated in the overlap section, in case of bolted connection, they do not propagate from the overlap to the individual plate.

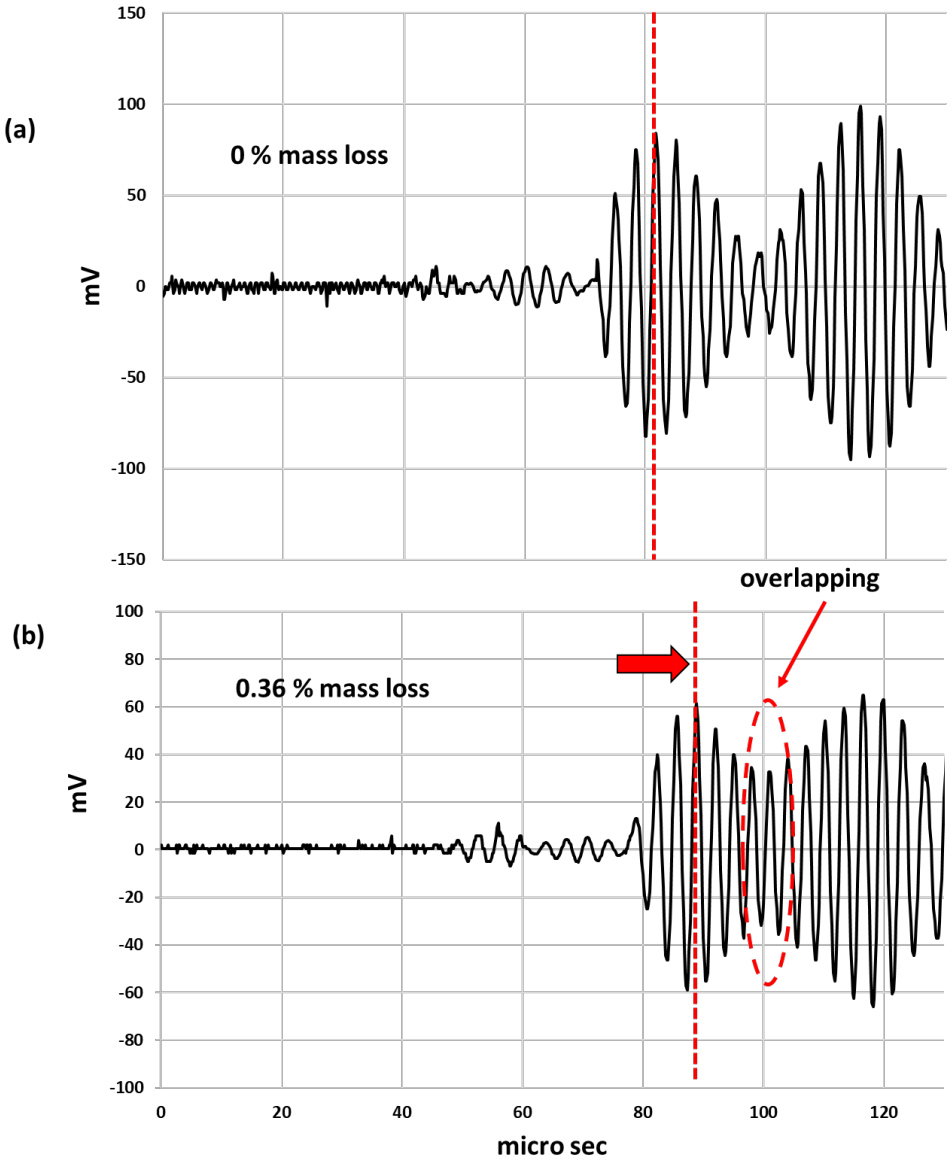

Figure 5- 7: Recorded signal for the specimen at (a) 0 % and (b) 0.36 % mass loss

In subsequent observation on the corroding joint, the pattern observed in the pristine specimen persisted for the first seven epochs of ultrasonic measurements. For 8th epoch (~0.36 % mass loss) as shown in Figure 5-7b, a noticeable change in the waveform was observed. A delay in the arrival time of first peak was observed whereas the arrival time of the second peak remained unchanged. As a result, the peaks, which were identified as S0 and A0 modes, got overlapped at around 100 µs. From the dispersion curves in Figure 5-3, it can be seen that as the plate thickness goes up from 5 mm the velocity of S0 goes down while that of A0 remains steady. Thus, the effect of corrosion at this stage is that of increasing the bond between the plates and thus increasing the effective thickness of the joint. From Figure 5-2, it is noticed

that as the effective thickness goes up from 5 mm, the velocity of mode A1 rises rapidly in comparison to that of A0 while S0 slows down. Therefore, we should expect higher contribution from A1 and relatively lower contribution from S0 within this time window, while A0 remains steady. As the thickness goes further up another mode, S1, approaches the velocity of A0. Hence, at that end, contributions from A0, A1 and S1 can be significant. From the modal distribution of Figure 5-3d, it is seen that for 10 mm plate thickness, contribution from A0, S1 and A1 dominates. Thus, the modal combinations give an excellent clue to the effective thickness of the joint. Along with the modal patterns the signal amplitudes were also noted. There is a noticeable drop in signal amplitude at 0.36% mass loss. This indicates that with advancing corrosion although the overlapped plates are behaving as a composite their interface is weakening due to accumulation of corrosion products.

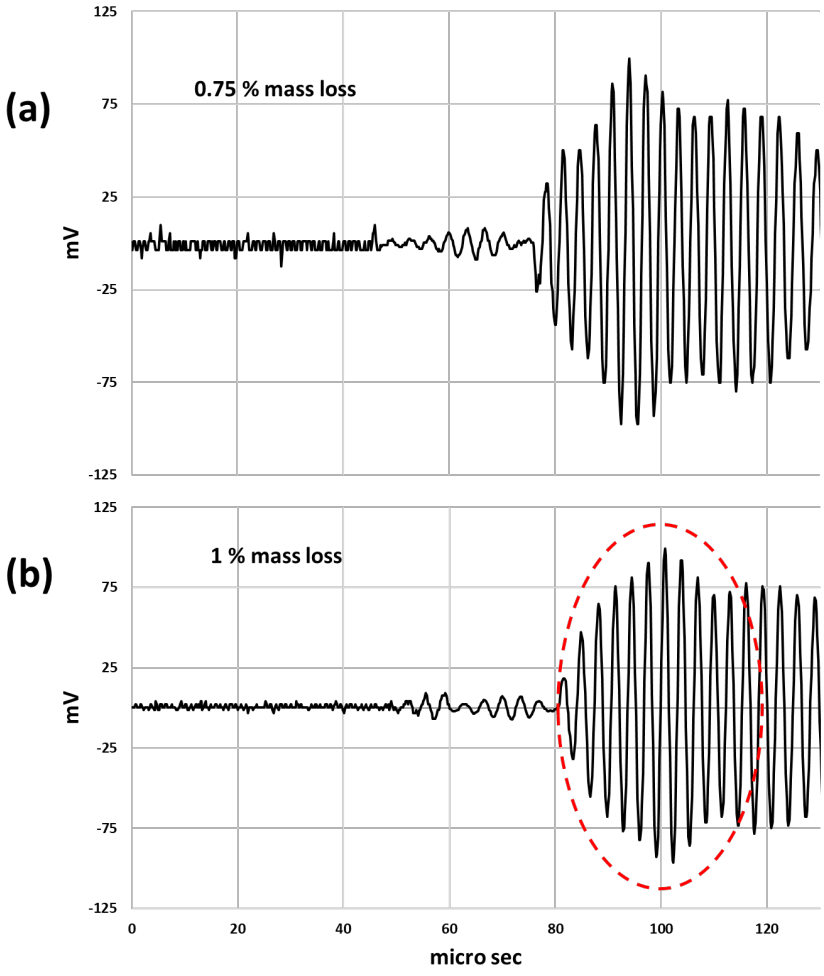

Figure 5- 8: Recorded signals for specimen at (a) 0.75 % and (b) 1 % mass loss

Figure 5- 8 shows the waveforms at 0.75 % and 1 % mass loss. It can be seen that the waveform emulates that of the 10 mm plate as obtained in Figure 5-3c. Thus, the effective thickness of

the plate at this stage is close to that of the sum of thicknesses of the individual plates. However, rust is significantly softer than steel. Although the corrosion products fill the void spaces between the plates, the softness is manifested through the drop in signal amplitude. Evidently, utilising the dispersion behaviour, the state of corrosion of the joint can be mapped.

5.6 Numerical Validation

To validate the hypothesis of the effective thickness presented in the previous Section a 3D finite element model was developed using ABAQUS® software. The model consists of the plates and the bolts as presented in Figure 5-4. The material properties are presented in Table 5-1. The interaction between the plates is modelled by imposing two conditions. In the areas where there is no relative displacement between the plates, a tied condition is used. Where there are gaps between the surfaces, a surface-to-surface interaction constraint is used. In this condition, the surfaces come in contact when there is compressive pressure, but they lose contact and move away from each other when pulled.

Table 5- 1: Material properties

Material	Density (kg/m^3)	Young's Modulus (GPa)	Poisson's ratio	Coeff friction
Mild steel	7800	200	0.3	0.2

In the vicinity of the tightened bolt, the contact pressure generated by the bolt tension keeps the plates in contact and there is no relative displacement between the plate surfaces. However, the contact pressure gradually goes down away from the bolt creating a condition when the plates can have space between them. This area is modelled with surface-to-surface interaction as shown in Figure 5-9. This condition affects the transmission of wave from one plate to the other. In the area where the two plates are in contact, the wave transmits through, while in the area they are separated, the wave reflects back. It is also to be noted that in case of tied surfaces, the plates behave like a composite of thickness measuring the sum of thicknesses of individual plates while in case of the surface-to-surface interaction, the composite action depends on the surface bonding properties chosen. At the pristine stage, the tied constraint is applied on a 30 mm square region around the bolt location while assigning interaction condition to the remaining area as shown in Figure 5-9.

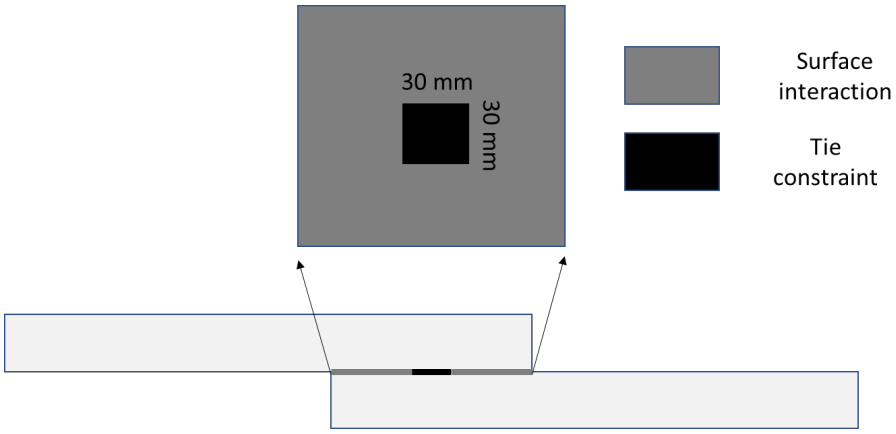

Figure 5- 9: Schematic for interfacial properties used to simulate pristine joint condition

Gradual increase in the composite behaviour due to corrosion of the joint has been modelled by expanding the tied fraction of the joint area while reducing the interaction zone. It is likely that the areas in the vicinity of the bolt would be filled by rust first gradually expanding to more remote areas. Figure 5-10 shows the interfacial conditions used in the model to simulate intermediate and advanced stage of corrosion.

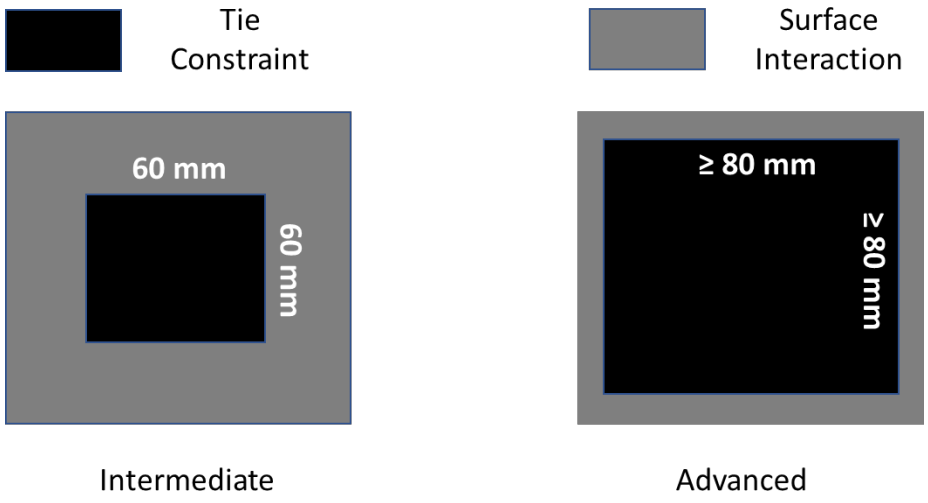

Figure 5- 10: Interfacial properties showing intermediate and advanced stages of corrosion

The model has been subjected to dynamic loading caused by the excitation from the piezo patches. An in-plane stress wave was generated by the application a force of 0.1 N maximum amplitude at the actuator location for ten cycles at a frequency of 300 kHz. Hanning window filter was used to simulate the experimental excitation. Dynamic explicit analysis has been performed at a time step of 10^{-7} s, which discretises each time period in about 30 time steps. Geometric non-linearities have been included in this analysis. Stresses were recorded at the

receiver location. It was averaged for 10 mm square region. The simulation was run for a total time period of 150 μs. It is sufficient to capture all the modes of interest.

5.6.1 Numerical simulation results

Figure 5-11 shows the effect of different interaction properties on the wave propagation across the lapped region. It can be seen that in the case of surface interaction, the compression waves propagate from the top plate to the bottom plate but the rarefaction waves do not. A significant portion of the wave energy remains trapped in the top plate, hence the specimen can be described as two interacting individual plates. For a tied interface, on the other hand, the signal transmission occurs both in compression and rarefaction phases. Thus, the joint behaves as a 10 mm thick composite.

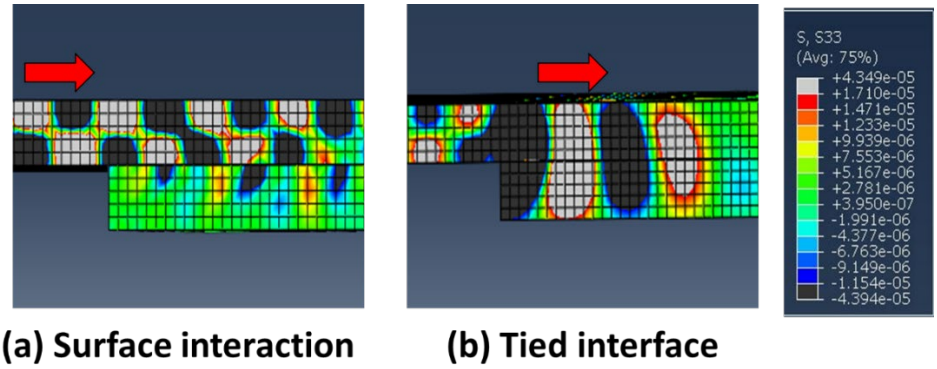

Figure 5- 11: Wave propagation across interface with (a) surface interaction and (b) Tie property

Figure 5-12 shows the waveform obtained for the pristine joint. It shows the two peaks as observed in the experiment. The timings of the peaks too agree very well with the experimental observation in Figure 5-7a. Based on the dispersion curves the peaks were identified as that of modes S0 and A0 (Figure 5-3b). This result validates our numerical model, especially modelling of the plate interfaces through the tie and the interaction conditions.

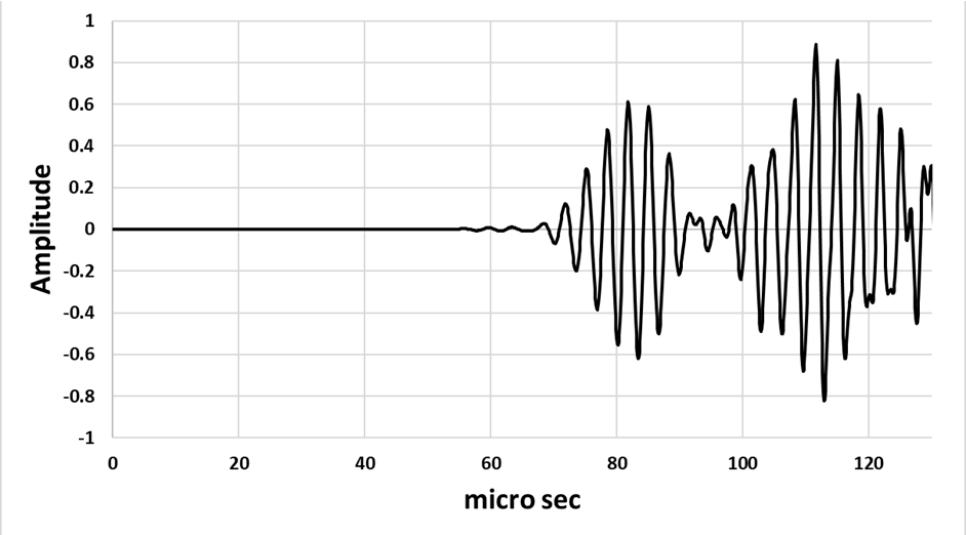

Figure 5- 12: Simulated result for a pristine joint

The tied zone of the model was gradually expanded to simulate corrosion. Figure 5-13a shows the waveform when the tied zone was 60 mm square. Clearly, the arrival of the S0 peak has been delayed, as expected. Also, the peaks have started to overlap as seen in the experiment after 0.36% mass loss (Figure 5-7b). As the tied area was increased further to 80 sqmm (Figure 5-13b) and 100 sqmm (Figure 5-13c), the distinct peaks gradually merged into one envelop. The waveforms have a close match with the experimentally observed ones after 0.75% and 1% mass loss. This validates the hypothesis that due to corrosion in the interfacial area, bolted joints behave increasingly like a plate of sum of thickness of the two joining plates. The overlapping of the distinct peaks is an excellent indicator of advancing corrosion.

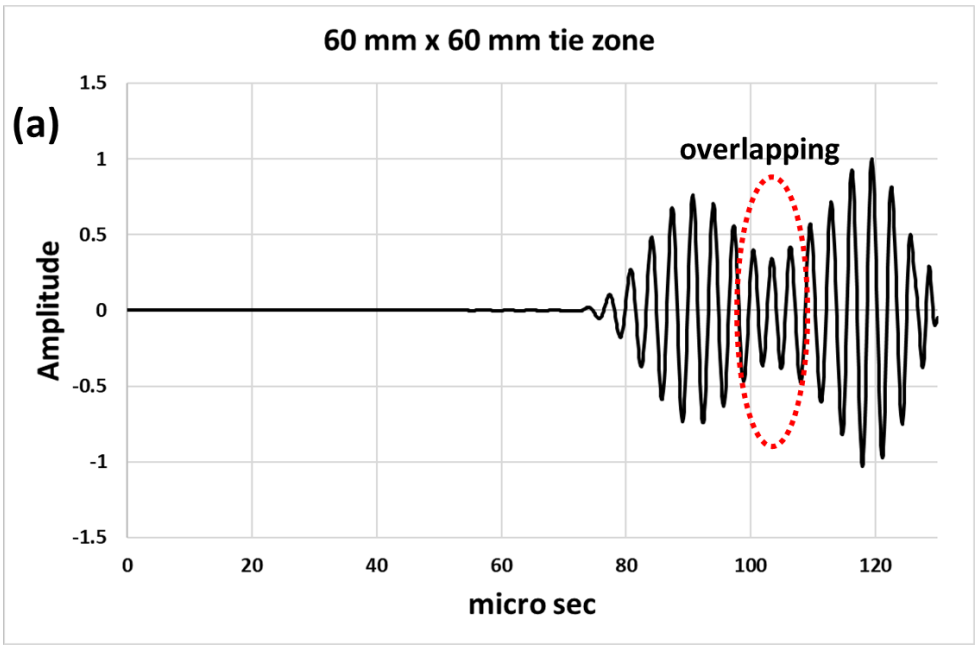

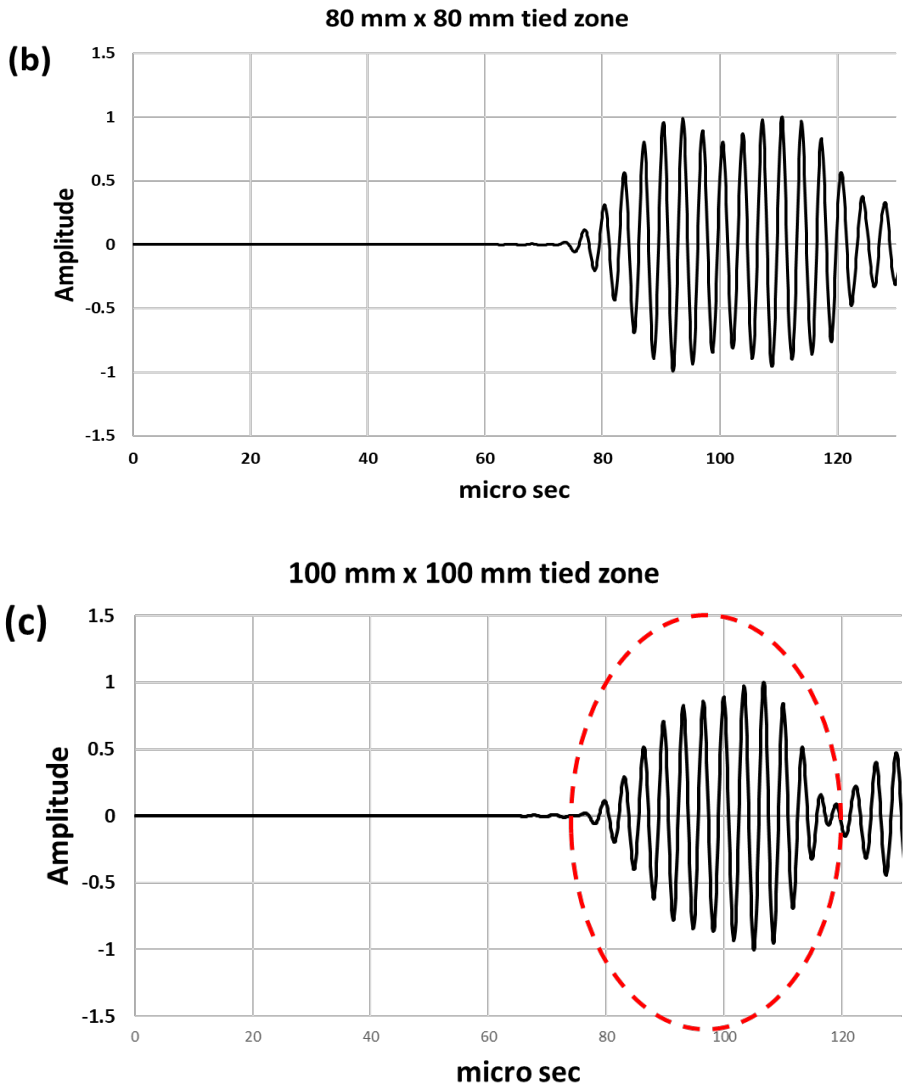

Figure 5- 13: Numerical results for (a) 60 mm (b) 80 mm and (c) 100 mm square tied region

5.7 Correlation of signals with corrosion

The energy (E) of the recorded signal in the time window 95 µs to 105 µs is used as a parameter to establish different stages of joint corrosion. The reason to choose this window is the gradual convergence of Lamb modes around 100 µs with the increase in corrosion. We have used equation 5-2 [19] to calculate the energy content.

$$E = \frac{1}{f_s}\sum_{t_i=95\mu s}^{t_f=105\ \mu s} V^2(t) \qquad (5\text{-}2)$$

Here f_s is the sampling frequency (6.25 MHz) and V is the amplitude of the signal at discrete times in the time window [t_i = 95 µs and t_f = 105 µs]. Prior to the calculation of E, the signal for each epoch of measurements was normalized with the respect to the maximum amplitude in that measurement. Different stages of interfacial corrosion can be discerned in the Figure 5-

14. The E remains relatively steady initially which can be associated with the time period when the initial mass loss takes place at the bolt head. This leads to the weakening of the interfacial contact hence creating pockets for the rust formation. A significant jump in the E at 0.36 % mass loss establishes the onset of interfacial corrosion. It resulted in the delay in the first peak as observed in Figure 5-7b. This was followed by further increase in E with the progress of corrosion. For higher mass loss, further increase in the E was observed representing the advanced stage of interfacial corrosion.

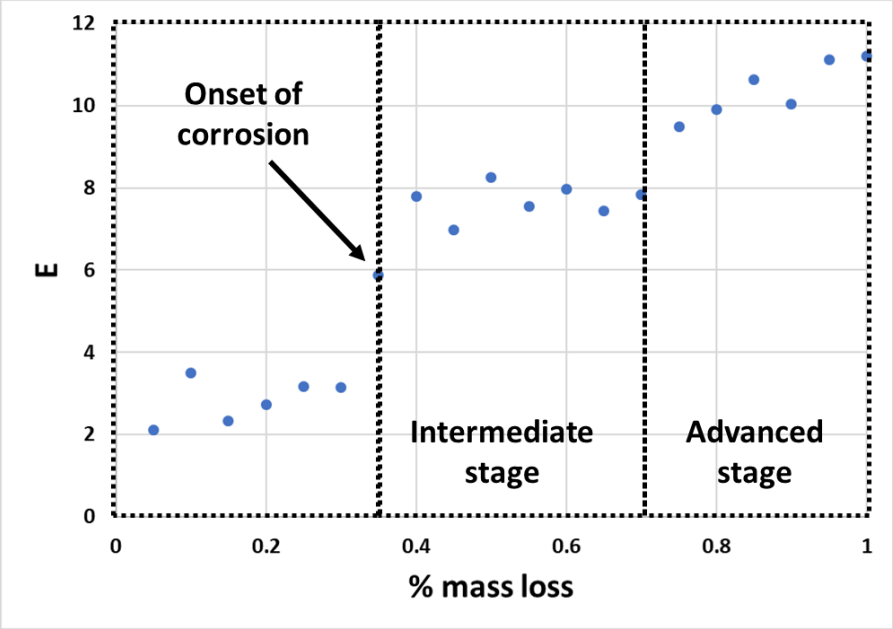

Figure 5- 14: (a) Variation in the energy with the % mass loss

Concluding remarks

This paper reports an experimental and numerical investigation on corroding bolted joint. A bolted joint specimen was subjected to accelerated corrosion and its effect was monitored through non-destructive ultrasonic testing. The corresponding to the Lamb wave modes are traced in the signal with advancing corrosion. Numerical studies using DISPERSE and ABAQUS® software are conducted to understand the outcome of experimental studies. Following are the major findings:

- A window of 1.5 to 3.0 MHz-mm is ideal for inspection of joints. Within this window, the relative contributions and velocities of different modes vary greatly while one reference mode remains steady. Thus, the interfacial bonding between the plates of a joint can be discerned by observing the passage of guided Lamb wave through the joint.
- The analysis of Lamb modes in single plate and overlapped region gives an insight to the experimental outcome.

- The propagating signal in pristine joints is dominated by Lamb wave modes of individual plates.
- Formation of rust at the interface increases the contact between the plates by filling up the interfacial voids. It can be tracked by the transition of wave modes in the propagating signal. As the corrosion advances, the joint behaves more as a composite.
- The generation of new wave modes corresponding to overlap region thickness indicates rust formation at the interface.
- The transition of wave modes from individual plate to overlapped region is a good indicator of the mass loss due to corrosion.
- The energy contained in the signal in a specific time window correlates well with the mass loss due to corrosion.

The present study evidences the efficacy of Lamb modes in discerning onset of corrosion of bolted steel plate joints. However, it is restricted to single bolt joints with a fixed torque and lap length. For a more general conclusion, the investigation must be expanded to more complex bolted joints. Moreover, specimens with different bolt torques must be tested in future.

Acknowledgements

The authors gratefully acknowledge Australian Research Council for funding this investigation through grant LP150100475. They are also thankful to Professor Michael Lowe for important suggestions for interpretation of the results.

References

Agarwala, V.., et al. (2000). *Corrosion detection and monitoring-A review.* Paper presented at the CORROSION 2000.

Ahn, J., et al. (2016). Clamping force loss of high-strength bolts as a result of bolt head corrosion damage: Experimental research A. *Engineering Failure Analysis, 59*, 509-525. doi:https://doi.org/10.1016/j.engfailanal.2015.08.037

Akinade, O., et al. (2015). Waste minimisation through deconstruction: A BIM based Deconstructability Assessment Score (BIM-DAS). *Resources, Conservation and Recycling, 105*, 167-176. doi:https://doi.org/10.1016/j.resconrec.2015.10.018

Amerini, F., et al. (2010). Detecting loosening/tightening of clamped structures using nonlinear vibration techniques. *19*(8), 085013.

Bayliss, D. (2004). *Steelwork corrosion control / D. A. Bayliss and D. H. Deacon* (2nd ed.. ed.): New York : Taylor & Francis.

Chaki, S., et al. (2006). Combination of Longitudinal and Transverse Ultrasonic Waves for In Situ Control of the Tightening of Bolts. *Journal of Pressure Vessel Technology, 129*(3), 383-390. doi:10.1115/1.2748821 %J Journal of Pressure Vessel Technology

Doyle, D., et al. (2010). Damage detection in bolted space structures. *21*(3), 251-264.

Hay, T., et al. (2006). A comparison of embedded sensor Lamb wave ultrasonic tomography approaches for material loss detection. *Smart Materials and Structures, 15*(4), 946-951. doi:10.1088/0964-1726/15/4/007

Kim, I., et al. (2016). Tensile behaviors of friction bolt connection with bolt head corrosion damage: Experimental research B. *59*, 526-543.

Kriesz, H. (1979). Radiographic ndt—a review. *NDT International, 12*(6), 270-273. doi:https://doi.org/10.1016/0308-9126(79)90086-5

Lowe, M,. (2013). DISPERSE.

Lowe, M., et al. (2000). The transmission of Lamb waves across adhesively bonded lap joints. *107*(3), 1333-1345.

Pickthall, T., et al. (2011). Corrosion Monitoring Equipment, A Review Of Application And Techniques. In.

Puthillath, P., et al. (2013). Ultrasonic guided wave propagation across waveguide transitions: Energy transfer and mode conversion. *133*(5), 2624-2633.

Raghavan, A. (2007). *Guided-wave structural health monitoring.*

Rathod, V.., et al. (2011). Ultrasonic Lamb wave based monitoring of corrosion type of damage in plate using a circular array of piezoelectric transducers. *NDT & E International, 44*(7), 628-636. doi:https://doi.org/10.1016/j.ndteint.2011.07.002

Rose, J. (2014). *Ultrasonic guided waves in solid media*: Cambridge university press.

Shah, J., et al. (2019). Ultrasonic monitoring of corroding bolted joints. *Engineering Failure Analysis, 102*, 7-19.

Shah, J., et al. (2020) Monitoring and Imaging of Bolted Steel Plate Joints Using Ultrasonic Guided Waves. *Journal of Nondestructive Evaluation, Diagnostics, Prognostics of Engineering Systems, 4*(1).

Sharma, S., et al. (2015). Ultrasonic guided waves for monitoring corrosion in submerged plates. *22*(1), 19-35. doi:10.1002/stc.1657

Sharma, S., et al. (2015). A non-contact technique for damage monitoring in submerged plates using guided waves. *43*(4), 776-791.

Silva, M., et al. (2003). Hidden corrosion detection in aircraft aluminum structures using laser ultrasonics and wavelet transform signal analysis. *Ultrasonics, 41*(4), 301-305. doi:https://doi.org/10.1016/S0041-624X(02)00455-9

Terrien, N., et al. (2007). Numerical predictions and experiments for optimizing hidden corrosion detection in aircraft structures using Lamb modes. *Ultrasonics, 46*(3), 251-265. doi:https://doi.org/10.1016/j.ultras.2007.02.004

Wang, H., et al. (2020). Corrosion-Induced Mechanical Degradation of High-Strength Bolted Steel Connection. *32*(8), 04020203. doi:doi:10.1061/(ASCE)MT.1943-5533.0003275

Wang, T., et al. (2013). Proof-of-concept study of monitoring bolt connection status using a piezoelectric based active sensing method. *22*(8), 087001.

Yang, Y., et al. (2019). Bolted joint integrity monitoring with second harmonic generated by guided waves. *18*(1), 193-204.

Yasui, H., et al. (1999). Ultrasonic measurement of axial stress in short bolts with consideration of nonlinear deformation. *42*(1), 111-118.

Zagrai, A., et al. (2010). Piezoelectric wafer active sensor structural health monitoring of space structures. *21*(9), 921-940.

Zampieri, P., et al. (2017). Influence of corrosion morphology on the Fatigue strength of Bolted joints. *Procedia Structural Integrity, 5*, 409-415. doi:https://doi.org/10.1016/j.prostr.2017.07.189

Zampieri, P., et al. (2017). Numerical analyses of corroded bolted connections. *5*, 592-599.

Zhang, M., et al. (2017). Application of subharmonic resonance for the detection of bolted joint looseness. *88*(3), 1643-1653.

Zhang, Z., et al. (2017). Vibro-acoustic modulation (VAM)-inspired structural integrity monitoring and its applications to bolted composite joints. *176*, 505-515.

Zhao, N., et al. (2020). A nonlinear ultrasonic method for real-time bolt looseness monitoring using PZT transducer–enabled vibro-acoustic modulation. *31*(3), 364-376.

Zhu, W., et al. (1998). Ultrasonic guided wave NDT for hidden corrosion detection. *10*(4), 205-225.

Chapter: 6 Monitoring of Corroding Bolted Interface Using Laser

6.1 Outline

This chapter reports the investigation on interfacial corrosion for a single bolt joint using a wide range of Lamb wave modes. The joint is subjected to electrochemical corrosion. The corroding joint is inspected concurrently with a contact and non-contact-based guided wave system. The former investigation is conducted through a piezoceramic patch-based system similar to Chapter 5. The latter investigation exploits the laser-based actuation and patch-based reception of the signal.

6.2 Specimen description

The specimen used in this study is two 400 mm x 100 mm x 5 mm mild steel plates are bolted together with an M16 bolt. The overlapped interfacial area is 100 mm x 100 mm. To achieve joint corrosion, a certain region on the top plate including the bolt head is submerged in an electrolytic bath. An electric circuit is formed with the bolt as the anode and an extra metal piece dipped in the electrolytic solution as the cathode to a DC power supply. Similar to Chapter 5, the electric current in the circuit is maintained at 0.1 A to induce a mass loss of 0.05% prior to each ultrasonic measurement. The details about the specimen and electrochemical corrosion can be learnt from the previous chapter.

6.3 Brief Recap

The existence of guided wave modes in solid media is dependent on the excitation frequency and the medium's thickness. The bolted joint consists of regions of different thickness: individual plate thickness and the overlapped thickness. These values are 5 mm and 10 mm in this study. In Chapter 5, only the interaction of zeroth and first-order guided wave modes with the corroding interface was studied. It was established that for a 300 kHz excitation, pristine joint supports the propagation of wave modes corresponding to the individual plate thickness (modes existing at 1.5 MHz-mm of Figure 6-1). However, with the progression in interfacial corrosion, a gradual transition to the modes corresponding to the joint thickness of the plates in the overlapped region (3 MHz-mm of Figure 6-1) was observed. It can be learnt from window I of Figure 6-1 that the identification of modes at lower frequency-thickness is relatively easier. Modes existing in this region are relatively less in number and have distinct velocities making them discernible at a different time of arrival. To estimate the arrival time of guided wave modes, the 'simulate' tool of DISPERSE software was used.

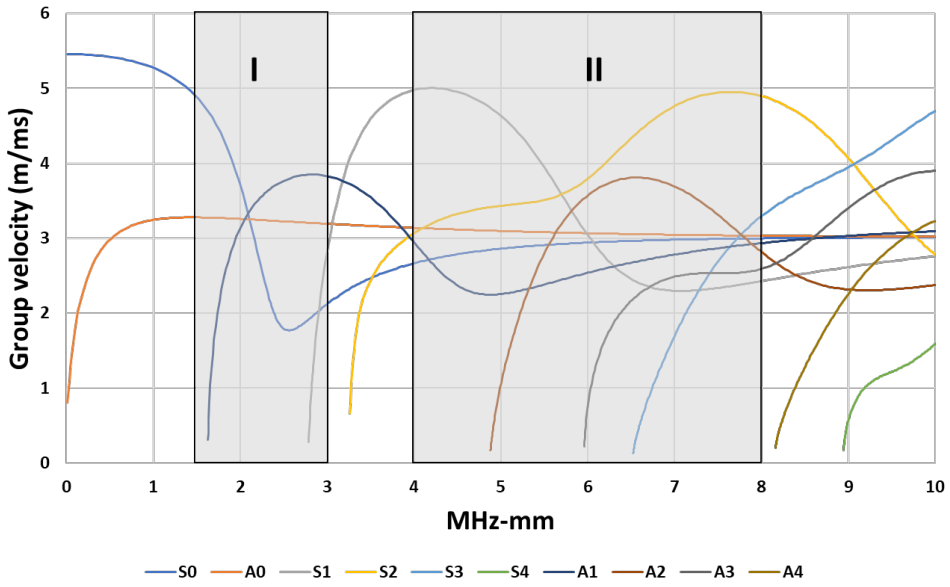

Figure 6- 1: Group velocity of Lamb modes existing in steel plate

6.4 Piezo patch-based inspection

6.4.1 The challenges with higher frequency modes

This section is the extension of the previous investigation with higher-order modes. In short, the previously used inspection window I in Figure 6-1 is slid across the frequency-thickness axis. This results in the generation of higher-order modes which are relatively in large number. In Chapter 5, an excitation frequency of 300 kHz and a path length (actuator to sensor distance) of 300 mm was chosen for the experimental investigation. For this frequency-length combination, the wave mode velocities and the shape of the transmitted signal were significantly different in the two thickness (5 mm and 10 mm) regions. In this chapter, the propagation length has been kept as a constant parameter. The upgrade is in the use of a wide range of excitation signals for the inspection.

It is to be understood that the interpretation of the transmitted signal can be a challenging task for higher MHz-mm range. The convergence of group velocities can be seen at higher MHz-mm. This results in the simultaneous arrival of multiple modes in the transmitted signal and their individual interaction with the corroding interface might not be possible to interpret. Therefore, observing the mode shift can be a formidable task. However, as these modes co-exist at the same excitation frequency, their cumulative contribution to the transmitted frequency component can provide a new insight into their interaction with the interfacial corrosion monitoring. For this purpose, excitation signals ranging from 300 kHz to 1 MHz in steps of 100 kHz are monitored for each round of ultrasonic measurement.

6.4.2 Patch based results

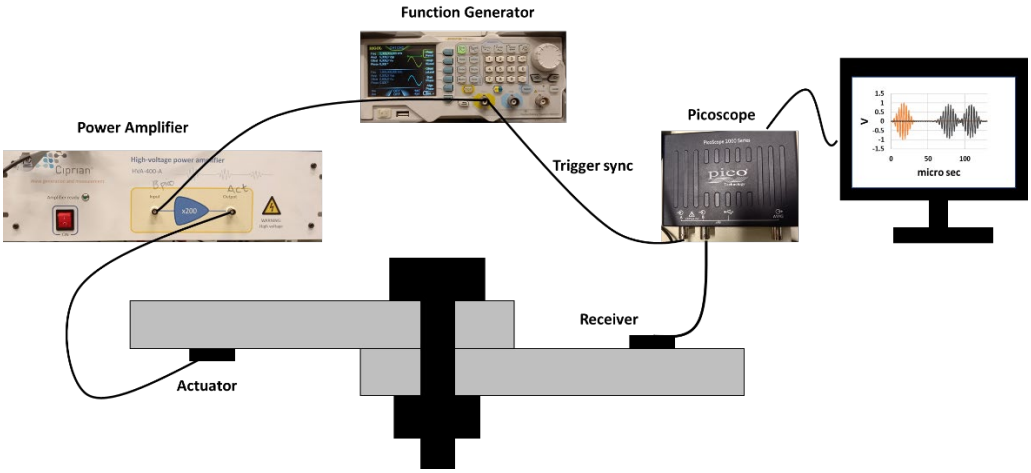

Figure 6- 2: Piezoceramic patch-based experimental setup

Figure 6-2 shows the measurement setup. The actuating patch is excited with a ten cycle Hanning windowed signal. The signal is generated using a function generator and further amplified prior to being fed to the actuating patch. The excitation frequency has been varied from 300 kHz to 1 MHz in steps of 100 kHz (8 measurements) for each round of ultrasonic measurement. The transmitted signal across the interface is recorded with an identical patch on the other plate. The total time period of the recorded signal is 200 µs. The results up to 0.5 % of mass loss are shown as no significant change in the signal is observed after that.

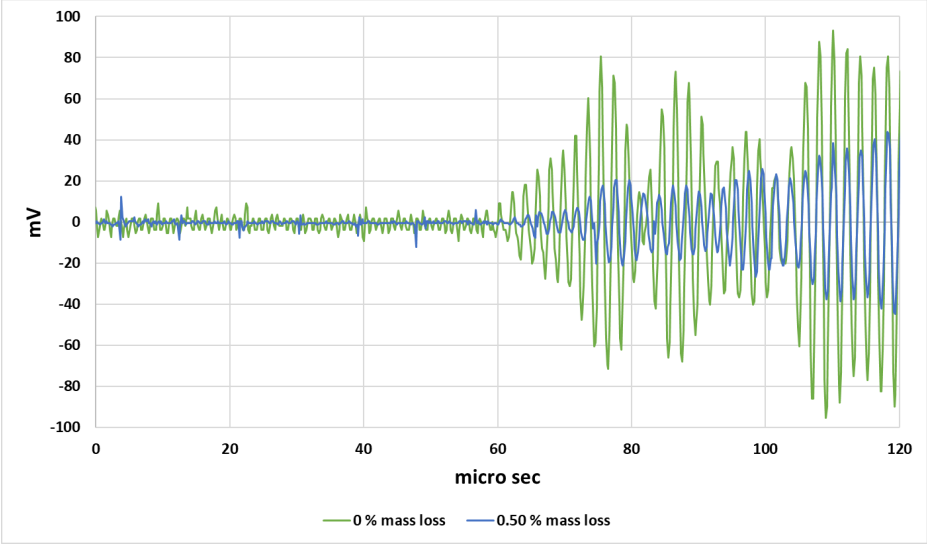

Figure 6- 3: Recorded signal for a 400 kHz excitation at (a) 0% and (b) 0.5% mass loss

Figure 6-3 shows the recorded time signal for a 400 kHz signal. It shows an overall drop in the signal strength. Fast Fourier transform of the recorded time signal has been used to monitor the change in the strength of the transmitted frequency. The change in the frequency strength

over different stages of mass loss is plotted in Figure 6-4. Each frequency results are normalized with respect to their maximum amplitude.

It can be seen that for the 300 kHz signal, the variation in the frequency amplitude saturates after 0.2% mass loss. However, the increasing rate of decline in the amplitude is observed for higher frequency excitations. It can be interpreted that the higher frequency signals interact more with the corroding interface and hence resulting in higher signal loss. In summary, higher frequency excitation can be used to identify interfacial corrosion at early stages.

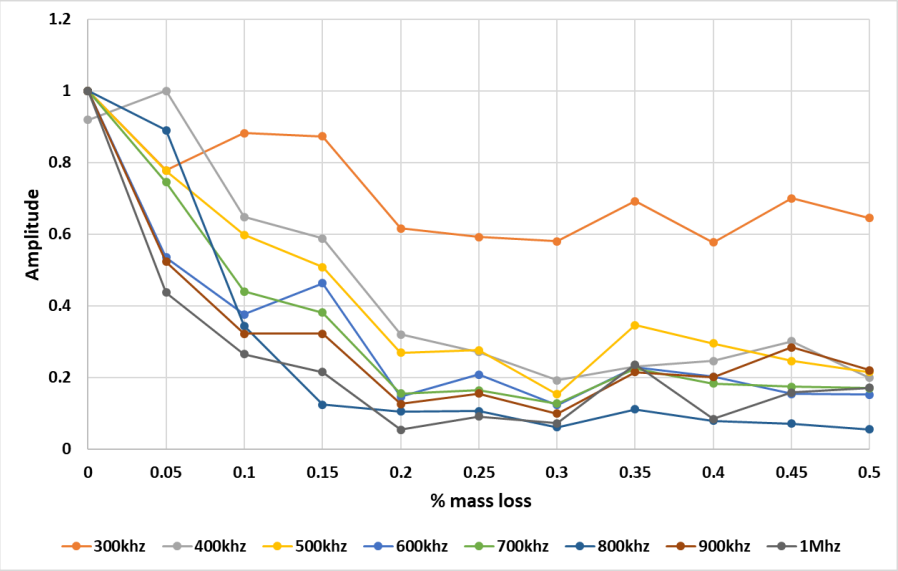

Figure 6- 4: Variation in transmitted frequency amplitude with % mass loss

6.5 Laser-based inspection

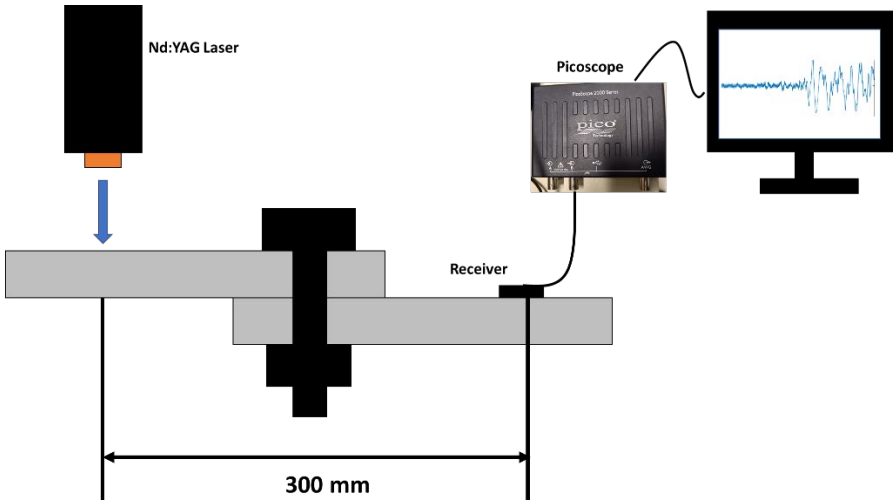

Figure 6- 5: Laser-based experimental setup

In general, patch-based excitation suffers the issue of low energy modes at especially at high-frequency excitation. It can be learnt from the transmitted signal strength in the mV range in Figure 6-3. Therefore, patch-based excitation has several limitations in monitoring large scale structure. Therefore, the actuating patch is replaced by an Nd: YAG laser as shown in Figure 6-5. The principle behind laser-based actuation is laser ablation. The increase in the local temperature at the point of excitation results in the generation of high-temperature plasma. It causes high energy particles to leave the metal surface. These particles have certain momentum associated with them resulting in a laser-based impulse. This impulse generates the required force to generate the stress waves in the specimen. The transmitted signal is recorded using a piezoceramic patch on the other plate. The distance between the point of Laser of excitation and the patch is kept fixed at 300 mm.

6.5.1 Laser-based results

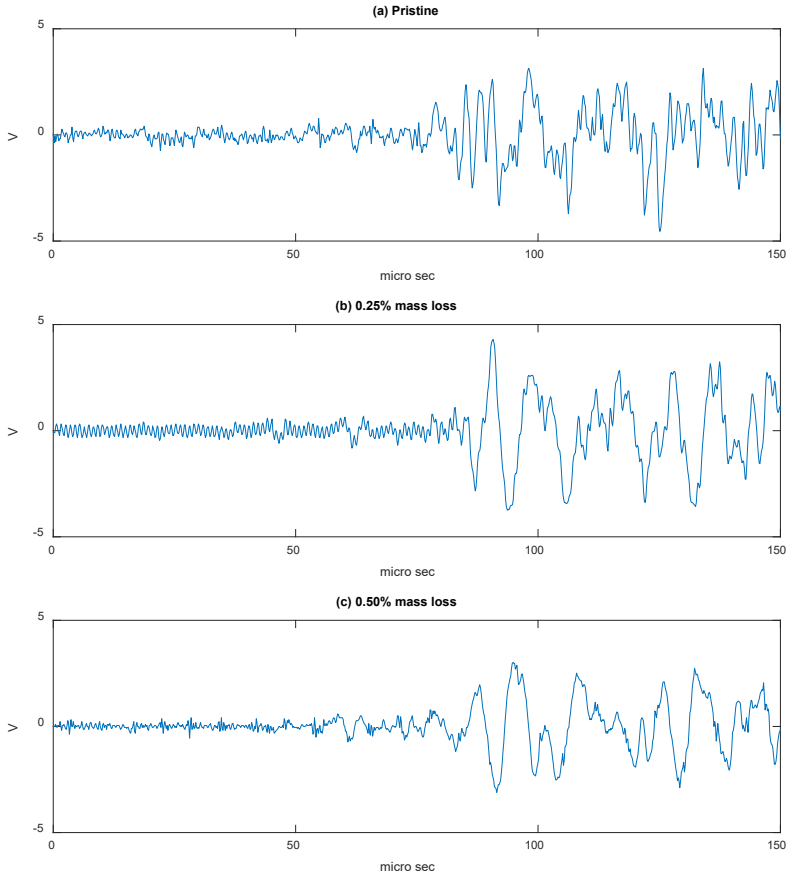

Figure 6- 6: Recorded transmitted signal for (a) 0%, (b) 0.25%, and (c) 0.50% mass loss

Figure 6-6 shows the recorded time signals for 0% (Pristine), 0.25%, and 0.50% mass loss. It can be seen that the laser-based signal actuation alleviated the issue of low energy output as the signal are in V order without any amplification. There is no significant change in the amplitude of the received signal with the mass loss. However, the reduction in the higher frequency components can be discerned intuitively in the time signal. Fast Fourier transform of the recorded signal in Figure represents the distribution of transmitted frequencies for different % mass loss. The frequency spectrum of the whole signal is extracted for a range of 0 – 1 MHz and then normalized with respect to the highest amplitude. The haphazard trend of frequency variation is best shown over five different bands {(200 (n-1) to 200 n) kHz, n = 1, 2, …., 5} is shown in Figure 6-7. The amplitude range is consistently the highest in the 0 – 200 kHz window. For higher-order bands, the reduction in the amplitudes can be seen.

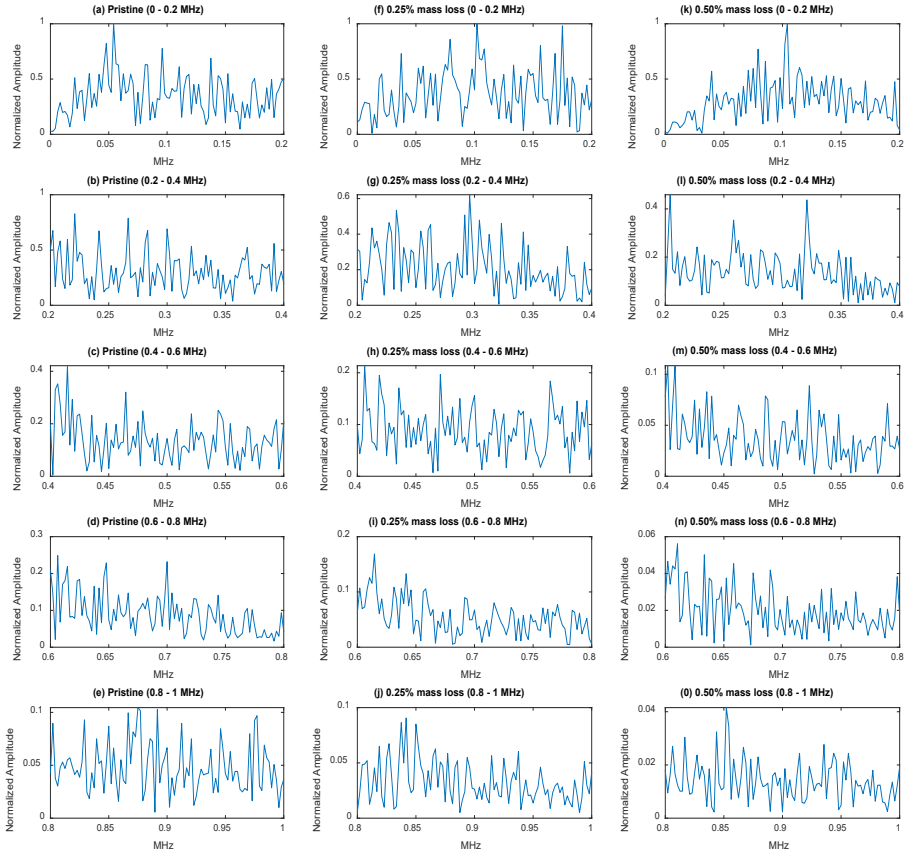

Figure 6- 7: Frequency spectra of laser-based investigation for different % mass loss

It is non-trivial to monitor the variation of a single frequency component due to poor control over excitation frequency, Therefore, the cumulative amplitude of the signal in each frequency band is monitored over different stages of % mass loss. Figure 6-8 shows that the lower order frequencies have relatively unchanged strength with the mass loss. However, an increasing decay rate for higher-order frequencies is observed. This pattern cross validates the results observed with the patch-based inspection.

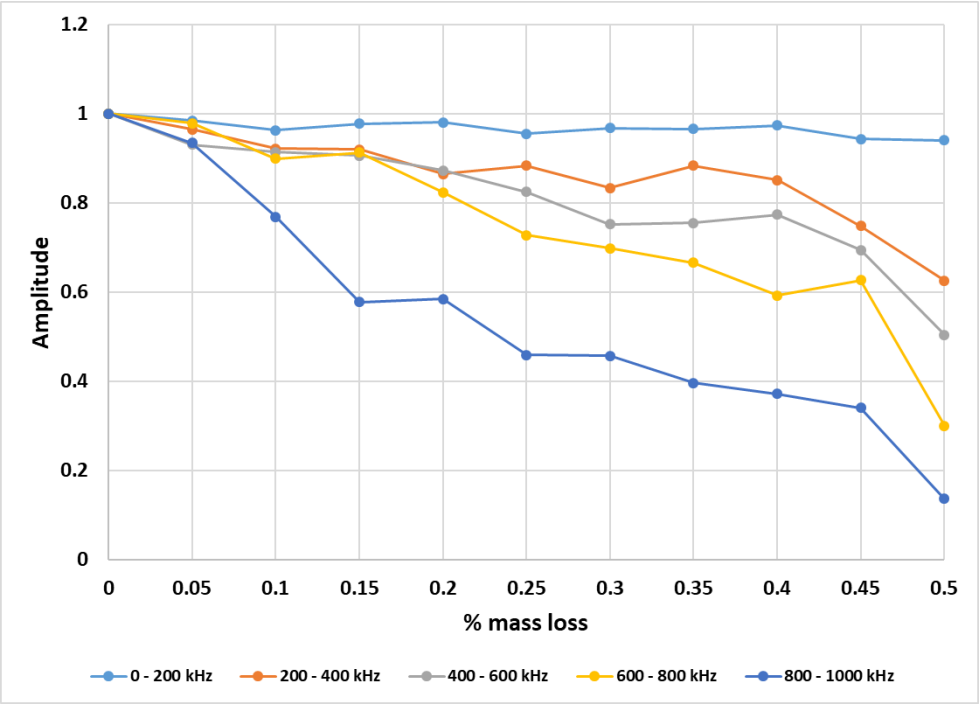

Figure 6- 8: Variation in frequency amplitude with % mass loss (laser-based excitation)

Summary

Both the investigations demonstrate that the higher-order signals are more sensitive to the interfacial corrosion. The strength of the transmitted frequencies decreases steeply for higher-order excitations. The Laser has the benefits of providing non-contact excitation which can be used for the inspection of large-scale structures. Another benefit is the generation of broad-band signals without compromising in their strength. This task would be unachievable with the patches.

Chapter: 7 Conclusions and Recommendations

Bolted steel structures play an important role in sustainable construction. However, bolted connections are inevitably prone to structural vibrations and harsh climatic conditions resulting in bolt loosening and joint corrosion. A significant number of guided wave-based investigations on bolted joints have been reported on torque loss conditions. The main motivation for this thesis is to establish the correlation between the bolt torque and the extent of interfacial corrosion. It has been argued that the generation of interfacial gaps between bolted plates during torque loss affects the integrity of joint. On exposure to corrosive conditions, these gaps can serve as an invisible site for interfacial corrosion. For the first time, this Ph.D. thesis will report a guided wave-based investigation on the correlation between bolt torque and interfacial corrosion. The key problems undertaken in this thesis are as follows:

The key objectives of this thesis were as follows:

1) Investigation of the correlation between bolt torque and interfacial corrosion.
2) To develop a baseline free technique to estimate the quality of interfacial contact.
3) To monitor interfacial corrosion using a wide range of guided wave modes.
4) To monitor joints using potentially non-contact and automated techniques.

These objectives have been accomplished and the findings have been reported in Chapter 3 to Chapter 6. The conclusions of these chapters have been summarized below:

Chapter 3 reports the potential of guided waves to trace the progression of corrosion in a bolted interface. Single lap joints consisting of two mild steel plates were investigated for different bolt torque, but similar corrosive conditions. In the preliminary study, the transmission of the ultrasonic waves across the interface is recorded when the bolt is tightened progressively in a pristine specimen. The findings demonstrate that the failure mode of a joint is dependent on the bolt torque. The nature of joint failure implicitly hints towards the contact quality between the plates. The strength of the transmitted signal increases with the increase in bolt torque or the interfacial contact. This is followed by monitoring of corroding joints initially tightened at different torque values. It was found that the nature and extent of corrosion depend on the initial bolt torque. Ultrasonic inspection can capture this difference. Through destructive tests, it was established that for the same level of corrosion in different tightened joints, the load capacity of a fully tightened joint significantly decreases relative to a loosely tightened joint.

Chapter 4 extends the concepts developed in Chapter 3. It exploits the fact that the contact between plates is dependent on the bolt torque. A loosened joint has poor contact between the plates. At the microscopic level, contact can be expressed in terms of interfacial gaps. These gaps gradually decrease as the bolt torque increases. It is observed that for a loose joint, the wave interacts dominantly with the bolt hole since there is no significant wave transfer between the two plates. As the wave transmission rises with the bolt torque, wave-bolt hole interaction gradually fades away. The ultrasonic monitoring has been conducted in a reflection mode configuration. The reflected signals from the bolted interface are recorded and used for developing the contact maps at the bolted interface. The developed hypothesis is further validated on a double-bolt specimen. Ultrasonic monitoring is able to discern the loosened bolt from the tightened one.

Chapter 5 reports a relatively sophisticated transmission-based investigation on the interaction of Lamb modes with the corroding interface. It utilizes Lamb modes existing in different thickness regions of the bolted specimen. A frequency-thickness window is chosen for the inspection. It is observed that for a pristine joint, modes corresponding to individual plates existed in the transmitted signal. With corrosion, these modes gradually convert into modes corresponding to the equivalent thickness of the overlapped region. It is hypothesized that the rust formation in the interfacial gaps increases the contact between the plates. Hence, during wave propagation, there is no relative displacement between the two surfaces. This results in the Lamb modes corresponding to the sum of two plate thicknesses. This hypothesis is further validated through a finite element based numerical model. The results are in good agreement.

Chapter 6 is the extension of Chapter 5 work where the interaction of Lamb modes with the corroding interface is studied over a wide range of excitation frequency. The preliminary investigation is done using a pair of piezoceramic patches. The results show that the decay rate in the transmission of higher-order frequencies is steeper than their lower-order counterpart. To alleviate the issue of low energy output of patches at a higher frequency, an Nd: YAG laser used to excite the stress wave. The output cross validates the preliminary outcomes. The study also highlights the potential of using non-contact laser-based excitation in joint monitoring.

7.1.1 Recommendations for future work:

1) The transmission of the ultrasonic wave as reported in Chapter 3 saturates at high torque values. Therefore, this approach cannot capture initial stages of bolt loosening. Further improvements in this technique which will facilitate monitoring of joint in a wide range

of torque loss would be beneficial. A relatively new study attempts to eliminate this saturation problem (Wang et al., 2020). This area needs to be developed further.

2) The imaging technique reported in Chapter 4 needs to be explored for joints with a higher number of bolts. Further development of the imaging algorithm will be required for the complex configuration of bolts.

3) Chapter 5 demonstrated the potential of individual Lamb mode inspection in determining the interfacial condition in a bolted joint. It reported the concept of mode conversion with the interfacial corrosion. However, it is learnt in Chapter 6 that the identification of individual modes to monitor mode conversion is a challenging task for higher-order excitation. Hence further research needs to be done to address the challenges of higher-order mode based joint monitoring.

Reference

Wang, F., et al. (2020). Monitoring of multi-bolt connection looseness using entropy-based active sensing and genetic algorithm-based least square support vector machine. *Mechanical Systems and Signal Processing, 136*, 106507.